STRUCTURAL AND OPTICAL PROPERTIES OF RARE-EARTH ELEMENT DOPED ZnO NANOSTRUCTURES

THESIS

Submitted in fulfillment of the requirement of the degree of

DOCTOR OF PHILOSOPHY

to

YMCA UNIVERSITY OF SCIENCE & TECHNOLOGY

by

DHIRENDRA KUMAR SHARMA

Registration No. YMCAUST/Ph01/2011

Under the Supervision of

DR. ANURADHA SHARMA
Supervisor
Assistant Professor
Department of Physics
YMCA University of Science & Technology, Faridabad

DR. VIPIN KUMAR
Co-Supervisor
Professor
Department of Applied Sciences
KIET Group of Institutions
Ghaziabad

Department of Physics

Faculty of Humanities & Sciences

YMCA University of Science & Technology

Sector-6, Mathura Road, Faridabad, Haryana, India

October, 2018

DEDICATION

First and foremost, I would like to thank *'God'*, for giving me courage and strength in successful completion of my thesis.

The research world has instilled in me the power of in depth thought, analysis and experience the happening. I owe my thanks to the field of research. The reason behind my existence is my parents my father Shri Shri Niwas Sharma, my mother Smt. Usha Sharma and my loving younger brother Virendra Sharma I give my heartfelt thanks to them.

I express my most sincere and heartfelt gratitude to my thesis supervisor Dr. Anuradha Sharma for her inspiring mentorship, valuable suggestions and propelling me towards rigorous effort. Her moral support and productive comments and also her hard work and vast knowledge in the research field helped me in the successful completion of this thesis. Her personal touch in the work of his/her mentee's makes me fill with gratitude and respect. It is indeed a rare privilege to work under her guidance.

Equally, I am extremely thankful to my thesis co-supervisor, Prof. Vipin Kumar for giving me this wonderful opportunity to work under his guidance and for the valuable suggestions and constant motivation throughout my research work.

It is a great pleasure for me to thank my wonderful colleagues at this moment, especially Dr. C.M. Batra (HOD of Applied Sciences) and Dr. Kapil Kumar Sharma for their immense help, kindness, motivation, moral support and encouragement and moreover for treating me as their family friend. In these years, the time I spend with them inside and outside the laboratory is invaluable and enjoyable.

I would also like to thank my other colleagues in my group Dr. Anshuman Sahai and Dr. Aditya Sharma for their timely help, kindness and invaluable discussions in performing and analyzing the samples.

At this moment, I owe my sincere gratitude and thanks to my former M. Tech. supervisor Dr. Navendu Goswami, JIIT, Noida (India) for introducing me to this world and new topic of research. The opportunity he gave me to work under his guidance is invaluable and appreciable.

I would also like to express my appreciation to my bosom friends for their presence at the time when I got demotivated. The friends who were constant support are Siddharth Bhardwaj, Vipin Goyal, Sweta Shukla, Monika Gaur and Deepika Gaur.

Lastly, I would like to state that I owe my research work also to my life-line my beloved wife Kalpana Sharma and my angel Vanshika Sharma (daughter) to whom I extend my great thanks.

CANDIDATE'S DECLARATION

I hereby declare that this thesis entitled "**STRUCTURAL AND OPTICAL PROPERTIES OF RARE-EARTH ELEMENT DOPED ZnO NANOSTRUCTURES"** by **DHIRENDRA KUMAR SHARMA,** being submitted in fulfillment of the requirements for the Degree of Doctor of Philosophy in **DEPARTMENT OF PHYSICS** under **FACULTY OF HUMANITIES & SCIENCES** of YMCA University of Science & Technology Faridabad, during the academic year 2018-19, is a bonafide record of my original work carried out under guidance and supervision of **DR. ANURADHA SHARMA, ASSISTANT PROFESSOR, DEPARTMENT OF PHYSICS, YMCAUST, FARIDABAD & DR. VIPIN KUMAR, PROFESSOR, DEPARTMENT OF PHYSICS, KIET GROUP OF INSTITUTIONS, GHAZIABAD** and has not been presented elsewhere.

I further declare that the thesis does not contain any part of any work which has been submitted for the award of any degree either in this university or in any other university.

DHIRENDRA KUMAR SHARMA

Registration No. Ph01/2011

CERTIFICATE OF THE SUPERVISORS

This is to certify that this Thesis entitled **"STRUCTURAL AND OPTICAL PROPERTIES OF RARE-EARTH ELEMENT DOPED ZnO NANOSTRUCTURES"** by **DHIRENDRA KUMAR SHARMA,** submitted in fulfillment of the requirement for the Degree of Doctor of Philosophy in **DEPARTMENT OF PHYSICS** under **FACULTY OF HUMANITIES & SCIENCES** of YMCA University of Science & Technology Faridabad, during the academic year 2018-19, is a bonafide record of work carried out under our guidance and supervision.

We further declare that to the best of our knowledge, the thesis does not contain any part of any work which has been submitted for the award of any degree either in this university or in any other university.

DR. ANURADHA SHARMA
Supervisor
Assistant Professor
Department of Physics
YMCA University of Science & Technology, Faridabad

DR. VIPIN KUMAR
Co-Supervisor
Professor
Department of Applied Sciences
KIET Group of Institutions
Ghaziabad

Date:

ACKNOWLEDGEMENT

I would like to express my sincere gratitude to my supervisors **DR. ANURADHA SHARMA** and **DR. VIPIN KUMAR** for giving me the opportunity to work in this area. It would never be possible for me to take this thesis to this level without his/her innovative ideas and his/her relentless support and encouragement.

DHIRENDRA KUMAR SHARMA

Registration No. Ph01/2011

ABSTRACT

Undoped ZnO, Ce^{3+} as well as Er^{3+} doped ZnO nanostructures with different concentrations of RE (Ce^{3+}, Er^{3+}) ions were successfully synthesized by the employ of chemical precipitation process, to fabricate rare earth activated zinc oxide nanophosphors. Though it's not an easy task to incorporate RE ions into the lattice of semiconductors that efficiently via chemical method as Ce/Er ion has large radius and there is a noticeable difference between their charges and chemical properties but this process was undertaken in this study effectively. The production of huge amounts of high uncontaminated samples at low cost is facilitated by the conventional chemical precipitation method. The phosphor powders were produced by sintering the precursor gels at 600˚C for 1 h and drying the dried gels at 60˚C for 40 h for Ce doped and Er doped ZnO nanostructures respectively. The prepared samples were characterized by XRD, TEM/HRSEM, EDX, UV/vis spectroscopy, PL and VSM. The improved structural transformation, luminescence, ferromagnetism characteristics and a decrease in band gap energy has been reported in this thesis.

From the X-ray diffraction conclusions, it was found that the pure and RE (Ce^{3+}, Er^{3+}) doped ZnO nanophosphors were in hexagonal wurtzite phase in nature regardless of the incorporation of Ce^{3+} or Er^{3+} ions and unnecessary compounds or precipitates were not formed during the growth. Energy dispersive X-ray spectrometer (EDX) analysis revealed homogeneous distribution of Zn, O, and RE^{3+} ions. The transmission electron microscope (TEM) analysis indicated that the pure and Ce^{3+} doped powders were composed of hexagonal homogeneously dispersed nanoparticles of high crystallinity with an average size range 20- 60 nm in diameter, which was in agreement with X-ray diffraction (XRD) analysis. High resolution scanning electron microscopy (HRSEM) analysis showed that the presence of Er^{3+} ions in crystal structure of ZnO can change the morphology i.e. nanorods transform to nanocones.

Optical band gap was extrapolated from the Ultraviolet Visible spectroscopy (UV- Vis) transmission spectra or absorption spectra using Tauc's relation and the considerable drop in optical band gap for the doped samples as compared to the pure sample was observed. Direct type of transition of band gaps was confirmed by transmission spectra occurring at 3.5 eV and 3.2 eV respectively for ZnO nanoparticles and Ce doped ZnO nanoparticles i.e. decrease of band gap energy with doping of Ce ions in ZnO nanoparticles. In UV- visible absorbance spectra, a red shift

was observed in the band gap of undoped ZnO and Er doped nanostructures with increasing Er concentration. Values of optical band gap decrease from 3.34 eV to 3.19 eV for undoped ZnO nanostructures and 1 to 7 at.% Er doped ZnO nanostructures respectively.

PL study showed that ZnO and Ce doped ZnO nanoparticles had an UV emissions and a green emission while the Ce ions doping induced a red shift in the UV emission with broadening in the green emission. The PL characterization of ZnO:Er^{3+} samples was studied by means of a 325 nm He-Cd laser line. It was examined that the undoped and doped nanostructures had an UV emission and a defect emission and the doping of Er ions induced a red shift in the UV emission and a small enhancement in the defect emission.

The magnetization/VSM study demonstrated that the RE (Ce^{3+}, Er^{3+}) doped nanophosphors exposed outstanding ferromagnetism property at room temperature while undoped ZnO nanostructures demonstrate diamagnetic behavior at room temperature.

Key Terms:

ZnO, Nanostructures, Chemical precipitation method, Rare earth, Cerium, Erbium, Ferromagnetism.

TABLE OF CONTENTS

LIST OF TABLES

LIST OF FIGURES

LIST OF ABBREVIATIONS

TITLE	ABBREVIATIONS
Zinc oxide	ZnO
Cerium	Ce
Erbium	Er
Rare earth	RE
Nano meter	Nm
X-ray diffraction	XRD
Energy dispersive X-ray spectroscopy	EDX
High resolution transmission electron microscope	HRTEM
High resolution scanning electron microscope	HRSEM
Ultraviolet visible spectroscopy	UV-Vis
Photoluminescence	PL
Vibrating sample magnetometer	VSM
Near-infrared	NIR
Light-emitting diode	LED
Organic light-emitting diode	OLED
Diluted magnetic semiconductor	DMS
Electron volt	eV

Conduction band	CB
Valence band	VB
Near-band edge	NBE
Deep level emission	DLE
Bound magnetic polaron	BMP
Field effect transistor	FET
Dye-sensitized solar cell	DSSC
Current-voltage	I-V
Chemical vapour deposition	CVD
De-ionized	DI

BRIEF PROFILE OF RESEARCH SCHOLAR

Dhirendra Kumar Sharma is presently working as Assistant Professor in Department of Physics, KIET Group of Institutions, Ghaziabad. He has obtained Bachelor's degree (B.Sc.) and Master's degree (M.Sc., Physics) from Jamia Millia Islamia, New Delhi. He has also obtained Master's degree (M. Tech.) in Material Science and Engineering from Jaypee Institute of Information Technology, Noida. He has qualified CSIR Net exam in June, 2011. He is pursuing Ph. D from YMCA University of Science and Technology Faridabad, India. He has presented his papers in International Conferences and National conferences. His papers are published in various International Journals and International Conferences. He has 10 years of teaching experience.

LIST OF PUBLICATIONS OUT OF THESIS

List of Papers Published in Journals

S. No	Title of the paper along with volume, Issue No, year of publication	Publisher	Impact factor	Refereed or Non Refereed	Whether you paid any money or not for publication
1.	Effect of Ce doping on the structural, optical and magnetic properties of ZnO nanoparticles Journal of materials science: materials in electronics Vol. 26, 2016, pp. 10330-10335	Springer	2.324	Referred (SCI & SCOPUS INDEXED)	No
2.	Synthesis of Er doped ZnO cone-like nanostructures with enhanced structural, optical and magnetic properties Journal of materials science: materials in electronics Vol. 29, 2018, pp. 3840-3849	Springer	2.324	Referred (SCI & SCOPUS INDEXED)	No

Paper Presented in National/ International Conferences

1. Functions of nanostructure phosphors in future technology

Dhirendra Kumar Sharma, Anuradha Sharma

[In National conference on "Science in Media" (SIM-2012), YMCA University of Science & Technology, Faridabad, 03-04 December, 2012]

2. A review on structural, optical and magnetic properties of rare earth element doped ZnO nanostructures

Dhirendra Kumar Sharma, Vipin Kumar, Kapil Kumar Sharma, Anuradha Sharma

[In AICTE sponsored 2nd International Conference on Communication & Electronics (ICCE- 2013), KIET Ghaziabad, 28-29 November, 2013, ISSN: 2320-8996]

3. Structural and optical study of Eu doped ZnO nanostructures

Dhirendra Kumar Sharma, Kapil Kumar Sharma, Vipin Kumar, Anuradha Sharma

[In National conference on Role of science and technology towards 'Make in India', YMCA University of Science & Technology, Faridabad, 05-07 March, 2016]

4. Enhanced photoluminescence emission from Ce: ZnO nanoparticles prepared by a chemical precipitation method

Dhirendra Kumar Sharma, Kapil Kumar Sharma, Vipin Kumar, Anuradha Sharma

[In International Conference on Frontiers of Science & Technology-17 (ICFST-17), KIET Ghaziabad, 06-07 January, 2017, ISBN: 978-83-85329-23-4]

CHAPTER I

INTRODUCTION

1.1 BACKGROUND OF NANOSCIENCE AND NANOTECHNOLOGY

Nanoscience and nanotechnology has grown immensely in the last few decades allowing us to do new things in almost every conceivable technological discipline. Nanoscience seems new but our history has already achieved a lot in this field in '*Ayurveda'* (in Sanskrit, Ayurveda meaning "knowledge for long life") in the form of *'bhasmas'*, which contained several minerals such as metal/metal-oxides nanoparticles in the form of ashes of gold, silver, copper, zinc, iron, nickel, mercury, etc. This is a fine proof of nanotechnology. *Bhasmas* are unique ayurvedic metallic/minerals preparations, treated with herbal juice or decoction and were used to cure various diseases between 3^{rd}-13^{th} centuries AD [1]. Different materials were made by various smiths for day to day utilities [2]. 'Lycurgus cup', made in 4^{th} century by a mixture of silver nanoparticles and colloidal gold, appears to shows different colours of appearance when light transmits or reflects from it [3]. Glittering pottery is another example of nanotechnology. Stained windows made of gold, chlorides and other metal oxides nanoparticles used in the Roman Catholic churches is also a fine example of nanoscience [2, 4]. Due to specific content of cementic nanowires and carbon nanotubes, 'Damascus' sabre blade possessed very high strength [4, 5]. This shows that people in ancient times were aware of nanotechnology and nanoscience but they may have given it some other name.

With the passage of time, nanotechnology has overwhelmed the modern era by rapidly attaining the target of giving luxury to human being. The modern era began in 1857 with Faraday's experiment on nanoscale gold particles. In this experiment, Faraday observed that the colour of gold kept changing when the size of gold particles was changed [6]. In 1947, Bardeen, Shockley and Walter invented semiconductor transistor at Bell Labs and expanded considerably the scientific information of semiconductor interfaces, laying the foundation for electronic devices and the "Information Age" [2]. In 1980, Klimov and co-workers noticed the size dependency

of optical spectra of semiconductors nanocrystals from experiment of semiconductors doped glass [7]. Prof. Feynman researched on designing the adaptability to manipulate, control, assemble, produce and manufacture things at atomic precision [8]. Richard Feynman delivered a lecture on 29th December, 1959 in the seminar of American Physical Society at the California Institute of Technology. This was published in February 1960 in the issue Caltech's Engineering and Science which owned the copyright but later on it was made available free of cost on web with his kind consent [9]. In the words of Sir Richard Feynman from the famous talk entitled 'There is plenty of room at the bottom', the importance can be summarised as: *"I would like to describe a field, in which little has been done, but in which enormous amount can be done in principle. The field is not quite the same as others in that it will not tell us much of fundamental physics (in the sense of, ―What are the strange particles?), but it is more like solid-state physics in the sense that it might tell us much of great interest about the strange phenomena that occur in complex situations. Furthermore, a point that is most important is that it would have an enormous number of technical applications. What I want to talk about is the problem of manipulating and controlling things on a small scale. . . . What I have demonstrated is that there is room—that you can decrease the size of things in a practical way. I now want to show that there is plenty of room. I will not now discuss how we are going to do it, but only what is possible in principle...We are not doing it simply because we haven't yet gotten around to it"* [8,9]. In 1974, Prof. Norio Taniguchi used the term "Nanotechnology" for the first time illustrating it as "the processing of separation, consolidation, and deformation of materials by one atom or one molecule" [10]. In 1981, Binnig and Rohrer at IBM's Zurich lab invented the scanning tunnelling microscope (STM), which allowed scientists to actually work at the direct spatial images of individual atoms for the first time [2]. This discovery led them to the Nobel Prize in 1986 [2]. In 1985, Kroto, Brien, Curl and Smalley discovered the Buckminsterfullerene (C_{60}), also known as the bucky ball, and were awarded Nobel Prize in Chemistry for this in 1996 [2]. In 1986, Atomic Force Microscope (AFM) was invented by Binning, Quate and Gerbe and the first book, namely "Engines of Creation" was written by K. Eric Drexler. In 1991, Sumio Iijima discovered carbon nanotube (CNT) [2]. In the last decade of 21st century nanotechnology played a vital role in day to day life of consumers and it has affected the market widely [2].

No exclusively precise definition of nanotechnology could be available, until in 2000, National Nanotechnology Initiative (NNI) was commenced in USA which gave the most relevant definition of nanotechnology as [2]: “Nanotechnology is the design of nanomaterials in size range of 1-100 nanometer (nm) and the applications of their fundamentally new properties and functions”. Nanotechnology can also be described as the formation and utilization of nanomaterials with structural features in between those of atoms and their bulk counterparts. The properties of the materials having dimensions at nanoscale show significant deviation from those at the atomic as well as macro scale. This could primarily be attributed to the large surface area to volume ratio exhibited by nanomaterials which improves their surface reactivity with the surrounding surface making them potential candidates for sensor applications. Therefore, nanomaterials hold promise for novel devices and technologies [11, 12].

Nanotechnology and nanoscience are the two most commonly used and misused terms. Nanotechnology offers an understanding and control of matter at dimensions approximately between 1 and 100 nm facilitating innovative applications of nanoparticles due to their distinct phenomena. Nanoscience is defined as the science fundamental to nanotechnology [13, 14]. Nanotechnology is a revolutionary field of science and technology with diverse applications in areas such environment, medical, biomedical, healthcare and life sciences, agriculture, food safety, security, energy production and conversion, energy storage, consumer goods, infrastructure, building and construction sector and aerospace [15–18]. The applications based on nanotechnology also provide faster response, low-cost, longer life time, ease of use and high efficiency of devices. Not only do nanotechnological applications offer new approaches to diagnosis and treatment of diseases, they also provide efficient environmental monitoring and unconventional methods for considerable energy production for the betterment of humanity. Thus nanotechnology has applications in almost every aspect world.

Luminescence, which was first named in 1888 by the German physicist Eilhard Wiedemann, is defined as the electromagnetic radiation from phosphors with suitable excitation. Wiedemann characterized the light emission originating from processes other than increase of temperature [19]. Luminescence, also called "cold light", is different from incandescence, which is light released by a substance as a result of heating. The classification of luminescence depending on the excitation source is given in Table 1.1. For optical characteristics in the present study, the focus will be on the first form of luminescence in the table i.e. photoluminescence, since it is most commonly used in solar cells [20].

Table 1.1: The different types of luminescence and their excitation source

Name	**Excitation source**
Photoluminescence	Light
Cathodoluminescence	Electrons
Radioluminescence	X-rays, α-, β-, or γ-rays
Thermoluminescence	Heating
Electroluminescence	Electric field or current
Triboluminescence	Mechanical energy
Sonoluminescence	Sound waves in liquids
Chemiluminescence and bioluminescence	Chemical reactions

The theory of luminescence was still in initial stages of development and this field was treated "*more as an art than science*". The production of valuable and efficient luminescent materials was more stressed upon. Lenard and his school undertook methodical and comprehensive investigations in the foundation properties of materials like alkaline earth sulphide phosphors [21]. Studies in luminescence which were motivated by application possibilities generated results of fundamental importance and facilitated consequent interpretative work in some simple cases at least. Hilsch,

Pohl and their collaborators studied the optical and electronic properties of alkali halide crystals and colour centres which can be considered as ground breaking in the progress for understanding the properties of luminescent crystals [21]. Further discussion on interest in luminescent materials and choice of luminescent dopant is presented in the next chapter.

Scientists the world over have taken tremendous interest in the synthesis and fabrication of efficient luminescent materials with nanometre dimensions. The control of shape and size of a new generation of light emitting materials at nanoscale known as ―*phosphors* and the investigation of their physical, optical and luminescent properties have drawn particular attraction [13, 22]. Phosphors are capable of absorbing energy from the incident radiations and emitting photons after series of energy transfer processes. To meet the demands of various applications, phosphors are generally used in powder form with elaborate requirements on particle size and morphology [23]. In the recent times, rare earth (RE) based phosphors have found wide-ranging applications in many fields such as cathode-ray tube (CRT) screens and liquid-crystal displays (LCD) which are the most commercially used display devices. The application of RE based phosphors in solar cells is a novel field. In this regard, the Fraunhofer Institute for Solar Energy Systems ISE and the Helmholtz Center, Berlin have jointly designed a solar cell with 44.7% efficiency. However, the maximum efficiency predicted theoretically by Trupke [24] and colleagues is approximately 63% for concentrated sunlight and 48% for non-concentrated sunlight.

The principal materials of interest in the current study are RE based phosphors. RE ions are used as activator centres in different host materials since they have high fluorescence efficiencies and very narrow line fluorescence bands. The RE doped Zinc Oxide (ZnO) nanostructures also show ferromagnetism property and this property has drawn great interest. These RE based nanostructures find applications in magneto-optical device applications i.e. communications, storage, quantum computation etc. [25, 26].

ZnO with a wide direct bandgap (3.37 eV) and a large excitation binding energy at room temperature (60 meV), is an ideal host candidate for RE ions [27]. Gali et al. and Erwin et al. [28, 29] reported low solubility of the dopant in the matrix resulting in a material exhibiting two phases due to the low temperature which comes across as a major challenge to the synthesis of RE doped ZnO phosphors. The fascination for optical study of lanthanide doped phosphors dates back to the 1880s.

Scientists such as Sir William Crookes, LeCoq de Boisbaudran, Eugène Demarçay or, later, Georges Urbain used luminescence as an analytical tool to test the purity of their crystallizations and to identify potential new elements [30].

Among other nanostructures such as nanorods, nanowires, nanotubes, nanoparticles etc, this study, focuses on a particular class of nanostructures called nanoparticles and cone-like nanostructures. Detailed discussion on these nanostructures will follow in the next chapter. In the present work, emphasis has been laid on the investigations of their enhanced structural, optical and magnetic properties.

Among all lanthanides which are luminescent except La^{3+} and Lu^{3+}, this study focuses on Cerium (Ce^{3+}) for which the *f-f* emission lines cover the entire spectrum in the visible region. Furthermore, we have also found interests on Erbium (Er^{3+}) which is luminescent in the near-infrared (NIR) region of the electromagnetic spectrum [31]. To the best of our knowledge, only few groups of researchers have reported their successful synthesis of luminescence materials based on ZnO nanostructures doped with lanthanides, in particular Ce^{3+} and Er^{3+} [32–48].

1.2 PROBLEM STATEMENT

Phosphors, with tuneable optical properties, have become a boon for new generation optical communication, high resolution and high efficiency luminescent devices. In the past, it has been examined that high definition display devices required submicron particle sizes to optimize screen resolution and luminescence efficiency [49]. Semiconductor nanostructures can be synthesized with sizes ranging from 2 to 10 nm and thus achieve the size requirement for quantum confinement process. With the invention of light emitting materials, nano-sized phosphors has shown attractive properties such as high quantum efficiency for photoluminescence, ultra-fast recombination time and increased energy band-gap for luminescence due to the low dimension of the particles [50-53]. Significant work in the field of luminescence started almost a decade ago and this has set unique significance of nanocomposites consisting of semiconductor nanocrystals. ZnO nanoparticles are usually doped in dielectric matrices such as glasses and polymers and are of great significance as phosphor materials for solar cell device fabrication. However, doping of RE ions into the semiconductor nanostructures efficiently via chemical precipitation method remains a challenge among the scientific community. The present study focuses on

developing RE^{3+} (Ce^{3+}, Er^{3+}) doped ZnO nanostructures in the size range 20-60 nm in order to improve the performance of optical and spintronic materials.

Due to its wide direct band gap (3.37 eV), large exciton binding energy (60 meV) and high optical gain (320 cm^{-1}), ZnO seems to be a promising material and the development of this phosphor can make a massive impact technologically worldwide. Structural, optical and magnetic studies will be carried out on the luminescent properties of semiconductor nanostructure powder phosphors. The transmission and absorption properties of these phosphors are of primary importance.

The present study proposes a procedure for doping RE ions into ZnO semiconductor nanostructures using chemical precipitation method. Chemical precipitation is used for its low energy consumption, good control of particle size and uniform morphology of the particles in the final product. The best part of this method is that although it has many features, it is still very economical.

1.3 STUDY OBJECTIVES

The prime objectives of this thesis are as follows:

- To synthesize pure and RE element doped (Ce^{3+} and Er^{3+}) ZnO nanostructures using chemical precipitation method.
- To study the structural, optical and magnetic properties of pure and RE doped ZnO nanostructures.
- Determination of the effect of doping on structural, morphological, optical and magnetic properties of $Zn_{1-x}Ce_xO$/ $Zn_{1-x}Er_xO$ nanostructures in comparison to undoped ZnO nanostructures.
- Exploration of prepared nanostructures for various technological applications.

1.4 PLAN OF THESIS

The thesis is composed of six chapters and organized as follows:

- **Chapter 1** gives the general introduction about nanoscience and nanotechnology and potential applications of nanotechnology in almost every aspect of science and technology. In this chapter, a brief background of luminescence and different types of luminescence with relevance to ZnO and RE doped ZnO nanostructures are also clearly highlighted.

- **Chapter 2** describes the technological applications of luminescent materials, fundamental properties of host material i.e. ZnO, fundamentals of doping and growth mechanism, historical introduction about RE elements and basic characteristics of RE element of Ce^{3+} and Er^{3+}.

- **Chapter 3** provides a brief review of the study of RE ions (Ce^{3+} and Er^{3+}) doped ZnO nanomaterials. A brief description on different methods of synthesizing the nanomaterials is also provided in this chapter along with details of chemical precipitation method which is employed in the present study for synthesis of pure and RE doped ZnO nanophosphors. The principles of the characterization techniques namely, X-ray Diffraction (XRD), Energy Dispersive X-Ray (EDX), Transmission Electron Microscopy (TEM), High Resolution Scanning Electron Microscopy (HRSEM), Ultraviolet-visible (UV-vis) spectroscopy, Photoluminescence (PL) spectroscopy and Vibrating Sample Magnetometer (VSM) used for the analysis of powder samples are also explained in brief.

- **Chapter 4** discusses the study of procedure and mechanism of synthesis of ZnO and Ce doped ZnO nanoparticles. The structural, compositional, morphological, optical and magnetic properties of the prepared samples were analyzed and discussed using XRD, EDX, TEM, UV-Visible (transmittance spectra), PL and VSM techniques respectively. The structural and morphological analysis revealed the hexagonal wurtzite phase of 20-60 nm size of nanoparticles. PL measurement of Ce doped ZnO nanoparticles revealed the red shift in the UV emission and green emission band for visible emission. UV-visible spectroscopy exhibited a considerable drop in the band gap after doping of Ce ions in ZnO nanoparticles. It was also found that the characteristic of ferromagnetism was prominent in Ce doped ZnO nanoparticles which was not at all visible in ZnO nanoparticles.

- **Chapter 5** presents the details of the synthesis method and reaction mechanism of ZnO and Er doped ZnO nanostructures via chemical precipitation. Structural, compositional, morphological, optical and magnetic properties of undoped and 1-7 at.% Er doped ZnO nanostructures have been systematically

studied. The prepared powder samples were characterized employing spectroscopic techniques namely XRD, EDX, HRSEM, UV-vis., PL and VSM. For prepared nanostructures, a regular morphological transformation from nanorods-like to nanocones-like, with Er incorporation in ZnO is shown through HRSEM. Er dopant has a strong consequence on structural and optical properties, which could be shown in a considerable red shift in the band gap, the formation of new states due to doping level and the presence of an oxygen vacancy. Values of optical band gap decrease from 3.34 eV to 3.19 eV for undoped ZnO nanostructures and 1 to 7 at.% Er doped ZnO nanostructures respectively. PL analysis revealed that the Er^{+3} ions doped ZnO has a high optical property and is a 'fascinating' PL material that shows multiemission peaks at the blue to yellowish-red region, which was attributed to the enhanced defects or oxygen vacancies in excess caused by erbium oxide dopant. At room temperature, hysteresis was observed in the M–H curves which show the presence of ferromagnetism in all Er doped ZnO samples. It is found that the coercivity, remanent magnetization and the saturation magnetization values of these samples increase as the doping concentration is gradually increased from 1-7 at.% Er.

- **Chapter 6** is about conclusion of the results and suggestions for possible future prospects.

CHAPTER II
BASIC LITERATURE

2.1 TECHNOLOGICAL INTEREST IN LUMINESCENT MATERIALS

The exclusive properties of luminescent materials because of the low dimensionality and their benefits provided by wide band gap semiconductor materials have become really significant for the researchers. The new technologies strongly depend on the exciting magnetic and spectroscopic properties of lanthanide ions. In particular, their ability to generate well-characterized and intense near-infrared (NIR) luminescence is exploited in modern fiber-optic telecommunication networks [54]. RE luminescent materials play a vital role in creating a wealth of advanced optical applications. Those materials involving NIR luminescence have stirred particular interest in view of exciting applications in telecommunications [55] and associated lasers and light-emitting diode (LED)/ organic light-emitting diode (OLED) devices [56–58] as well as in bio-sciences [55, 57–65] and solar energy conversion [66–70]. In the recent years, the importance of crystalline and wide gap oxides doped with trivalent lanthanide ions has increased for its applications in optoelectronics and lighting devices, in photo-catalysis, optical imaging and also in photon frequency down- and up- conversion. For the latter, the optical frequency conversion through photoluminescence has been suggested in the 70's in solar cells coupled with luminescent concentrators [71]. Different processes have been proposed to overcome the efficiency losses and all of these methods concentrate on better exploitation of the solar spectrum like quantum dot concentrators, multijunction solar cells, interband transitions, photon frequency down conversion [69, 72] (one high energy photon can be splitted into two or more lower energy photons that can be absorbed) and up-conversion [73] (two lower energy photons can be added together to obtain one high energy photons) etc. Specifically, photon frequency conversion [74-76] is an appreciable approach which allows us to modify the solar spectrum by shifting or converting a spectral range to a region where the solar cell has a better response, as the mismatch between incident solar spectrum and the spectral response is one of the main reasons for the efficiency loss in solar cells. Since the pioneering studies [54], this frequency conversion approach was coupled with luminescent concentrators

employing organic dye molecules. In comparison, due to the low quantum efficiency and stability of these organic materials, significant steps have been taken on finding new nanostructured materials (particularly quantum dots, doped wide band gap oxide semiconductors). This explanation has created interest in this topic and many scientific works have been done to study these materials. The process of photon absorption in oxide semiconductors followed by an energy transfer toward some levels of the ions of rare earth is particularly effective [77]. In the literature, many works have been reported on doping of oxide semiconductors by numerous lanthanide ions, investigating the effect on the luminescence and structural properties [78-84]. It has been demonstrated that the properties of oxides can be tuned through the addition of variety of dopant ions and also the processing conditions [85-87]. Concerning to the luminescence applications in UV, Visible and NIR emissions, wide band gap oxides are the most suitable host matrix for intentionally doping impurities for many technological applications. In recent years, RE doped wide band gap semiconducting nanomaterials have attracted use in various applications such as thin film electroluminescent (TFEL) devices, optoelectronic or cathodoluminescent devices [88, 89]. RE doped insulators are used in telecommunication, lasers and amplifiers, medical analysis and phosphors [90, 91].

RE doped nanostructured materials can significantly increase the efficiency of Si solar cells i.e. they can address the problem of inefficient use of high energy photons. In this chapter, an overview of the luminescent materials, basics of doping, fundamental properties of host material i.e. ZnO and finally the characteristics of Ce^{3+} and Er^{3+} materials will be discussed.

2.2 SEARCH FOR A HOST MATERIAL FOR LUMINESCENT CENTRE

In the class of semiconductor metal oxides, group II-VI nanoscale semiconductors are recognized for their unique and vast potential applications in optoelectronic devices, diluted magnetic semiconductors (DMS), field effect transistors, solar cells, photoluminescence devices and so on [92-94]. In particular, ZnO has a significant advantage for above mentioned applications. As a result, doping ZnO with various elements has been a popular technique to manipulate and control ZnO's extrinsic properties for device applications [95]. Specially, RE and transition metal doped ZnO systems exhibit interesting structural, optical and magnetic properties, which do not

exist in undoped ZnO. So in this section, fundamental, crystal and luminescence properties are discussed.

2.2.1 Fundamental Properties of ZnO

ZnO is a wide band gap semiconductor (3.4 eV) having a large exciton binding energy of 60 meV at room temperature, considered to be the most promising semiconductor for many technological applications [95-98]. Many particular features of ZnO are determined by the fact that, among the elements of the sixth group, the ionization energy of oxygen is the highest, which leads to a strongest interaction between the Zn*3d* and O*2p*- orbitals [99]. Zinc oxide is a versatile material that has been used in variety of applications such as UV absorption, sunscreen lotions, antibacterial treatments [100], catalysts [101], photocatalysis [102], and as an additive in many industrial applications. ZnO nanostructures are also attractive for solar cells [103] and liquid crystal displays. The lack of a centre of symmetry in wurtzite structure combined with large electromechanical coupling results in piezoelectric and pyroelectric properties which can be used in mechanical actuators and piezoelectric sensors [104-108].

2.2.2 Crystal Structure of ZnO

ZnO crystallizes in the hexagonal wurtzite structure. The other structural forms of ZnO are cubic blende and cubic rocksalt. At ambient pressure and temperature conditions, ZnO exhibits the thermodynamically stable wurtzite structure as shown in the Fig. 2.1. At high pressures, a cubic structure is formed (NaCl lattice); cubic ZnO is an indirect gap semiconductor with a band gap width of Eg = 2.7 eV [99]. As ZnO belongs to hexagonal lattice, it belongs to the space group of P63mc or C^4_{6v} with two lattice constants “a: 0.32539 nm” and “c: 0.52098 nm” in the ratio of $\frac{c}{a} = \sqrt{\frac{8}{3}}$=1.6333. A schematic representation of wurtzite structure is shown in the Fig. 2.1.

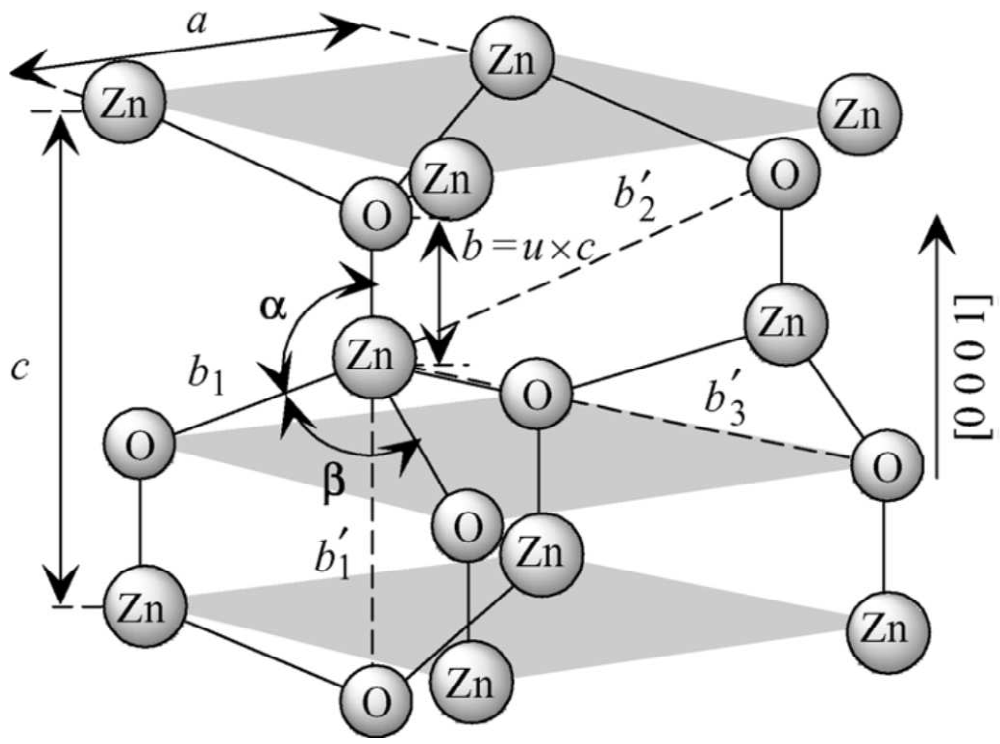

Figure 2.1: Schematic representation of a wurtzitic ZnO structure having lattice constants "a" in the basal plane and "c" in the basal direction, u parameter, which is expressed as the bond length or the nearest-neighbor distance b divided by c (0.375 in ideal crystal), a and b (109.47° in ideal crystal) bond angles. [Figure adapted from reference 109]

As ZnO crystallizes in hexagonal structure, each anion (O^{2-}) is surrounded by four cations (Zn^{2+}) at the four corners of tetrahedron. The structure is composed of two interconnecting hexagonal close packed (hcp) sub lattices of Zn^{2+} and O^{2-}, each of which consists of one type of atom displaced with respect to each other along the threefold c-axis. Another important characteristic of ZnO is polar surface and the most common polar surface is basal plane. Besides the stable polar plane [0001], two non-polar surfaces $[2\bar{1}\bar{1}0]$ and $[01\bar{1}0]$ and one polar $[000\bar{1}]$ facets exist in the structure [95].

Table 2.1: The summary of the basic physical parameters of ZnO

Physical Parameters	Values
Stable phase at 300K	Wurtzite
Lattice Parameters	a= 0.32495 nm and c= 0.52069 nm
Density	5.606 g/cm^3
Melting Point	1975°C
Refractive Index	2.008
Band Gap	3.4 eV, Direct
Electron effective mass	0.24
Hole effective mass	0.59
Static dielectric constant	8.656
Exciton binding energy	60 meV

2.2.3. Optical Properties of ZnO

The optical studies of a semiconductor are linked to its intrinsic and extrinsic features. Intrinsic optical properties are linked to the relation between electrons in the conduction band (CB) and holes in the valence band (VB), including excitonic effects due to the Coulomb interaction. Extrinsic properties are related to dopants or defects introduced in the semiconductor, which create discrete electronic states between CB and VB [95]. Optical transitions in ZnO have been studied by various experimental methods such as optical absorption, transmission, reflection, photoluminescence, cathodeluminescence, etc. Among these techniques, the PL technique has been widely employed to study the optical properties of ZnO nanostructures. Typically, room temperature PL spectrum of ZnO shows UV emission and one or two visible emissions induced by defects, including vacancies (missing atoms at regular lattice positions), interstitials (extra atoms occupying interstices in the lattice), antisites (a Zn

atom occupying an O lattice site or vice versa) and complex defects [110, 111]. At room temperature, ZnO shows a wide and direct band gap of 3.37 eV with relatively large exciton energy of 60 meV. The value of exciton energy of ZnO (60 meV) is much larger than that of GaN (25 meV) which makes efficient exciton emission at room temperature under low excitation energy. Therefore, ZnO is one of the most encouraging photonic materials in the blue-UV region [112]. For ZnO nanorods, photoluminescence spectroscopy has been employed to study the optical properties, which gives information such as band gap, defects and crystal quality [112, 113]. Room temperature PL study of ZnO nanorods shows a near-band edge (NBE) UV emission and a broader band emission linked to deep level defects. Deep level emissions (DLE) have been seen in ZnO nanorods with low impurity concentrations and there is only one emission occurring at UV emission (varies in a range from 3.236 to 3.307 eV) [114]. The UV emission ascribed to the NBE emission of the wide band gap ZnO and the DLE bands within the visible range are attributed to the defects in the ZnO nanostructure such as Oxygen vacancy (V_O), Zinc vacancy (V_{Zn}), Oxygen interstitial (O_i), Zinc interstitial (Zn_i) and extrinsic impurities [112, 114]. The relative intensity between the NBE emission and DLE emission can be used as a sign of the optical quality of the ZnO nanostructures. Therefore, the optical quality of the ZnO nanostructures can be studied by the ratio of the intensity of the near band edge emission to the intensity of the deep level emission (I_{NBE}/I_{DLE}). A large ratio of the I_{NBE}/I_{DLE} means a lower concentration of the deep level defect [114].

2.2.4 Magnetic Properties of ZnO

The magnetic semiconductors are classified on the basis of the alignment the electron spins in semiconductor host lattice. They can be divided into three categories: (a) Magnetic semiconductors (b) Diluted magnetic semiconductors (c) Non-magnetic semiconductors. Magnetic semiconductors have only periodic arrangement of magnetic elements which are aligned in periodic fashion as shown in Fig. 2.2 (a). Diluted magnetic semiconductors are alloys of magnetic element and non-magnetic semiconductors as shown in Fig. 2.2 (b). Another class is nonmagnetic semiconductor in which there is no magnetic impurity present in the semiconductor host lattice, which is shown in Fig. 2.2 (c). In order to achieve ferromagnetic semiconductors, introduce different transition and/or rare-earth atoms of impurity, such as Mn, Cr, Co,

Ni, Fe, Cu, Eu, Gd, Sm etc., into the structure of non-magnetic semiconductors known as diluted magnetic semiconductors (Fig. 2.2 (b)).

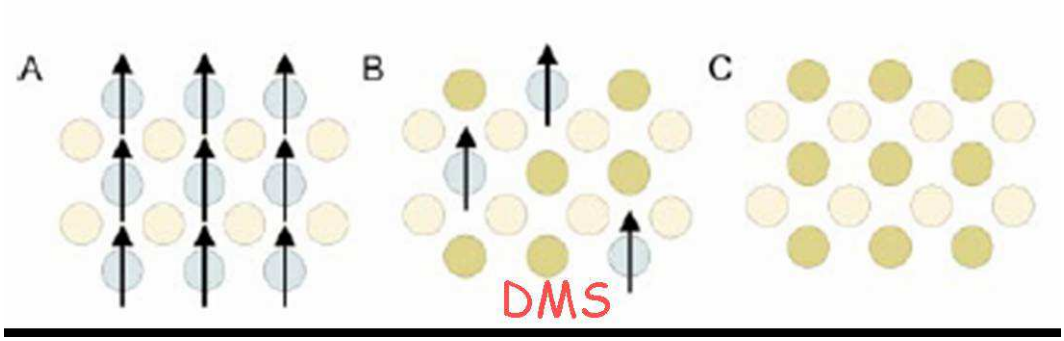

Figure 2.2: Three types of semiconductor: (a) a magnetic semiconductor, in which a periodic arrangement is present; (b) a dilute magnetic semiconductor and magnetic element; (c) a nonmagnetic semiconductor, which has no magnetic ions. [Figure adapted from reference 115]

The procedure of purposely introducing impurities into an intrinsic semiconductor in order to change its physical properties is called doping. Many reports were published on DMS in bulk form [116-122]. The attempts to dope semiconductor nanocrystals have also been reported [123, 124]. There is rapidly rising interest in considering the fundamental physical properties of nanoscale DMS in the forms of quantum dots, wires and wells for spin-based electronics applications [121-123, 125]. These materials are created through the doping of transition metal ions, such as Co, Fe, Mn and Cr or rare earth ions into semiconductor. Both the ions have moderately filled *d* and *f* shells, respectively, which give rise to unpaired electrons. The 3*d* band of the Mn^{2+} ion is accurately half-filled with an energy gap between the up-spin (↑) occupied states and empty down-spin (↓) states. In other transition metals such as Co, Co and Ni, one of the bands is partially filled (down or up). In general, 3d transition-metal ions substitute for the cations of the host semiconductors. In case of ZnO, the particular transition-metal element, for example Mn, imparts its $4s^2$ electrons to the s-p^3 bonding and substitutionally replaces the Zn in the tetrahedral bonding to form a Mn^{2+} charge state. The transition metal's d bands hybridize with host valence bands (O-p bands in ZnO) to figure the tetrahedral bonding. This hybridization ascends to exchange interaction between the localized carriers in the host valence band and 3*d* spins and thus induces local magnetic

moment in the sample. The magnetic behaviour of these materials depends on the amount of the transition metal ions in crystal, the carrier density and the crystal quality.

The inspiration for studying semiconducting oxides, mainly ZnO, for spintronics had been stimulated by the work of Dietl et al [126]. The projected mean field theory predicts that common diamagnetic semiconductors would exhibit high Curie temperature if doped with 5 atomic % Mn and a hole concentration 3.5 x 10^{20} cm^{-3}. Simulations indicate Curie temperature above 300 K in case of ZnO and GaN [126]. The mean field Zener model predicated by Dietl is based on an indirect exchange mechanism, where the ferromagnetism between magnetic dopants is mediated by holes in the valence band [126].

The carrier's role is an essential part of the model as it indicates that the magnetic property is tuned by modifying the carrier density in the materials. Initially, p-type material was predicted as good candidate for high Curie temperature because the exchange integral parameter and the density of states are higher in the valence band than the conduction band. Due to the difficulties in formation of p- type ZnO, the theory of Dietl is not applicable to ZnO.

Coey et al. [127] introduced a model that indicates the influence of defect states on ferromagnetic properties of DMS. According to them, donor defects (oxygen vacancies or zinc interstials in case of ZnO) overlap at huge dopant concentration and form an impurity band. The impurity band can interact with local magnetic moment via formation of bound magnetic polaron (BMP). Within each BMP, the bound carrier interacts with the magnetic dopants inside its radius and can align the spins of the magnetic dopants parallel to one another. Ferromagnetism is achieved when the BMPs overlap to form a continuous chain throughout the material, thus percolating ferromagnetism in the DMS.

DMS nanocrystals is a special class of system which integrates quantum confinement effect and magnetic properties occurring because of the DMS nature of the system. Direct exchange of cations or anions of host material by dopant ions in nanocrystals includes some artificial challenges [128-131]. A major barrier is to accomplish the nanocrystals with dopant ions incorporated homogeneously within the lattice of host material. The high surface area to volume proportion in nanocrystals have initiated to improve impurity segregation to the nanocrystals surface through a "self annealing" process in the core. Hence dopants are likely to stay on the surface

giving trap levels. However, synthesis method to obtain doped nanocrystals plays a significant role. There are various reports, which recommend successful incorporation of dopant in host materials [125, 128, 129].

The basic method for introducing magnetism into ZnO is confined to doping a tiny quantity of transition or RE atoms. However, there are various controversies about substitutional inclusion of transition or RE ions in host material and derivation of magnetism in transition or RE doped ZnO. The transition metals are inherently magnetic and their precipitates or secondary magnetic phases in the host semiconductor can be the primary reason for the observed ferromagnetism. If DMS is studied systematically by associating all its properties, the disagreement over the presence of magnetic precipitates can be sorted out.

A great excitement has been generated in the observation of room temperature ferromagnetism in metal oxide nanocrystals. Comparing with the corresponding bulk material, the surface-to-volume ratio is high in nanocrystals, and therefore the surface effects are pronounced with decreasing nanocrystals size. The impact of uncompensated surface spins on the saturation magnetization plays a vital role in the magnetic properties. Different metal oxides such as ZnO, Al_2O_3, and HfO_2 that are diamagnetic in their bulk structure show ferromagnetic ordering in nanocrystalline regime [132]. The origin of ferromagnetism in these materials can be attributed exchange interactions between localized electron spin moment from the oxygen vacancies at the surfaces of the nanocrystals [132]. The occurrence of room temperature ferromagnetic ordering is also detected in chemically grown ZnO nanocrystals capped by different capping agents. Modification of surface charge states via attached ligand can encourage spin polarization [133-135]. This work shows that the magnetic properties of nanocrystals are not only associated with the presence of magnetic ions but is also firmly determined by existence of surface defects [132-137].

2.2.5 Applications of ZnO

Arnold et al. [138] have prepared field effect transistors (FET) using individual nanobelts. Large packets of ZnO nanobelts were dispersed in ethanol by ultrasonication until most of the individual nanobelts were isolated. These ethanol dispersions were dried onto a SiO_2/Si substrate for imaging by non-contact mode atomic force microscopy (AFM). ZnO field effect transistors were fabricated by depositing ZnO nanobelt dispersions onto SiO_2/Si(p^+) substrates. This was followed by treatment in an oxygen atmosphere at 800°C for 2 hours. The SiO_2/Si substrates were then spin coated with PMMA, baked, exposed to electron-beam lithography for the definition of electrode arrays and developed. A 30 nm thick layer of titanium was deposited by electron-beam evaporation to serve as the source and drain electrodes and the remaining PMMA was lifted off in hot acetone. The concept of this device is that controlling the gate voltage would control the current flowing from the source to the drain.

Nano-dimensional ZnO structures, such as nanorods, nanowires and nanobelts, have been identified as favourable candidates for gas sensing [139, 140]. Zinc oxide nanostructures have been widely used as a gas sensing layer in conductometric [141] and FET [142] based gas sensors. In recent years, some work has been reported on electrical and gas sensing studies of Schottky diodes based on nanostructured ZnO [143]. In one of these studies, electrical characterization of an individual single crystalline ZnO nanobelt, which was kept between two palladium contacts was performed in air and NH_3 (1% and 3%) balanced in ambient air at room temperature. The current-voltage (I-V) curves of this device indicated rectifying nature in both ambient air and NH_3. Upon exposure to NH_3 gas, a voltage shift in the I-V curves was seen in both forward and reverse bias operations. Zhang et al. [144] also observed rectifying behaviour in the I-V characteristics of Schottky diode based on a single ZnO nanorods lined up across paired Ag contacts. The device was investigated for NH_3 gas (50 and 1000 ppm) at room temperature and showed an increase in the forward and reverse currents, indicating a high sensitivity to NH_3 gas. Another study of gas sensing performance of ZnO nanostructured Schottky diodes was reported by Yu et al. [145]. They presented the preparation of a ZnO nanorod Schottky diode and investigated it for hydrogen gas over a temperature range of 280°C to 430°C. The sensor showed larger lateral voltage shift in the I-V plot upon exposure to hydrogen under reverse bias condition as compared to the forward bias. They exhibited that

upon exposure to hydrogen, the effective change in free carrier concentration at the ZnO nanorod interface was magnified by an enhancement factor, effectively lowering the reverse barrier, producing a large voltage shift. Hydrogen gas sensing performance of ZnO single nanowire Schottky diodes were also investigated by Das et al. [146]. The sensor revealed good sensing characteristics (sensitivity ≈ 90%) at room temperature with response time of approximately 55 seconds.

Dye-sensitized solar cells (DSSCs) are encouraging devices for low-cost solar energy conversion and are rigorously studied nowadays. ZnO is obviously one of the best prospects among semiconductors for DSSC applications as it can be prepared comfortably and economically in number of shapes and sizes by different methods and is eco-friendly and stable [109]. A typical DSSC structure is mainly composed of four parts: (1) a photoanode - a thick film (~10 μm) of a wide band gap semiconductor, such as ZnO or TiO_2 nanoparticles, (2) a dye sensitizer - a monolayer of dye molecules adsorbed on the semiconductor nanostructures, (3) an electrolyte - a redox couple (traditionally I^-/I_3^-) that percolates in between the dye-coated nanostructure, serving as charge carrier and (4) a counter electrode–metal coated transparent conducting oxide glass plate [147]. The semiconductor nanoparticles bring in the electrons from photo-excited dye molecules and move them to the collecting anode. In the mean time, the oxidized dyes are reduced by redox species that convey electrons from the counter electrode [148]. So far, various ZnO nanostructures have been widely studied for DSSCs. ZnO arrays of one dimensional (1D) nanostructures, such as nanowires and nanotubes have been extensively used to significantly improve the electron transport velocity within the photoanode by giving a direct conduction pathway for the rapid collection of photogenerated electrons [149]. However, the insufficient internal surface area of these 1D nanostructure arrays limits the power conversion efficiency at a relatively low level, for example, only 1.5% for ZnO nanowires [150] and 1.6% for nanotubes [151]. In addition, 2D and 3D ZnO nanostructures have also been studied for DSSC applications due to their large specific surface area. Xu et al. [149] have shown DSSC based on hierarchical ZnO nanowire-nanosheet architectures, which show a power conversion efficiency of 4.8%. Wu et al. [152] have designed a 3D ZnO nanodendrite/nanoparticle composite DSSC with an efficiency of 3.74%. Irene et al. [153] have reported the highest efficiency up to date is 7.2% achieved with a porous single crystal.

ZnO nanoparticles exhibit high luminescent properties. Daniele et al. [154] prepared ZnO nanoparticles by co-precipitation method using different amounts of aminopropyltriethoxy silane (APTS). They produced LED devices based on the organo-modified ZnO nanoparticles with the photoemission and find their higher luminescent properties. In another study, Liu et al. [155] reported a photodetector based on flexible nanoparticle-assembled ZnO cloth, which was prepared via a carbon cloth templated hydrothermal method. Under UV irradiation, the conductance of the device increased more than 600 times having response and decay time to be around 3.2 seconds and 2.8 seconds, respectively.

The ZnO nanoparticles were suggested by Bagabas et al. [156] for environmental applications. They follow room temperature wet chemical route based on cyclohexylamine for synthesizing ZnO nanoparticles in aqueous and enthanolic media and also investigated the photodegradation of cyanide ions. They concluded that the morphology was crucial in enhancing the cyanide ion photocatalytic degradation efficiency. Also ZnO nanoparticles were produced by calcination of precursor by the precipitation method with grafting polystyrene onto the surface of ZnO nanoparticles to enhance the dispersion of the particles. They reported that ZnO nanoparticles possess high photocatalytic activity [157].

The nanoparticles with luminescent and magnetic properties show applications both in vitro and in vivo as detection probes and drug carriers etc. Due to their good biocompatibility [158] and low cost, these nanoparticles have shown promising potential in bioimaging and drug delivery [159]. Recently, Matsuyama et al. [160] suggested the biological applications of ZnO nanoparticles by the use of silica-coated ZnO-nanoparticle quantum dots (QDs) with biotin as fluorescent probe in cell-labeling applications and have suggested the selective destruction of tumor cell applications [161]. Also, ZnO nanoparticles have been proved as a promising candidate for the realization of dye sensitized solar cells [162] and are employed for sunscreens lotion as UV blockers [163]. Sun et al. [164] suggested a flexible nanogenerator made of ZnO nanoparticles which may bring out some important and interesting applications in energy harvesting.

2.3 FUNDAMENTALS OF DOPING

The doping is the best utilized way of moderating the properties of semiconductor. Doping can also be stated as “controlled impurity” if addition to the material is done in a homogeneous way. If major amounts of dopants are added to the material, either a mixed oxide phase or a second phase may form which is based upon the solubility limit of the two components. The dependence of doping levels/limit and doping efficiency is basically on the ionic size and the electro-negativity may be on growth process too. Doping is used as a modification method for altering phase structure, electronic structure and surface structure [165]. Dopants may be used either as substitutional or interstitial. Dopants are initiated in a semiconductor by method of defects or impurities. Defects may enact as a donors or acceptors. The general defects that could be witnessed include vacancies, interstitials, dislocations and anitisites. The free carrier creation needs not only the existence of impurities, but also that the impurities emit electrons to the conduction band in which case they are called *donors* or that they may emit holes to the valence band in which case they are called *acceptors.*

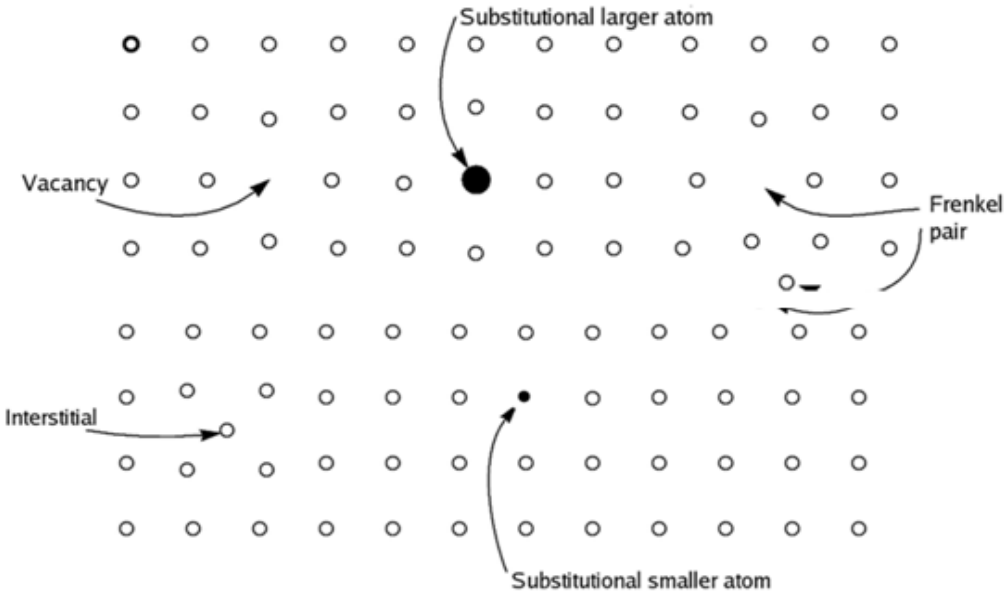

Figure 2.3: Schematic representation of possibilities of dopants in lattice sites. [Figure adapted from reference 166]

Intrinsic doping

Intrinsic doping is present due to defects in the crystal lattice, away from stoichiometry. This leads to the oxygen deficiency and thus to oxygen vacancies in those materials. These oxygen vacancies give rise to shallow donor states just below the conduction band and act as an n-type impurity band [167].

Extrinsic doping

The incorporation of extrinsic defects (cations or anions doping) into the host lattice leads to the formation of donors and acceptors when their valency is higher and lower than that of host lattice ions. Several approaches for ZnO modification have been proposed: metal-ion implanted ZnO (e.g. Al, In, Cu, Fe, Ga, Mn, Co, Cr, Ni), reduced ZnO photocatalysts, non-metal doped- ZnO (e.g. N, B, F), composites of ZnO with semiconductor having lower band gap energy (e.g. CdS, SnO_2), sensitizing of ZnO with dyes (e.g. Reactive Orange 29 (RO29)) and ZnO doped with upconversion luminescence agent [168].

2.4 DOPING AND GROWTH MECHANISM

The choice of host materials is of great importance in designing a rare earth ion based luminescence for efficient energy applications. Generally, luminescent materials require a host matrix with high crystalline structure. The characteristic luminescence properties can be achieved by doping the host matrix with relatively a small loading of rare earth ions. It is rather difficult to incorporate RE ions into the lattice of semiconductors that efficiently via chemical method as RE ion has large radius and there is a noticeable difference between their charges and chemical properties.

In this frame work, Reza Zamiri et al. [169] reported a work based on doping effect of RE ions on morphology on ZnO nanostructures prepared via chemical method. Interestingly, different kinds of growth mechanism have been proposed and these mechanisms lead to different morphological evolution of nanostructure as nanorods and nanorods-like to nanoplates-like. According to them, doping of ZnO with Er and Yb remarkably changed the morphology of the nanostructures from nanorod-like to nanoplate-like. These morphological changes cannot be attributed to variation in the precipitating conditions, as they were kept constant to avoid any influence on the nucleation and crystal growth processes and on the morphology of precipitated crystals. Therefore, the observed changes can only be attributed to the

effects of dopants, which might act as structure driving agents through selectively adsorbing onto ZnO crystalline planes.

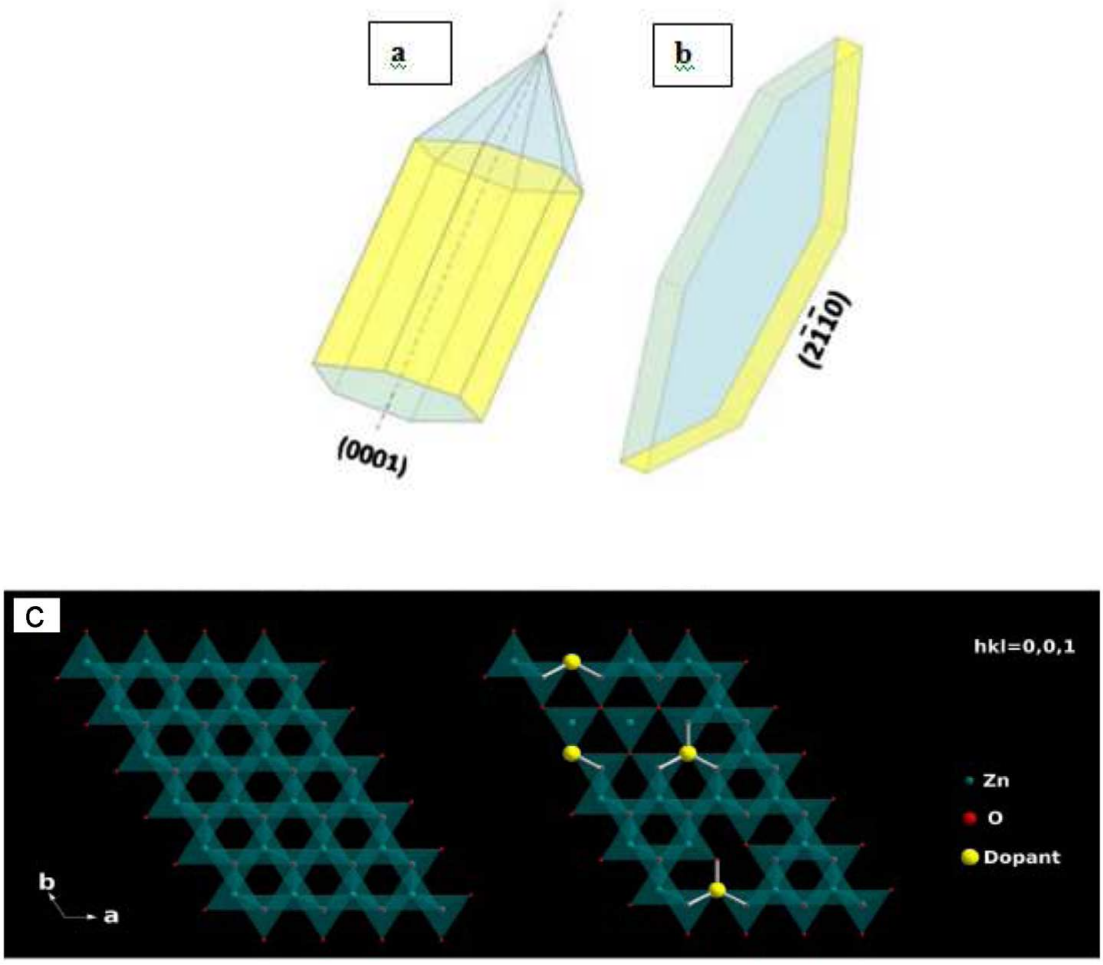

Figure 2.4: Schematic representation of (a) growth of ZnO crystal in c-axis direction (0001), (b) after doping change in morphology from nanorods-like to nanoplates-like in (2110) direction, and (c) crystal disturbance and growth in lateral directions after doping. [Figure and concepts adapted from reference 169]

According to several literature reports, ZnO has structurally three types of crystalline planes, two non-polar (2110) and (0110) planes and a polar (0001) basal plane with C_{6V} symmetry. The (0001) plane has higher surface energy and therefore the growth of crystal in c-axis direction is faster which leads to the formation of nanorods shape crystals as it is indicated in Fig. 2.4 (a). However, doping of RE ions in ZnO revealed a drastic change from nanorod-like to nanoplate-like (Fig. 2.4 (b)).

Here, the (0001) surfaces of ZnO with tetrahedral structure usually expose terminal OH^- ligands to the solution [170, 171]. The presence of the three valence ions instead of Zn^{2+} ions in the ZnO crystal is likely to enhance the adsorption of OH^- ligands onto these basal surfaces. These ligands will prevent further extensive deposition of Zn species at that surfaces leading to a decreased growth rate of ZnO nanocrystallites along the c-axis direction. This means that the crystal growth along the (0001) direction is significantly suppressed under this condition, where as the nanocrystallites can still grow sideways along the (2110) directions. Schematic of crystal structure disturbance of ZnO lattice with doping has been shown in Fig. 2.4 (c) which shows crystal growth oriented along lateral directions. The drastic morphological changes observed for the RE ions doped ZnO samples can therefore be regarded as a proof of the incorporation of these elements in the ZnO lattice.

2.5 CHOICE OF LUMINESCENT DOPANTS

ZnO was frequently doped with group III, IV, V and VI elements. Due to its potential optoelectronic and spintronic applications, nowdays the RE (e.g. Eu, Tb, Er, Tm) doped ZnO is an interesting field of study [172-175]. Part of this interest lies in the shielded 4*f* levels of RE^{3+}, which can make various well-defined narrow optical transitions happen between the spin orbit levels split under the different manifolds weak crystal field.

2.5.1 History of Rare Earth Elements

The RE elements are classified as a group of chemical elements created from scandium, yttrium and the lanthanides. According to the periodic table, the lanthanides are a group of 15 chemically similar elements with atomic numbers 57 through 71, inclusive. Even though not a lanthanide, yttrium (atomic number 39), is counted in the RE group because it frequently occurs with them in nature, having similar chemical properties. Scandium (atomic number 21), is also taken in this group, although it typically occurs in RE ores only in slight quantities because of its smaller atomic and ionic size [176].

RE elements are obtained from the rare earths ores as bastnasite, monazite, xenotime and ion-adsorption clay. Bastnasite is the world's primary source of RE and is found in China and the United States. Considerable amount of RE are also

recuperated from the mineral monazite. From xenotime and ion-adsorption clays, a much smaller part of the total production is obtained but these are important sources of yttrium and other heavy atomic number of RE elements.

The detection of the RE elements swings around two basic facts. In 1794, the Swedish mineralogist F. Cronsted found a new mineral from which, J. J. Berzelius and W. Hisinger segregated a new oxide which was known as "ceric earth" (in Latin *Ceres* = the creator). In the meantime, the Finn chemist J. Gadolin, found a new mineral extracted from a quarry close to Ytterby town in Sweden, acquired and nominated it as “yttrica earth”. In the coming years, it has been found that in reality, the stated oxides were a mixture of quite a few elements progressively segregated and identified. The history of the classification of the lanthanide elements finished in 1907 with the finding of Lutetium [177]. Between 1839 and 1848, the Swedish chemist Carl Gustav Mosander (1797-1858) found a variety of lanthanides from ytterite.

Later on, German chemist Martin Heinrich Klaproth (1743-1817) and Swedish chemist Wilhelm Hisinger (1766-1852) studied the material discovered by Crönstedt, and both concluded that this had to be a new element. It was named **Cerium** (**Ce**) in honor of Ceres, an asteroid between Mars and Jupiter. Only in 1875, was cerium actually extracted from an ore. A pure **Erbium** (**Er**) oxide, following Mosander discovery in 1843, was prepared in 1905 by French chemist Georges Urbain (1872-1938) and American chemist Charles James (1880-1928), but the pure metal form was only found in 1934.

Lanthanides are characterized by the progressive filling of the 4*f* orbitals with an electronic configuration [Xe]$4f^n5d^n6s^n$ [178, 179]. The oxidation states are included between 2^+(Yb) and 4^+(Sm and Eu), but 3^+ is by far the most common. Some general properties of the rare earth elements are shown in Table 2.2. [180]

Table 2.2: Electronic structure and selected physico-chemical properties of the RE elements

Element	**Symbol**	**Atomic No.**	**Configuration Ln^{3+}**	**Ground state Ln^{3+}**	**Density (ρ) gm/cm^3**	**Melting Point (K)**	**Boiling Point (K)**
Lanthanum	La	57	[Xe]	$^1S_0$	6.146	1193	3743
Cerium	**Ce**	**58**	**[Xe]$4f^1$**	**$^2F_{5/2}$**	**6.689**	**1068**	**3633**
Praseodymium	Pr	59	[Xe] $4f^2$	$^3H_4$	6.640	1208	3563
Neodymium	Nd	60	[Xe] $4f^3$	$^4I_{9/2}$	6.800	1297	3373
Promethium	Pm	61	[Xe] $4f^4$	$^5I_4$	7.264	1373	3273
Samarium	Sm	62	[Xe] $4f^5$	$^6H_{5/2}$	7.353	1345	2076
Europium	Eu	63	[Xe] $4f^6$	$^7F_0$	5.244	1099	1800
Gadolinium	Gd	64	[Xe] $4f^7$	$^8S_{7/2}$	7.901	1585	3523
Terbium	Tb	65	[Xe] $4f^8$	$^7F_6$	8.219	1629	3503
Dysprosium	Dy	66	[Xe] $4f^9$	$^6H_{15/2}$	8.551	1680	2840
Holmium	Ho	67	[Xe] $4f^{10}$	$^5I_8$	8.795	1734	2993
Erbium	**Er**	**68**	**[Xe] $4f^{11}$**	**$^4I_{15/2}$**	**9.066**	**1770**	**3141**
Thulium	Tm	69	[Xe] $4f^{12}$	$^3H_6$	9.321	1818	2223
Ytterbium	Yb	70	[Xe] $4f^{13}$	$^2F_{7/2}$	6.570	1097	1469
Lutetium	Lu	71	[Xe] $4f^{14}$	$^1S_0$	9.841	1925	3675

2.5.2 Rare Earth Ions as Active Luminescent Centres

RE ions – jewels for functional materials of the future [181] are rigorously examined concerning their optical and exclusive spectroscopic properties due to their electronic configurations.

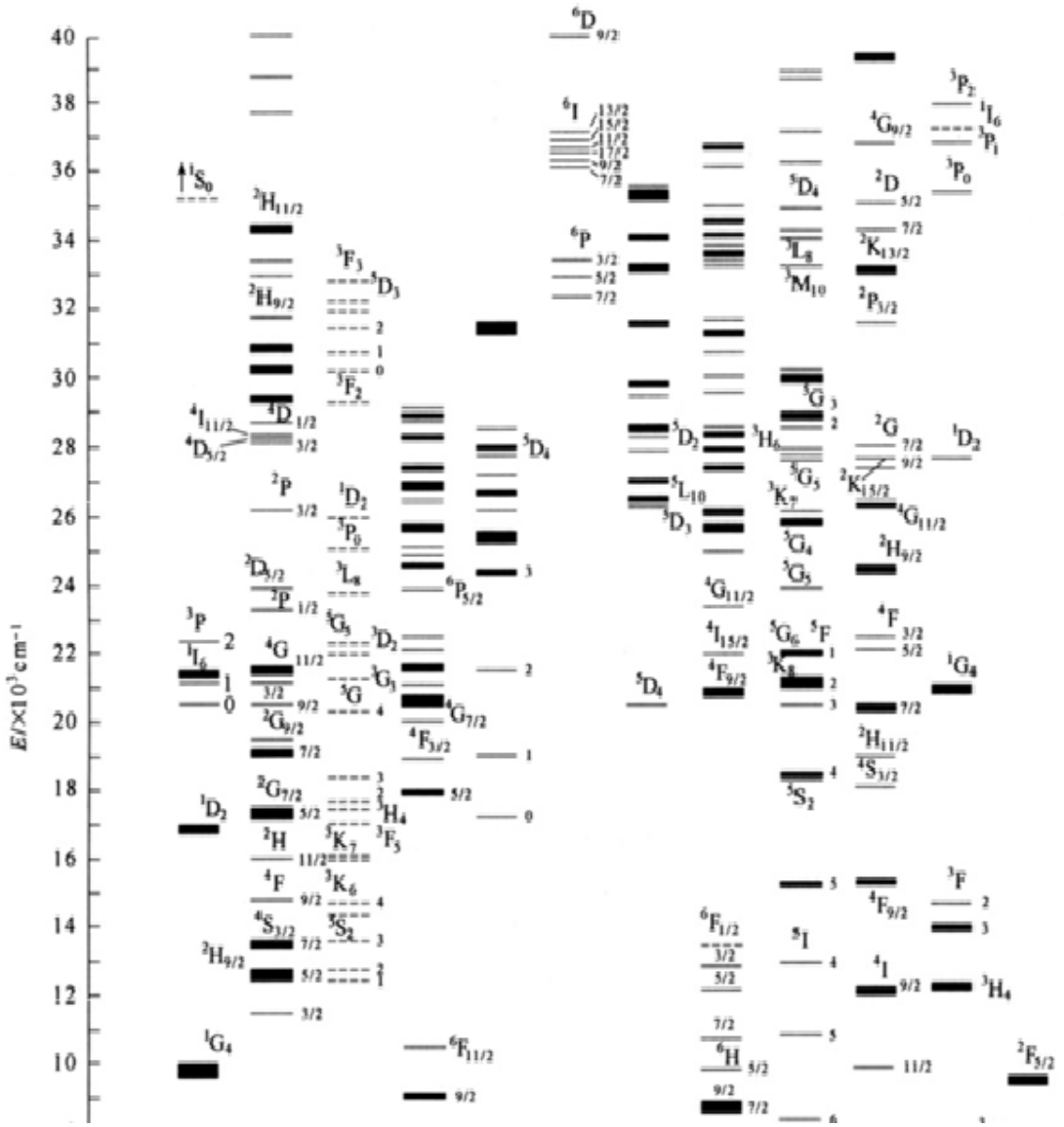

Figure 2.5: Energy level structure (Dieke diagram) of rare earth ions. [Figure adapted from reference 182]

RE ions are used in wide range of applications such as lighting, displays, lasers and fibre amplifiers and bio-medical applications including imaging and labelling [183-185].The lanthanide ions are a group of elements that are listed at the bottom of the periodic table after lanthanum. They are isotopically stable and the outer electronic configurations of trivalent ions with dominant oxidation state of RE^{3+} having a general form of [Xe] $5s^2 5p^6 4f^n$ with n refers to the number of 4*f* electrons.

The partially filled 4*f* electrons are responsible for the characteristic optical transition properties for Ln^{3+}. The group of elements from cerium (58) to ytterbium (70) are often denoted as rare earth ions.

The partially filled 4*f* orbitals have different energies exhibiting rich energy level structure and wavelengths covering from ultraviolet, visible to infra-red part of the spectrum. The rich energy level structure makes lanthanide ion as perfect "photon managers" that can be used to efficiently convert the radiation into photons of any desired wavelength [91, 186]. The vast difference between the transition metal ion and the lanthanide ions lies in the nature of 4*f* orbitals. The characteristic energy level structure of rare earth ions is illustrated in the Fig. 2.5, which is also called as Dieke Diagram [182]. Since the 4*f* electrons are shielded by the completely filled outer $5s^2$ and $5p^6$ electrons, they are only weakly affected from the ions in the surrounding medium in the host matrix. Due to this shielding, all the trivalent ions result in very narrow sharp optical absorption and emission bands which are relatively independent of the host matrix. The transition between the parity forbidden 4*f*-4*f* states (no change in the dipole moment) and the shielding by outer electrons, minimizes the interactions between the doped ions and the host matrix and thus the excited states have relatively longer lifetimes; up to milliseconds.

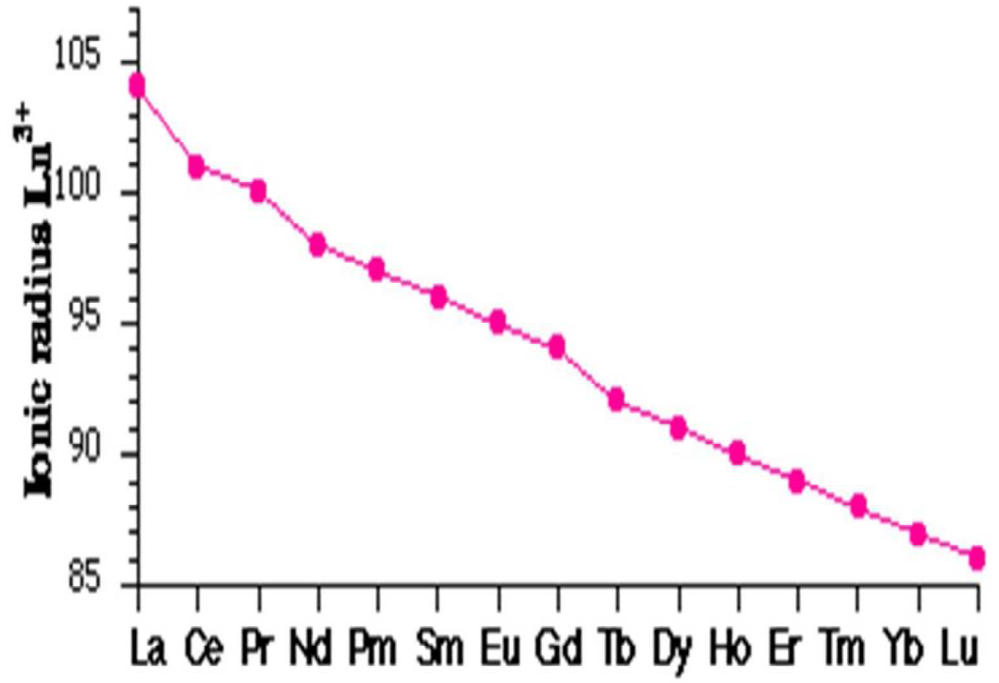

Figure 2.6: Ionic Radii of the trivalent lanthanide ions. [Figure adapted from reference 182]

The poor shielding of the 4*f* electrons provides a progressive increment of the effective nuclear charge resulting in a smaller atomic radius. This trend is therefore so called lanthanide contraction [179]. The ionic radii of the lanthanides decrease from 103 pm (La^{3+}) to 86 pm (Lu^{3+}) in the lanthanide series [187].

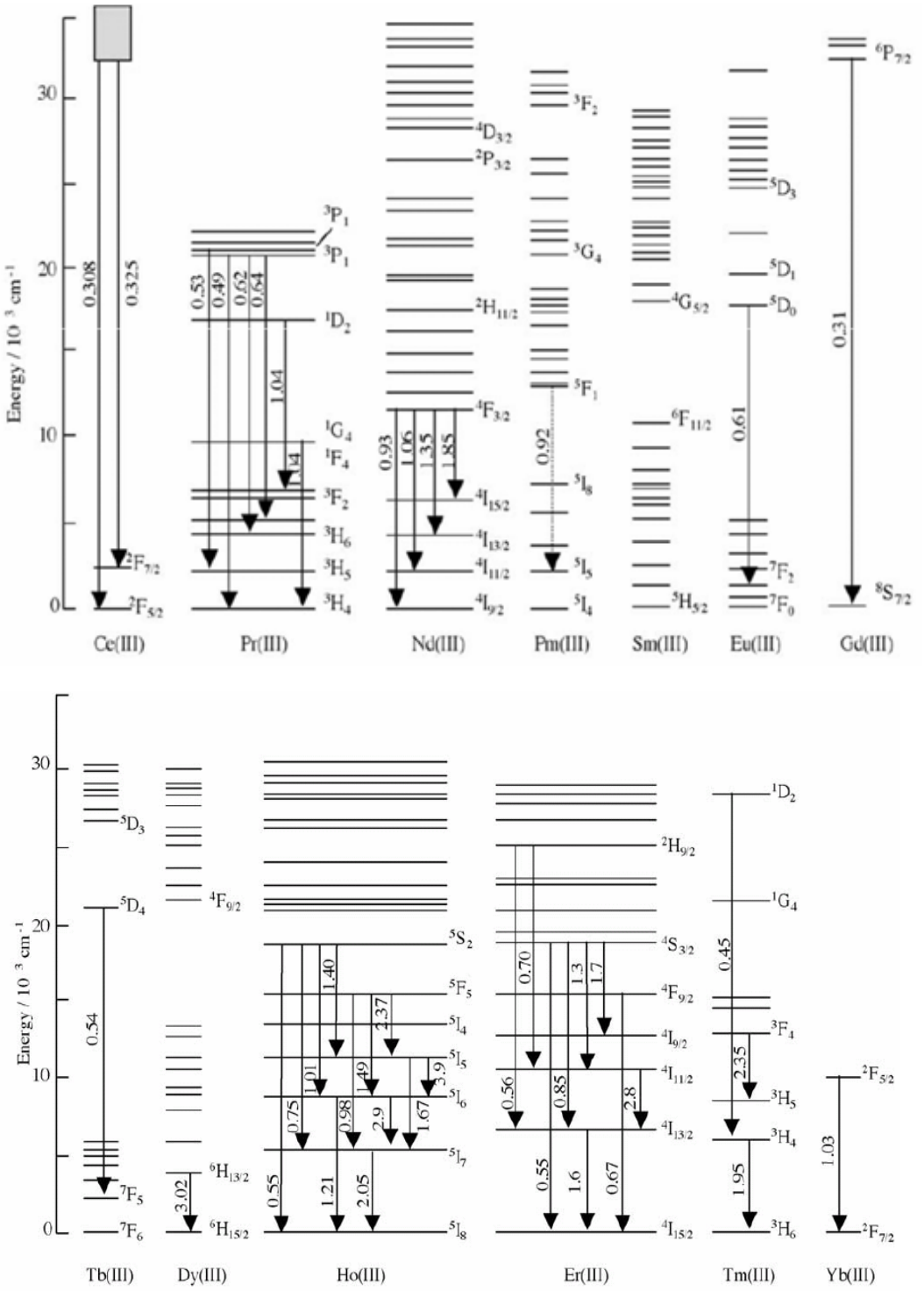

Figure 2.7: Electronic states (Dieke diagram) for Ln(III) ions. Solid black arrows indicate radiative transitions. [Figure adapted from reference 183]

From the classical approximation, the Russel-Saunders (RS) coupling allows the representation of the electronic states (Dieke diagram) denoted as $^{2S+1}L_j$ where (L) the orbital angular momentum, (s) the spin angular momentum and (j) total angular quantum momentum, respectively. S and j are represented with numbers 0, ½, 1, 3/2 etc. L represents orbitals S, P, D, F… when L is equal to 0, 1, 2, 3, 4… respectively [188, 189].

2.5.3 Characteristics of Cerium (Ce^{3+})

Recently, much interest has been paid to Lanthanide ion doped ZnO for potential applications in visible emitting phosphors in displays, high power lasers, and other optoelectronic devices [173, 190, 191]. Herein, we have chosen cerium (Ce) as a suitable dopant for ZnO matrix.

However, Ce^{3+} is different because there is only one electron in the first shell of the 4*f* orbital ($4f^1$ electronic configuration) and its luminescence transition (4*f*–5*d*) can occupy only low symmetry sites in the matrix i.e. ZnO and appears as distinct bands in the excitation spectra. Consequently, electrons are excited and emitted from the high-energy 5*d*–orbitals. The relative energy of the 5*d* orbitals is highly dependent on the host lattice [192].

Since CeO_2 has a band gap of~ 3 eV and shows interesting optical properties such as optical transparency and strong UV absorption that are similar to that of ZnO, the mixed CeO_2-ZnO have been investigated for searching highly efficient catalysts or UV filters [193-196]. Ce doped ZnO nanostructures have been designed and studied for degradation of dyes [197], cyclohexanol conversion [194], detoxification of cyanide [198], infrared emissivity [199], photoluminescence [200], oxidative and steam reforming of methanol to produce hydrogen [201].

2.5.4 Characteristics of Erbium (Er^{3+})

Er is a rare earth element and in its trivalent state (Er^{3+}, $4f^{11}$) doped into semiconductors and is widely used because of its intra-shell transitions allowing it to be used as structural probes [202]. The direct Er^{3+} ion excitation can be a difficult process to achieve due to the forbidden non-effective intra 4*f* transitions of rare earth ions and the emission quenching from $4I_{13/2}$ level by phonon assisted molecule collisions [203].

Er-doped semiconductor materials such as GaN, GaAs, and Si have been of interest for the optical applications ranging from visible to infrared (IR) region [174, 204, 205]. To improve 1.54 mm IR emission properties, it is known that oxygen co-doped and wide-band gap semiconductors are more effective [206, 207]. For this purpose, ZnO is proposed to be a host semiconductor for erbium, not only because of its wide band gap (~3.3 eV), which is applicable to the excitation of erbium, but also because of its high electrical conductivity that are essential for the realization of current injection optoelectronic devices [208]. Er-doped ZnO films have been known to be reliable materials for laser diodes, light-emitting diodes, photo-induced piezo-optics and nonlinear optics [209].

CHAPTER III

LITERATURE REVIEW AND EXPERIMENTAL DETAILS

3.1 BRIEF REVIEW

ZnO is no stranger to scientific study. It has featured as subject of extensive research back as early as 1935. Alteration of ZnO properties by impurity/dopant inclusion has become a hot topic. Doping of RE ions in ZnO will make scientists tailor its optical, electrical and magnetic properties through altering its electronic structure. This results in enhancement in different applications like optoelectronic, electronic, spintronic, photocatalytic, antibacterial and other applications due to its direct wide band gap energy, high electron mobility, strong room-temperature luminescence and controversial room-temperature ferromagnetic behaviour in different forms like single crystals, thin films, powders and nanostructure. Much of the research interest is focused on the development of nanomaterials based on wide band gap semiconductors doped with the trivalent lanthanide ions as they constitute unique applications in optoelectronic and light emitting devices, plasma display panels, photovoltaic and so on [210].

3.1.1 Review of the Study of Cerium (Ce) Doped ZnO Nanomaterials

G.-R. Li et al. [32], in 2008, reported the synthesis of Ce^{4+}-doped different ZnO nanostructures i.e. nanotubes, nanorods and nanocages via electrochemical deposition. In this report, the results of XRD, EDS, XPS, HRTEM, and SAED revealed that the prepared Ce^{4+}-doped ZnO deposits are composed of single crystal structures with preferential growth in the (0001) direction. The PL spectra showed that the Ce^{4+}-doped ZnO has high optical property and is an exciting PL material that illustrates multiemission peaks at blue-green region. Furthermore, the direct electrochemical method represents a significant improvement for the synthesis of adulterated ZnO samples because it allows superior control over the nanostructures and may therefore give a better experimental basis for understanding and finally controlling the optoelectronic properties of this class of materials. J. Yang et al. [33], in 2008,

prepared ZnO and Ce-doped ZnO nanorods through sol–gel method. The X-Ray diffraction results showed that when Ce was doped into ZnO nanorods, no diffraction peaks of Ce or cerium oxide were observed in the pattern. The PL spectra of Ce-doped ZnO showed a strong UV emission band located at 377 nm and a weak visible emission. More electrons could be contributed by cerium dopants so that the radiative recombination of these excess excitons will lead to a blue shift and broadening of UV emission peak. Raman peaks proved that Ce-doped nanorods maintain their high crystal quality. The simplistic, reproducible and useful route presented here provides a useful method for the RE^{3+}-doped ZnO system. J. Lang et al. [35], in 2010, synthesized Ce-doped ZnO nanorods through the hydrothermal method. XRD and XPS results exhibited that Ce ions were successfully incorporated into the lattice position of Zn ions in ZnO. TEM images illustrated that the average diameter of Ce-doped ZnO nanorods was 8 nm. PL measurements revealed that both the undoped and Ce-doped ZnO nanorods had an UV emission and a defect emission and the Ce ions doping induced a red shift in the UV emission and a small enhancement in the defect emission. The slight shift in A_{1L} and E_{1L} in Raman spectra increasing with the Ce ions doping also indicated that the Ce doping changed the free carrier concentration in the ZnO nanorods. A. George et al. [37] reported, in 2011, the refluxing synthesis of ZnO and Ce doped ZnO nanocrystals with spherical morphology. Spherical morphology is designated to the crucial role played by ethylene glycol during synthesis. XRD analysis showed highly crystalline phase of synthesized nanopowders and no additional signatures were observed. With the increase in Ce concentration, the variation in lattice parameters is negligible. Williamson–Hall plot provide crucial values for crystallite size and is approximated at~ 15 nm. The value is in good agreement with the TEM results i.e. 20 nm. For pristine samples, PL is broad in nature with maxima at various positions in visible region of electromagnetic spectrum. For Ce doped ZnO samples, the emission intensity decreases and is anticipated to be due to formation of additional surface defects. The higher wavelength bands are assigned to either emission from Ce lowest band (Eg) or to the formation of some new type of defects during synthesis. N.F. Djaja et al. [34], in 2012, reported the preparation of a series of Ce-doped ZnO nanoparticles by co-precipitation method. The structural, optical and photocatalytic activation of Ce-doped ZnO nanoparticles, as a function of doping concentration were investigated. The nanoparticles showed X-ray diffraction pattern that harmonized with ZnO in its

wurtzite structure. It was also found that the average grain size was in the between range of 13-16 nm. UV-Vis measurements showed that there was a red shift in the photophysical response of ZnO after doping. This was exhibited in reflection spectra in the visible region in the range 300-800 nm i.e. there was a significant reduction in the band gap. It has also been found from electron spin resonance (ESR) measurements that defects, which are likely to be oxygen vacancy and an electron trapped at cerium site, were formed in these Ce-doped ZnO nanoparticles. The photocatalytic activities of Ce-doped ZnO were studied by irradiating the nanoparticles solution with ultraviolet light by taking methyl orange as organic dye. It revealed that the photo- degradation increased as doping concentrations increased at first and then decreased when the doping concentration exceeded 9 at%. It is proposed that the photocatalytic activity is strongly dependent on the formation of oxygen vacancy and an electron trapped at cerium site. Y.-I. Jung et al. [36] in 2012 prepared Ce-doped ZnO nanorods on Si substrates through the hydrothermal method. The structural properties examined by FE-SEM, EDS and XRD confirmed that the Ce^{3+} ions are effectively included into the ZnO lattice sites. The growth of ZnO nanorods was not affected by the doping of Ce atoms and unwanted Ce-related compounds or precipitates were not formed during the growth of Ce-doped ZnO nanorods. The PL results demonstrated that the Ce^{3+}doped ions in the ZnO nanorods act as a proficient luminescence centre at 540 nm. This corresponds to the optical transition of 5d→4f orbitals in the Ce^{3+} ions. Since the energy transfer of the excited electrons in ZnO to the Ce^{3+} ions would be enhanced by increased Ce^{3+} ions, therefore the photoluminescence intensity of the Ce-doped ZnO nanorods increased with the increasing molarity of the Ce-doping agent. The detailed synthesis and studies on highly efficient photocatalyst Ce doped ZnO nanorods under mild hydrothermal conditions using the polyamines TETA as the cross-linking agents were reported by M. Faisal et al. [39] in 2013 for the first time. The choice of surfactant in the preparation procedure is playing an important role in obtaining nanorod structures. The sharp diffraction peaks demonstrate that the ZnO nanorods are highly crystalline. Moreover, the cubic CeO_2 phase was also identified in the cerium doped ZnO. The XPS analysis confirms that the cerium doped ZnO nanorods contain mainly Ce^{3+}, Ce^{4+} and Zn^{2+} ions. The SEM images reveal that with increasing Ce doping, very thin fluffy or porous like structures on smooth ZnO nanorods appeared. All Ce doped samples are more photoactive than either undoped ZnO or commercially available

TiO_2 (UV100). 0.5% Ce doped ZnO exhibits highest photocatalytic activity among the prepared samples. Ce acts as an electron reservoir and inhibits the photogenerated electrons–hole pair recombination and helps in the improvement of photocatalytic performance of Ce doped samples. The improved efficiency and low-cost synthesis suggest that this material might be practically useful for environmental remediation. K. Singh et al. [38] reported, in 2014, the synthesis of well-crystalline CeO_2–ZnO nanoellipsoids by hydrothermal route at low-temperature and characterized in terms of their optical, compositional, morphological and structural properties. The detailed morphological studies showed that the prepared nanomaterials have ellipsoidal shape grown in high density. The structural and compositional properties confirmed that the synthesized structure possess both cubic fluorite type of CeO_2 and wurtzite hexagonal ZnO structure. Importantly, the prepared CeO_2–ZnO nanoellipsoids were used as an effective electron mediator in the fabrication of 4-Nitrophenol (4NP) chemical sensor. The constructed 4NP chemical sensor exhibited a reasonable and reproducible sensitivity of ~ 0.120 μA/nMcm^2 and detection limit of 1.163 μM. This research opens a new way that efficient chemical sensors can be made by simply synthesizing CeO_2–ZnO nanomaterials.

3.1.2 Review of the Study of Erbium (Er) Doped ZnO Nanomaterials

Er doped ZnO thin films were synthesized by Y. Chen et al. [45] in 2011 on glass substrates by direct current co-reactive magnetron sputtering technique. The XRD and XPS analysis showed that Er doping leads to a disorder of ZnO film and the Er doped ZnO film deposited at room temperature shows an amorphous phase. The optical band gap increases after Er doping. The amorphous Er doped ZnO film has the largest band gap, which is about 3.99 eV. The crystallinity of the Er doped films become well and the band gap of the films reduces with increasing substrate temperature. The main reason for the broadening of the band gap is attributed to the amorphous phase in the Er-doped ZnO film. R. John et al. [48] in 2012 reported the synthesis of Er^{3+} doped ZnO nanoparticles at different concentrations by solid state reaction method. The synthesized nanoparticles were characterized by XRD, UV-absorption spectroscopy, SEM, PL study and vibrating sample magnetometer. The XRD studies exhibit the presence of wurtzite crystal structure similar to the parent compound ZnO in 1% Er^{3+} doped ZnO, suggesting that doped Er^{3+} ions sit at the regular Zn^{2+} sites. However, same studies spread over the samples with Er^{3+} content >1% reveals the occurrence of

secondary phase. SEM images of 1% Er^{3+} doped ZnO show the polycrystalline nature of the synthesized sample. UV-visible absorption spectrum of Er^{3+} doped ZnO nanocrystals shows a strong absorption peak at 388 nm due to ZnO band to band transition. The PL study exhibits emission in the visible region, due to excitonic as well as defect related transitions. The magnetization- field curve of Er^{3+} doped ZnO nanocrystals reveals ferromagnetic property at room-temperature. L. Miao et al. [46] reported, in 2013, the preparation of ZnO:Er thin films with different doping levels and configurations on quartz substrate by a sol–gel spin coating method. Spectroscopic ellipsometry (SE) analysis reveal the significant effect of Er doping and annealing temperatures on the modification of optical band gap, dielectric property and luminescence of ZnO films. The alternations of optical constants, dielectric functions, optical band gaps, and Urbach energy of Er light doping ZnO films are found strongly dependent on the local strain, structure disorder, crystallinity change and non-homogeneous distribution of the minor impurities. Excellent agreement has been achieved between the SE analyses and those of XRD and PL emission. J.-C. Sin et al. [40], in 2013, synthesized Er-doped spherical-like ZnO hierarchical nanostructures by a facile chemical solution route confirmed by XRD, FESEM, EDX, TEM, UV–vis DRS and PL measurements. X-ray diffraction and energy dispersive X-ray results revealed that Er ion was successfully doped into ZnO. UV–vis DRS spectra revealed that Er doping increased the visible light absorption ability of Er/ZnO and a red shift for Er/ZnO appeared when compared to pure ZnO. Analysis of the PL spectra indicated that the as-prepared ZnO products have oxygen vacancy and the content of Er/ZnO was larger than that of the pure ZnO. The photocatalytic results showed that doping of Er into ZnO can significantly improve the photocatalytic efficiency of ZnO under visible light irradiation. The obtained ZnO products contain very developed free surfaces and grain boundaries which can show ferromagnetic behaviour. A. Khataee and his group [41], in 2015 prepared Er doped ZnO nanoparticles by a sonochemical method and their sonocatalytic activity was evaluated for the decolorization of Reactive Orange 29 (RO29). The successful synthesis and the different properties of pure and Er doped ZnO samples were characterized using XRD, SEM, TEM, UV–Vis spectroscopy and XPS analysis. The strong and sharp peaks of the XRD patterns confirm the complete crystalline structure of the prepared samples. The structure of ZnO nanoparticles was not changed by the embedding of Er dopant in the ZnO lattice. The decolorization efficiency of doped

ZnO was higher than that of undoped ZnO for all doping contents, and 4% Er doped ZnO showed the best sonocatalytic performance with a decolorization efficiency of 88%. The effect of different operational parameters including the catalyst dosage, initial dye concentration, and ultrasound power was investigated on the sonocatalysis efficiency. The decolorization efficiency of RO29 was decreased by the addition of radical scavengers and improved by the addition of enhancers such as $K_2S_2O_8$ and H_2O_2 to the dye solution. The synthesized sonocatalyst showed good durability after several consecutive decolorization runs. The intermediates of dye degradation were identified by GC-Mass analysis. R. Vettumperumal and his group [44], in 2015 reported detailed synthesis and studies on Er doped ZnO sol–gel thin films. These thin films were prepared on glass substrate using the spin coating method. The effect of erbium concentration and annealing temperature on structural and optical properties was studied. The annealed film was analysed by XRD, SEM with EDX, micro-Raman, PL and UV–vis spectroscopy. All the films showed a wurtzite structure of polycrystalline nature with an average crystal size of 27.44 nm at 500°C and 29.28 nm at 600°C. The Raman spectra confirmed the absence of secondary phases in the Er doped ZnO films and the longitudinal optical phonon mode was upto the fifth order. Densely packed surfaces of the films were observed from SEM images. The presence and distribution of Zn, O and Er elements in the deposited films were confirmed by EDX analysis. The calculated value of exciton binding energy of ZnO film was 60 meV with a maximum value of 72 meV being observed for Er doped films. The near infra-red emission peak was observed at 1.63 eV through PL spectra studies. The average transmission was 80% with the calculated value of optical band gap being 3.26–3.32 eV. An increase in the refractive index value predicts the substitutional incorporation of Er ions in ZnO with the maximum optical conductivity being observed in the UV region. E. Asikuzun et al. [42] in 2016 reported preparation, growth, structure and optical properties of high-quality c-axis oriented non-vacuum ZnO films coated as a function of Er concentrations by sol–gel dip-coating technique. XRD data of the films show (002) orientation of films increases with increasing Er doping. This result is supported by calculation of degree of (002) orientation. Lattice parameters and plane parameters are calculated. *c* lattice parameter increases with increasing Er doping. While plane stress (σ) is negative for undoped ZnO thin film, it exhibits positive behaviour for Er doped ZnO thin films. Thus, it is observed that all films have tensile stress. Also, values of ZnO bond length increase with increasing Er

content rate. According to SEM analysis, it is observed that grain size decreases with Er doping. Values of optical transmittance are determined as 81%, 89%, 87%, 84%, 86% and 87% for x=0.0, 0.1, 0.2, 0.3, 0.4 and 0.5 respectively at 405 nm. Values of optical band gap decreases from 3.28 eV to 3.24 eV. In addition, the Urbach energy value decreases with increasing Er concentration. There is a relationship between the steepness parameter and the Urbach energy. J. Lang and his group [43], in 2016, synthesized Er^{3+} doped ZnO nanosheets via a two-step hydrothermal method accompanied by post-annealing treatment. Based on the XRD, Raman, EDS, SEM, TEM and PL spectral analyses, the effect of erbium doping on the structural and photoluminescence properties of ZnO nanosheets with irregular porous microstructures is revealed. The results showed that Er^{3+} ions were successfully incorporated into the crystal lattice of ZnO host and some irregular porous microstructure with diameter of 3–10 nm could be seen on ZnO nanosheets with various doping concentrations. It was found that the crystallization and photoluminescence properties of ZnO nanosheets were strongly influenced by erbium doping concentration. The ultraviolet emission and deep level emission both appeared in PL spectra and the intensity of the whole deep level emission was enhanced with erbium doping, indicating that deep-level-defect luminescent centres were increased in the doped samples. Moreover, the crystallization of the samples became worse due to more defects by erbium doping. N.K. Divya et al. [47] in 2016 prepared erbium doped ZnO via simple solid state reaction route and investigated their structural, morphological and optical properties. Since RE elements have larger ionic radii compared to Zinc, the incorporation of trivalent RE ions into ZnO host lattice can cause a significant distortion in the ZnO crystal lattice. The crystallite size is calculated using Scherrer formula and is found to decrease with doping. Effect of Er^{3+} ion incorporation on bond length, volume, average microstrain, specific surface area and dislocation density was studied. The incorporation of Er in ZnO was confirmed using EDAX as well as XPS analysis. Large irregular shaped morphology of heat treated ZnO is changed to small nanosized rods with optimum doping concentration and was analysed using SEM images. Samples show weak emission in the UV region and enhanced emission in the visible region with erbium doping. The induced defects like antisite oxygen O_{Zn} and interstitial oxygen O_i due to the doping of Er can be considered as the reason for the enhanced visible emission. Photocatalytic activity of ZnO is enhanced to a large extent with erbium doping. The time taken for the

degradation of 96.76% of MB dye is only 25 minutes while 0.6 wt% erbium doped ZnO is taken as the catalyst instead of pure ZnO. Both the photocatalytic activity and photoluminescence property of ZnO show their maximum at 0.6 wt% erbium doping. The stability test indicates that the prepared sample (0.6 wt% erbium doped ZnO) is a good photocatalyst and can be used repeatedly.

3.2 DESCRIPTION OF SYNTHESIS METHOD

Synthesis of nanomaterials with severe control over size, shape, density, surface area, and crystalline structure has become very vital for the applications of nanotechnology in various fields including, electronics, catalysis, coatings, sports and medicinal fields. There are two approaches to fabricating at the nano scale:

a. Top-down: this approach involves the reduction of size from bulk materials

b. Bottom-up: in this approach material synthesis is done from atom level

a. Top-down approach

The Top-down approach uses traditional methods to guide the synthesis of nanoscale materials. This approach begins from a bulk piece of material, which is then gradually or step-by-step removed to form objects in the nanometer-size regime (~1 billionth of a meter or 10^{-9} m). This approach may involve crushing, cutting, milling, grinding, or attrition. Usually this route is not suitable for preparing uniformly shaped materials; it is very difficult to realize very small particles even with high energy consumption. The biggest problem with top-down approach is the surface defects (imperfection). Such surface defects introduce internal stress which has a significant impact on physical properties and surface chemistry of nanomaterials. It is well known that the conventional top-down technique can cause significant crystallographic damage to the processed patterns. Basically nanostructures from top- down approach can be synthesized by following methods:

i. Plasma synthesis

ii. Electro synthesis

iii. Spray pyrolysis

iv. Laser ablation

v. High energy ball milling

vi. Inert gas condensation

vii. Arc discharge method

b. Bottom-up approach

The bottom-up approach mode of nanomaterials production involves the condensation of atoms or molecular entities in solution or a gas phase to get the material in the nanometer range. In this approach, nanoparticles are built up atom by atom, molecule by molecule and cluster by cluster from the bottom. The later approach is preferred in the synthesis of nanostructures due to several advantages associated with it. This route is more often used for preparing most of the nano-scale materials with the ability to generate a uniform size, shape and distribution. The controlling of size and shape is done by adjusting the ratio of the concentration of the chemicals making nanoparticle. It effectively covers chemical synthesis and precisely controlled the reaction to inhibit further particle growth. Although the bottom-up approach is nothing new, it plays an important role in the fabrication and processing of nanostructures and nanomaterials.

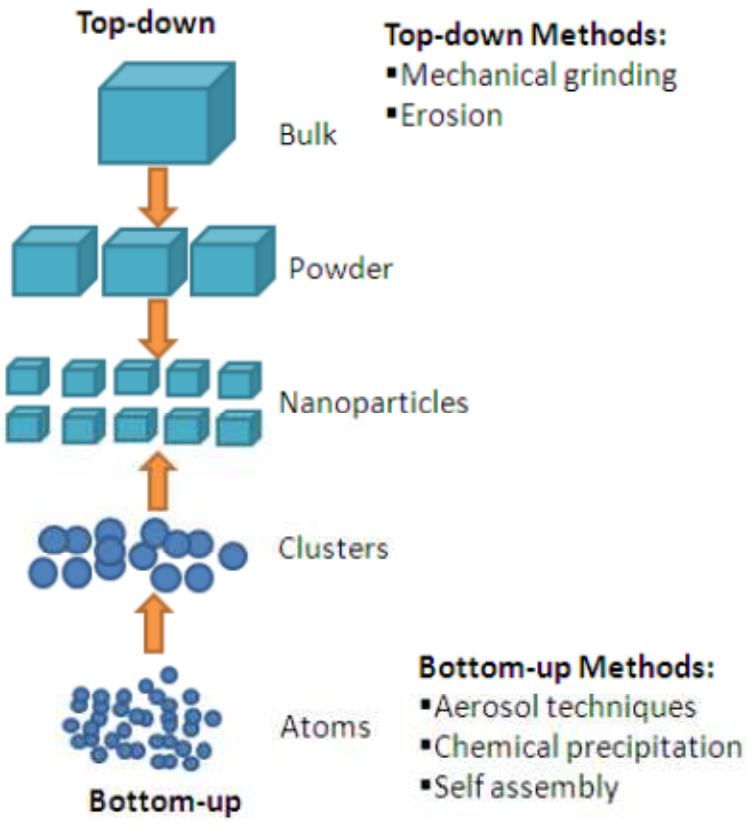

Figure 3.1: Schematic representation of top-down and bottom-up approaches.

There are number of bottom-up methods of synthesizing metal oxide nanomaterials, such as: self-assembly of nanoparticles or monomer/polymer molecules, chemical or electrochemical reactions for precipitation of nanostructures, laser pyrolysis, chemical vapour deposition (CVD), plasma or flame spraying synthesis, and atomic or molecular condensation, microwave synthesis and wet chemical process, etc. Synthesis of nanoparticles to have a better control over particles size distribution, morphology, purity, quantity and quality, by employing environment friendly economical processes has always been a challenge for the researchers [211]. There are mainly five methods of synthesizing of nanomaterials under wet chemical process, these are:

i. Sol-gel method

ii. Hydrothermal(thermal hydrolysis) method

iii. Polyol process

iv. Micro-emulsion process

v. Chemical precipitation method

This section will discuss briefly about all the wet chemical process of the above mentioned processes. The present research work focuses on chemical precipitation technique because the method of synthesis used in this investigation is the chemical precipitation. The chemical precipitation process is a wet chemical synthesis technique that is used for the preparation of gels, glasses, and ceramic powders. It has been selected because of its advantages over other synthesis methods among which are the potential for achieving very high levels of molecular homogeneity, the possibility to control both the morphology and size of the powders as well as its low processing temperature [212].

i. Sol-Gel Method

The sol-gel process is a versatile soft chemical process, widely used for synthesizing metal oxides, ceramic and glass materials. It is a many step process that involves chemical and physical processes associated with the phenomena of condensation, hydrolysis, polymerization, gelation, drying and densification [213]. This process generally starts with the mixing of metal alkoxides and its salts or organometallic inorganic salts as precursors in water or in a suitable solvent (usually an alcohol) at ambient or slightly high temperatures [213, 214]. In this process, initial control of the pH in solution is very important to avoid the precipitation as well as the formation of homogenous gel, which can achieved by the addition of acidic or basic solutions [215]. Apart from the above, organic compounds having hydrophilic functional groups such as hydroxides, carboxylates etc. and small acidic molecules such as citric acid, succinic acid, oxalic acid, tartaric acid, acrylic acid, malonic acid**,** etc. and polymers like polyacrylic acid (PAA), polymethacrylic acid (PMA), and polyvinyl pynolidone (PVP) can be used with metal ion sources to form the sol as well as to control the shape, morphology and textual properties of the final materials [215-217]. Chelation of metal ions by carboxylic groups leads to a homogeneous distribution of the constituent ions in the obtained gel [218]. The gel intermediate is further heated between 150°C and 300°C to eliminate volatile components, excess water, etc., which results in dried intermediate powders. Single phase nanocrystalline metal oxides are

obtained after calcining the dried gel powder at 400-800°C and it depends on the chemical nature of the precursor [219, 220].

$$MOR + H_2O \rightarrow MOH + ROH \text{ (hydrolysis)}$$

$$MOH + ROM \rightarrow M\text{-}O\text{-}M + ROH \text{ (condensation)}$$

Sol-gel method of synthesizing nanomaterials is very popular amongst chemists and is widely employed to prepare oxide materials

Advantages of Sol-Gel Process

1. Less energy consumption: there is no need to melting temperature to achieve network structure i.e. low temperature processing and consolidation is possible.

2. Smaller particle size and morphological control in powder synthesis.

3. Better homogeneity due to mixing at the molecular level and high purity compared to traditional ceramic method.

4. No need for special or expensive equipment.

Disadvantages of Sol-Gel Process

1. Metal alkoxides are the most preferred precursor. But they are expensive as compared to mineral based metal ion sources.

2. Due to the use of organic reagents in preparative steps, products would contain high carbon content and this would inhibit densification during sintering.

3. Close monitoring of the process is required because multi steps are involved in this process.

4. Moreover, formation of gel is a slow process, which makes sol gel a time consuming fabrication technique as compared to other methods.

ii. Hydrothermal Process

One of the important branches of inorganic synthesis is hydrothermal process. Water is an excellent eco-friendly solvent for many ionic compounds. It can dissolve even non-ionic compounds under high pressure and high temperature. In this method, the

above property of water has been effectively exploited for the preparation of fine powders of metal oxides [221-223]. Under the hydrothermal conditions, water plays two different roles: as pressure transmitting medium and as a solvent for the precursors. These conditions effectively brings down the activation energy for the formation of final phase, which speeds up the reaction between the precursors, otherwise it would occur only at very high temperatures [224, 225]. An autoclave is invariably employed to achieve hydrothermal conditions. The pressures attained are in the range of 10 to 150 kilo bar which depends on the chosen temperature of water (>373 K). Depending on hydrothermal conditions powders are either crystalline or amorphous [226-229]. Hydrothermal method has certain advantages as well as some disadvantages, which are listed below.

Advantages of Hydrothermal Process

1. Powders are formed directly from the solution.

2. It is possible to control particle size and shapes by using different starting materials and hydrothermal conditions.

3. Resulting powders are highly reactive, which aid in low temperature sintering.

4. Hydrothermal process is useful to control particle morphology, crystalline phase and surface chemistry through regulation of the solution composition, reaction temperature, pressure, solvent properties, additives and aging time.

Disadvantages of Hydrothermal Process

1. Prior knowledge on solubility of starting materials is required.

2. Hydrothermal slurries are potentially corrosive.

3. Accidental explosion of the high pressure vessel cannot be ruled out.

iii. Polyol Process

The polyol method involves suspending the metal precursor in a glycol solvent and subsequently heating the solution to a refluxing temperature. This technique has been used to synthesize metallic, oxide and semiconductor nanoparticles. The good capabilities of polyols to solubilize the starting materials allow the use of simple and

cheap metal precursors as starting compounds. Ethylene glycol has been widely used in the polyol process for the synthesis of metal (both pure and alloyed) nanoparticles due to its strong reducing power and relatively high boiling point (~197°C) [230, 231]. Recently, it has been widely used for the synthesis of nanocrystalline ceramic powders which involves complexation with ethylene glycol, followed by polymerization [231-234]. In addition, ethylene glycol has been used to fabricate meso structures of titania, tin dioxide, zirconia, and niobium oxide by forming glycolate precursors because of its coordination ability with transition metal ions. This process involves hydrolysis and inorganic polymerization carried out on the salts dissolved in a polyol medium [234]. The selection of polyol for the preparation of nanoparticles is because of its high relative permittivity, boiling point and reduction potential. It allows one to carry out hydrolysis reactions under atmospheric pressure in a large temperature range up to the boiling point of the polyol [235, 236]. The chelating ability of polyol is a beneficial factor to control key features, such as nucleation, growth, and agglomeration of the particles. Another important advantage of polyol's is that the reductive ability at elevated temperatures can reduce the metal solution readily to form metal nanoparticles.

Advantages of Polyol Process

1. It is a low temperature process.

2. Highly pure organic free powders are synthesized.

3. Polyol process has ability to control the particle properties such as narrow size distribution, uniform shape, and morphology, etc.

Disadvantages of Polyol Process

1. Huge amount of poly-hydroxy alcohol required for this process.

2. During synthesis of multi component oxides phase separation is observed.

3. It is difficult to choose the suitable polyhydroxy alcohol for individual processes.

4. There are complications in Collecting and purifying the intermediate particles.

iv. Micro-emulsion Process

Micro-emulsions are clear, transparent dispersions with droplet size 10-100 nm. They tend to be thermodynamically more stable and hence form spontaneously. Microemulsions can generally be formed by gentle mixing of the ingredients which require intense agitation for their formation. Micro-emulsion constitute the smaller droplets dispersed in an immiscible solvent and an amphiphilic surfactant species on the surface of the micelle. The micro- emulsion technique promises to be one of the versatile preparation method which enables to control the particle properties such as mechanisms of particle size control, geometry, morphology, homogeneity and surface area, which can achieved through modification of micelle [237-241].

v. Chemical precipitation process

In chemical precipitation method, a solid substance is derived from a solution, either by converting the substance into an insoluble form or by changing the composition of the solvent to diminish the solubility of the substance in it. In this process, the required metal cations are obtained through some chemical reaction in a solution from a common medium and finally resulting in the form of co-precipitated usually as hydroxides, carbonates, oxalates, sulphates, formates or citrates [242-244]. These precipitates are subsequently calcined at appropriate temperatures to yield the final powder. It is the most adaptable, less expensive and high throughput procedure. It is possible to synthesize nanostructures via chemical precipitation method because basic precursors like acetates, carbonates, nitrates are highly soluble in water forming a homogeneous solution and for achieving high homogeneity, the solubility products of the precipitate of metal cations must be closer [245]. Chemical precipitation results in atomic scale mixing and hence, the calcining temperature required for the formation of final product is low, which lead to lower particle size [246]. All the synthesis requires its own special conditions, precursor reactions, solvents, etc. Also, chemical precipitation process required to control the concentration of the solution, pH, temperature and stirring speed of the mixture in order to obtain the final product with required properties [212, 247]. The synthesis procedure for the undoped and Ce, Er doped ZnO nanostructures via chemical precipitation method are discussed and shown in chapter 4 and 5 by the flowchart (Figure 4.1, 4.2, 5.1 and 5.2).

Advantages of Chemical precipitation Process

1. Homogeneous mixing of reactant precipitates reduces the reaction temperature of the process.

2. Simple direct process for the synthesis of fine metal oxide powders, which are highly reactive in low temperature sintering.

Disadvantages of Chemical Precipitation Process

1. This process is not suitable for the preparation of highly pure and accurate stoichiometric phases.

2. In chemical precipitation method, reactants have very different solubility as well as different precipitate rate due to which it does not work well.

3. It does not have universal experimental condition for the synthesis of various types of metal oxides.

3.3 DESCRIPTION OF CHARACTERIZATION TECHNIQUES

Characterization and manipulation of individual nanostructures require not only extreme sensitivity and accuracy, but also atomic level resolution. It therefore leads to various microscopies that will play a central role in characterization and measurements of nanostructured materials and nanostructures. In this study, various characterization methods that are most widely used in characterizing nanostructures are first discussed. These include: X-ray diffraction (XRD), Energy dispersive X-ray (EDX), Transmission electron microscopy (TEM), High resolution scanning electron microscopy (HRSEM), UV-visible spectroscopy, Photoluminescence spectroscopy (PL) and Vibrating sample magnetometer (VSM). The discussion in this chapter is focused mainly on the fundamentals and basic principles of the characterization techniques and physical methods. The aim of this chapter is to provide the basic information on the fundamentals that the characterization techniques are based on.

3.3.1 X-Ray Diffraction (XRD)

X-ray diffraction techniques are a family of non destructive analytical techniques which reveal the information about the crystallographic structure, chemical composition and physical properties of materials and thin films. These techniques are based on observing the scattered intensity of an X-ray beam hitting a sample as a function of incident and scattered angle, polarization and wavelength or energy. Further, X-ray diffraction method can be used to distinguish crystalline materials from nanocrystalline (amorphous) materials. The structure identification is made from the X-ray diffraction pattern analysis and comparing it with the standard powder diffraction files published by the international centre for diffraction data (ICDD).

From X-ray diffraction pattern, we can obtain the following information:-

(i) Identification of phases present in the material
(ii) Study the formation of a particular material system
(iii) Estimation of unit cell structure, lattice parameters and miller indices
(iv) Estimation of crystalline/amorphous content in the sample.
(v) Evaluation of the average crystalline size from the width of the peak in a particular phase pattern. Large grain size gives rise to sharp peaks, while the peak width increases with decreasing grain/particle size.
(vi) Analysis of structural distortion arising as a result of variation in d-spacing caused by the strain and thermal distortion

The X-ray diffraction study has been the most popular method to guess the crystallite size in nanomaterials. The assessment of crystallite sizes in the nanometer range warrants careful analytical skills. The broadening of the Bragg peaks is attributed to the growth of the crystallite refinement and internal stain. To size broadening and strain broadening, the full width at half maximum (FWHM) of the Bragg peaks as a function of the diffraction angle is analyzed. Crystallite size of the deposits is calculated by the XRD peak broadening. The diffraction patterns are obtained using Cu-Kα radiation at a scan rate of 1º/min. The FWHM of the diffraction peaks were estimated by pseudo-Voigt curve fitting. After subtracting the instrumental line broadening, which is estimated using quartz and silicon standards; the grain size can be estimated using the Debye Scherrer formula.

Principle: When a monochromatic X-ray impinges upon the atoms in a crystal lattice, each atom acts as a source of scattering the radiations of same wavelength. The intensity of the reflected beam at a certain angle will be maximum, when path difference between two reflected waves from two different planes is an integral multiple of wavelength.

Diffraction and Bragg Equation: Diffraction of an X-ray beam striking a crystal occurs because the wavelength of the X-ray beams is of the order of the spacing of atoms in materials (1-10 Å). When an X-ray beam encounters the regular 3-D arrangement of atoms on a crystal, most of the X-ray will destructively interfere with each other and cancel out each other, but in specific direction they constructively interfere and reinforce each other.

W.L. Bragg showed that the diffracted X-rays act as if they were reflected from a family of planes within crystals. Bragg's planes are the rows of atoms that constitute the crystal structure. These reflections were shown to only occur under certain conditions which satisfy the following equation:

$$n\lambda = 2d\sin\theta \qquad (3.1)$$

This equation is called Bragg's equation where n is integer, λ is wavelength, d is the distance between two planes and θ is the angle of incidence. The path length difference between two incident X-ray beams is 2d sinθ. Fig. 3.2 shows the diffraction of X-ray from set of planes.

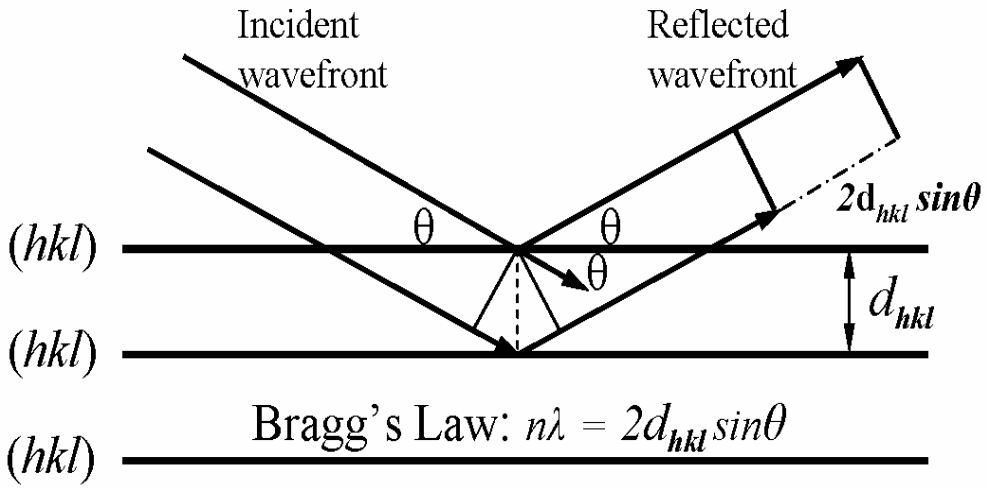

Figure 3.2: Geometrical illustrations of crystal planes and Bragg's law.

Determination of structural parameters:

1. Inter-planner distance (d): For the XRD profiles, the inter-planner distance d can be calculated by using the Bragg's equation [248].

$$n\lambda/ 2\sin\theta = d \qquad (3.2)$$

where n is the order of diffraction, λ is the wavelength of X-rays, and θ is the glancing angle.

2. Average crystallite size/grain size (D): The crystallite size (D) can be estimated by using the Debye Scherrer's formula given by equation by (3.3),

$$D = \frac{0.9\lambda}{\beta Cos\theta} \qquad (3.3)$$

where 'β' is the FWHM in radians. In the present work, the crystal structure of the undoped and doped ZnO samples were studied using XRD (Philips X'pert Materials Research X-ray diffractometer) with CuKα radiation (λ= 1.54 Å).

3.3.2 Energy Dispersive X-Ray (EDX)

It is a technique used for identifying the elemental composition of the specimen and an area of interest thereof. During EDX analysis, the specimen is bombarded with an electron beam inside the scanning electron microscope. The bombarding electrons collide with the specimen atom's own electrons, knocking some of them off in the process. A position vacated by an ejected inner shell electron is ultimately occupied by a higher-energy electron from an outer shell. To be able to do so, however, the transferring outer electron must give up some of its energy by emitting an X-ray. The amount of energy released by the transferring electron depends on which shell it is transferring from, as well as which shell it is transferring to. Furthermore, the atom of every element releases X-rays with unique amounts of energy during the transferring process. Thus, by measuring the energy of the X-rays emitted by a specimen during electron beam bombardment, the identity of the atom from which the X-ray was emitted can be established.

The output of an EDX analysis is an EDX spectra, which is a plot of how frequently an X-ray is received for each energy level. An EDX spectra normally displays peaks corresponding to the energy levels for which the most X-rays had been

received. Each of these peaks is unique to an atom, and therefore corresponds to a single element. The higher a peak in a spectrum, the more concentrated the element is in the specimen. An EDX spectra plot not only identifies the element corresponding to each of its peaks, but the type of X-ray to which it corresponds as well. For example, a peak corresponding to the amount of energy possessed by X-rays emitted by an electron in the L-shell going down to the K-shell is identified as a K_α peak. The peak corresponding to X-rays emitted by M-shell electrons going to the K-shell is identified as a K_β peak as shown in Fig. 3.3.

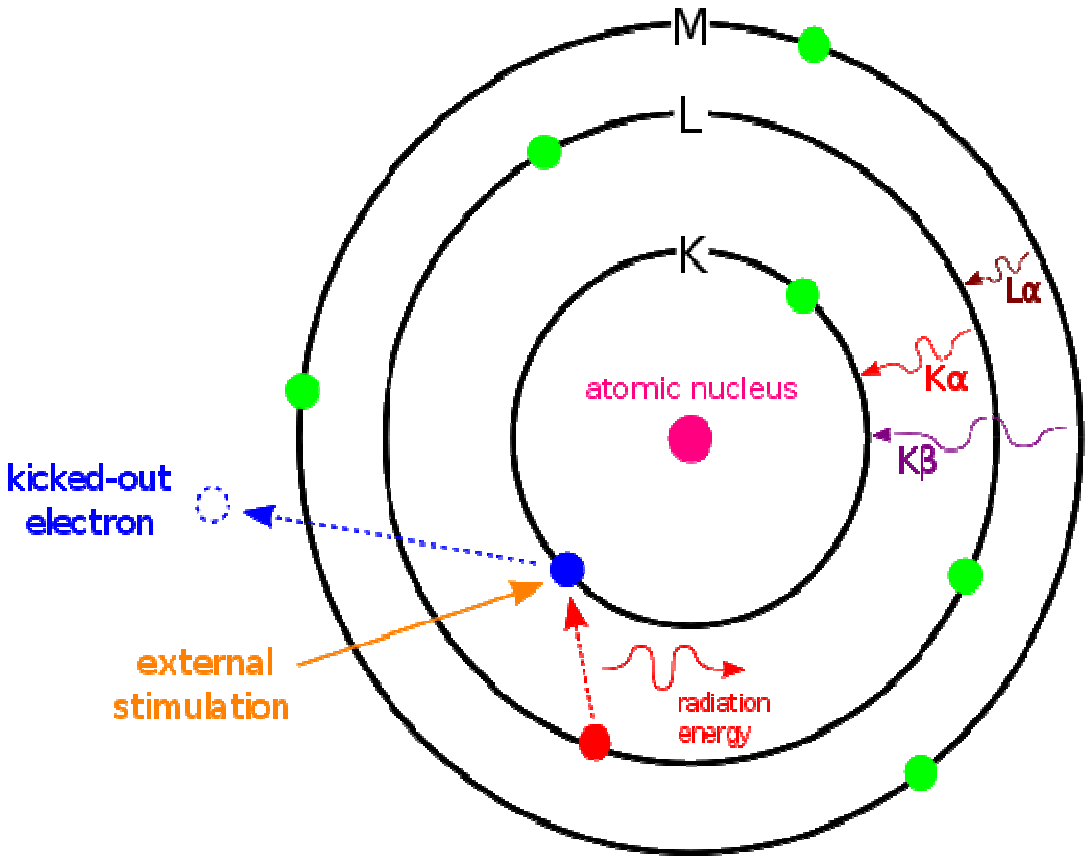

Figure 3.3: The emission of X-rays.

3.3.3 Transmission Electron Microscopy (TEM)

Transmission Electron Microscopy (TEM) has become an essential characterization technique for materials scientists. TEM's strong cards are its high lateral spatial resolution (better than 0.2 nm "point to-point'' on some instruments) and its capability to provide both image and diffraction information from a single specimen. In addition, the highly energetic beam of electrons used in TEM interacts with specimen matter to produce characteristic radiation and particles; these signals are regularly measured to provide materials characterization using EDS, backscattered and secondary electron imaging, to name a few possible methods. In TEM, a focused electron beam is incident on a thin (less than 200 nm) specimen. The signal in TEM is obtained from both undeflected and deflected electrons that penetrate the specimen thickness. A series of magnetic lenses at and below the specimen position are responsible for delivering the signal to a detector, usually a fluorescent screen, a film plate, or a video camera. Accompanying this signal transmission is a magnification of the spatial information in the signal by as little as 50 times to as much as a factor of 10^6. This remarkable magnification range is facilitated by the small wavelength of the incident electrons, and is the key to the unique capabilities associated with TEM analysis. TEM offers two methods of specimen observation, diffraction mode and image mode. In diffraction mode, an electron diffraction pattern is obtained on the fluorescent screen, originating from the specimen area illuminated by the electron beam. The diffraction pattern is entirely equivalent to an X-ray diffraction pattern: a single crystal will produce a spot pattern on the screen, a poly-crystal will produce a powder or ring pattern (assuming the illuminated area includes a sufficient quantity of crystallites) and a glassy or amorphous material will produce a series of diffuse halos. The image mode produces an image of the illuminated sample area. The image can contain contrast brought about by several mechanisms: mass contrast, due to spatial separations between distinct atomic constituents; thickness contrast, due to non uniformity in specimen thickness; diffraction contrast, which in the case of crystalline materials results from scattering of the incident electron wave by structural defects; and phase contrast. Alternating between image and diffraction mode on a TEM involves nothing more than the flick of a switch. The reason for this simplicity is buried in the difficult electron optics technology that makes the practice of TEM possible. There are a number of limitations of the TEM technique. Many materials

require extensive specimen preparation to produce a specimen thin enough to be electron transparent, which makes TEM analysis a relatively time consuming process with a low throughput of specimens. The structure of the specimen may also be changed during the preparation process. Also the field of view is relatively small, raising the possibility that the region analyzed may not be characteristic of the whole specimen. There is potential that the specimen may be damaged by the electron beam, particularly in the case of biological materials. The dimension and crystallinity of the undoped and doped ZnO specimens were analyzed using a transmission electron microscope (Philips CM-12).

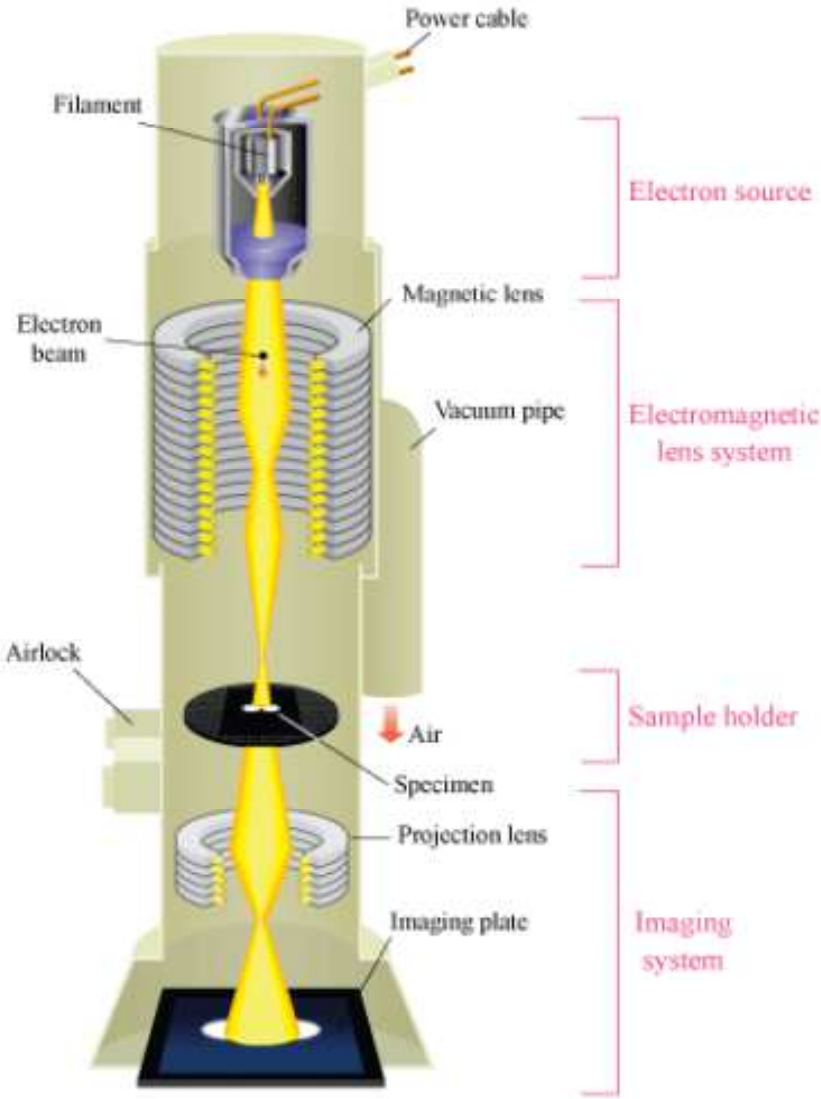

Figure 3.4: Schematic diagram of TEM instrumentation.

3.3.4 High Resolution Scanning Electron Microscopy (HRSEM)

The High resolution scanning electron microscope (HRSEM) is a type of electron microscope that helps in forming an image of the specimen surface by scanning in the surface to generate signals that shed valuable light on properties like composition, topography and electrical conductivity. The so called “signals” produced by an SEM include secondary and back-scattered electrons, characteristic X-rays, specimen current and light (due to cathodoluminescence). SEM helps in obtaining high resolution images of specimens ranging in size from those visible to the naked eye to those which are just a few nanometers. In a typical SEM, an electron beam is thermionically emitted from an electron gun fitted with a tungsten filament cathode. The electron beam, which typically has an energy ranging from 0.5 to 40 KeV, is focused by one or two condenser lenses to a spot about 0.4 to 5 nm in diameter. The beam passes through pair of scanning coils or pair of deflector plates in the electron column, typically in the final lens, which deflect the beam in the x and y axes so that it scans in a raster fashion over a rectangular area of the specimen surface. The image may be captured by photography from a high resolution cathode ray tube, but in modern machines, is digitally captured and displayed on a computer monitor and saved to a computer's hard disk. Schematic diagram of HRSEM instrumentation is shown in Fig. 3.5.

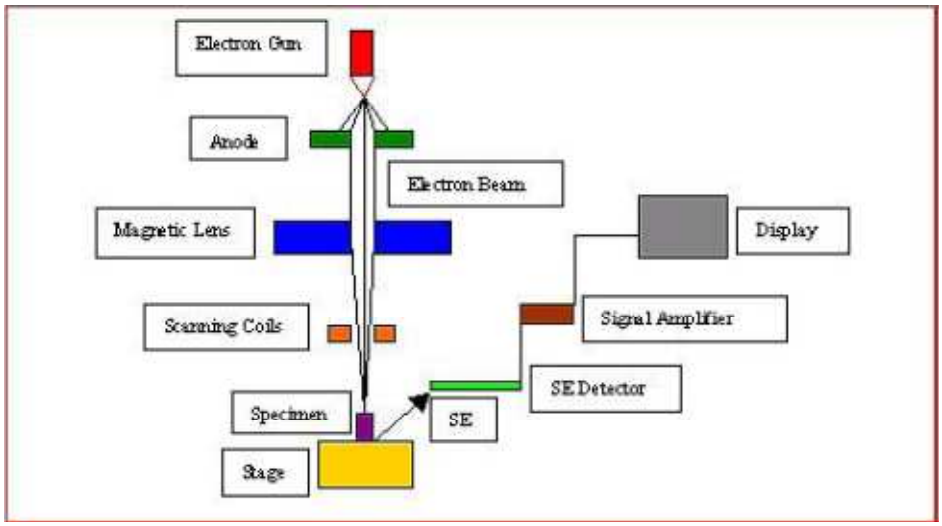

Figure 3.5: Schematic diagram of HRSEM instrumentation.

Applications

(i) HRSEM is a widely used to identify phases based on qualitative chemical analysis and/or crystalline structure

(ii) Backscattered electron images (BSE) can be used for rapid discrimination of phases in multiphase samples

Advantages

(i) Better resolution and depth of field than light microscopes

(ii) Minimal specimen preparation

(iii) Modern SEMs generate data in digital formats, which are highly portable

3.3.5 UV-Visible Spectroscopy (UV-vis)

Ultraviolet-visible (UV-vis) spectroscopy is used to obtain the absorbance spectra of a compound in solution or as a solid. What is actually being observed spectroscopically is the absorbance of light energy or electromagnetic radiation, which excites electrons from the ground state to the first singlet excited state of the compound or material. The UV-visible region of energy for the electromagnetic spectra covers 1.5-6.2 eV which relates to a wavelength range of 800-200 nm. It measures the intensity of light passing through a sample (I) and compares it to the intensity of light before it passes through the sample (Io). The ratio I/Io is called transmittance and is usually expressed as a percentage (%T).

The basic parts of a spectrophotometer are a light source, a holder for the specimen, a diffraction grating or monochromator separating the different wavelengths of light, and a detector as shown in Fig. 3.6. The radiation source is often a tungsten filament (300-2500 nm), a deuterium arc lamp which is continuous over the ultraviolet region (190-400 nm) and more recently LED and xenon arc lamps for the visible wavelengths. The detector is typically a photodiode or a charge couple device (CCD). Photodiodes are used with monochromator, which filter the light so that only light of a single wavelength reaches the detector. Diffraction gratings are used with CCDs which collects light of different wavelengths on different pixels. Specimens for UV-vis spectrophotometer are most often liquids, although the absorbance of gases and even of solids can also be measured. Samples are typically placed in a transparent cell, known as a cuvette. Cuvettes are typically rectangular in

shape, commonly with an internal width of 1 cm. The most widely applicable cuvettes are made of high quality quartz glass, because these are transparent throughout the UV, visible and near infrared regions. Absorbance is directly proportional to the path length and the concentration of the absorbing species.

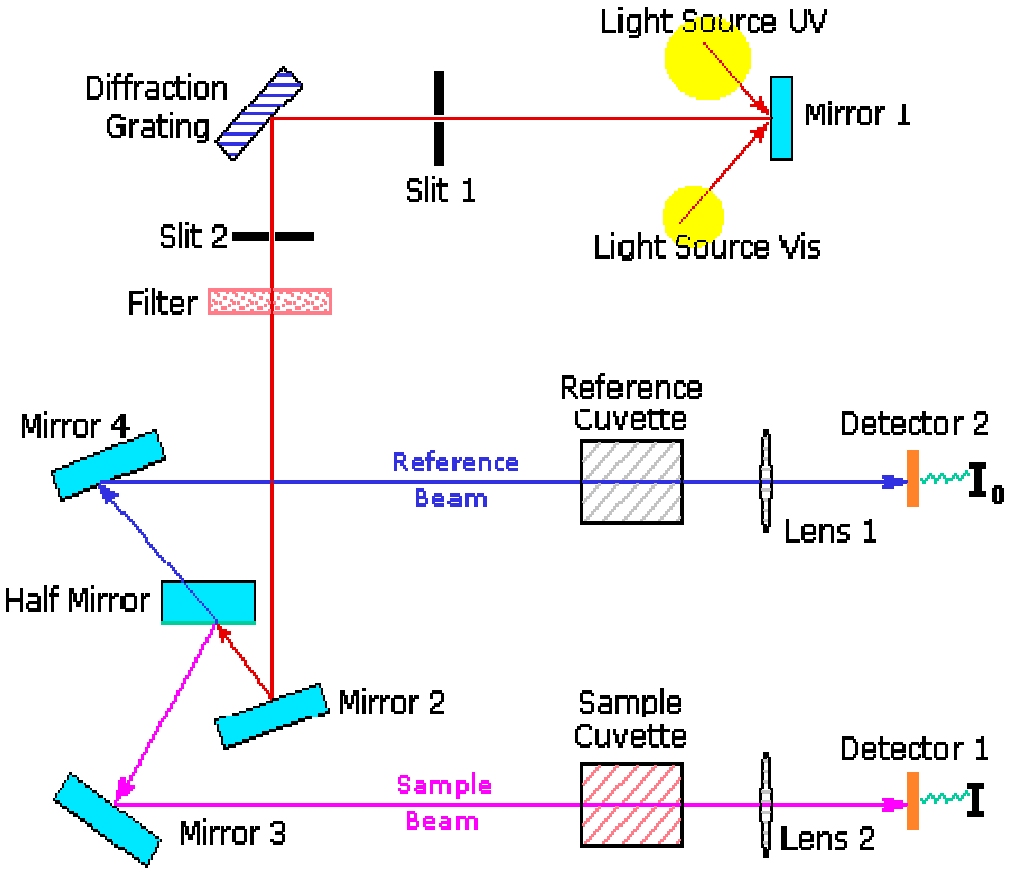

Figure 3.6: Schematic diagram of UV-Vis spectroscopy.

The wavelength at the maximum of the absorption band will give information about the structure of the molecule or ion and the extent of the absorption is proportional with the amount of the species absorbing the light. Quantitative measurements are based on Beer's Law given by equation which states that,

$$A = \varepsilon bc \qquad (3.4)$$

Where ε – constant of proportionality, b – path length, c – concentration

Different molecules absorb radiation of different wavelengths. Absorption spectra will show a number of absorption bands corresponding to structural groups within the molecule.

3.3.6 Photoluminescence Spectroscopy (PL)

PL spectroscopy concerns monitoring the light emitted from atoms or molecules after they have absorbed photons. It is suitable for materials that exhibit photoluminescence. PL spectroscopy is suitable for the characterization of both organic and inorganic materials of virtually any size and the samples can be in solid, liquid or gaseous forms.

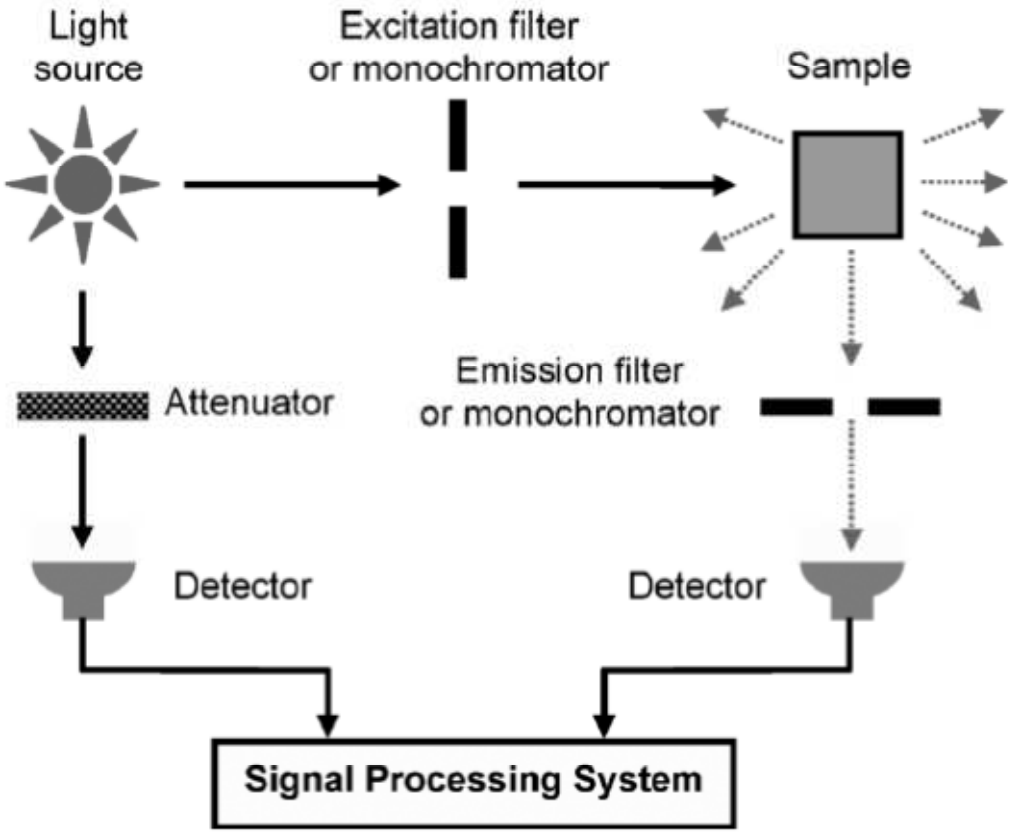

Figure 3.7: Schematic diagram of PL spectrophotometer.

Electromagnetic radiation in the UV and visible ranges is utilized in PL spectroscopy. The specimen's PL emission properties are characterized by four parameters: intensity, emission wavelength, bandwidth of the emission peak and the emission stability. The PL properties of a material can change in different ambient

environments, or in the presence of other molecules. Furthermore, as dimensions are reduced to the nanoscale, PL emission properties can change, in particular a size dependent shift in the emission wavelength can be observed. Additionally, because the released photon corresponds to the energy difference between the states, PL spectroscopy can be utilized to study material properties such as band gap, recombination mechanisms and impurity levels. In a typical PL spectroscopy setup for liquid samples is shown in Figure 3.7, a solution containing the sample is placed in a quartz cuvette with a known path length. Double beam optics is generally employed. The first beam passes through an excitation filter or monochromator, then through the specimen and onto a detector. This impinging light causes photoluminescence, which is emitted in all directions. A small portion of the emitted light arrives at the detector after passing through an optional emission filter or monochromator. A second reference beam is attenuated and compared with the beam from the specimen. Solid specimen can also be analyzed, with the incident beam impinging on the material (thin film, powder etc.). Generally an emission spectrum is recorded where the specimen is irradiated with a single wavelength and the intensity of the luminescence emission is recorded as a function of wavelength. The fluorescence of a specimen can also be monitored as a function of time, after excitation by a flash of light. This technique is called time resolved fluorescence spectroscopy.

3.3.7 Vibrating Sample Magnetometer (VSM)

VSM is the basic instrument for characterizing magnetic materials to measure the basic magnetic properties of materials as a function of magnetic field and temperature. The VSM consists of an electromagnet which provides the magnetizing field (DC), a vibrator mechanism to vibrate the sample in the magnetic field and detection coils, which generate the signal voltage due to the changing flux emanating from the vibrating sample. The VSM represents by far the most commonly used type of magnetometer. A small sample of a given geometry is magnetized and allowed to vibrate in proximity of coils. The induced in the coils as the flux linked with the coils changes due to the vibration of the sample. The various components are monitored through a computer interface. Using controlling and monitoring software, the system gives information about the amount of magnetization of the sample and how its magnetization depends on the strength of the constant magnetic field. The schematic diagram of VSM is represented in Fig. 3.8.

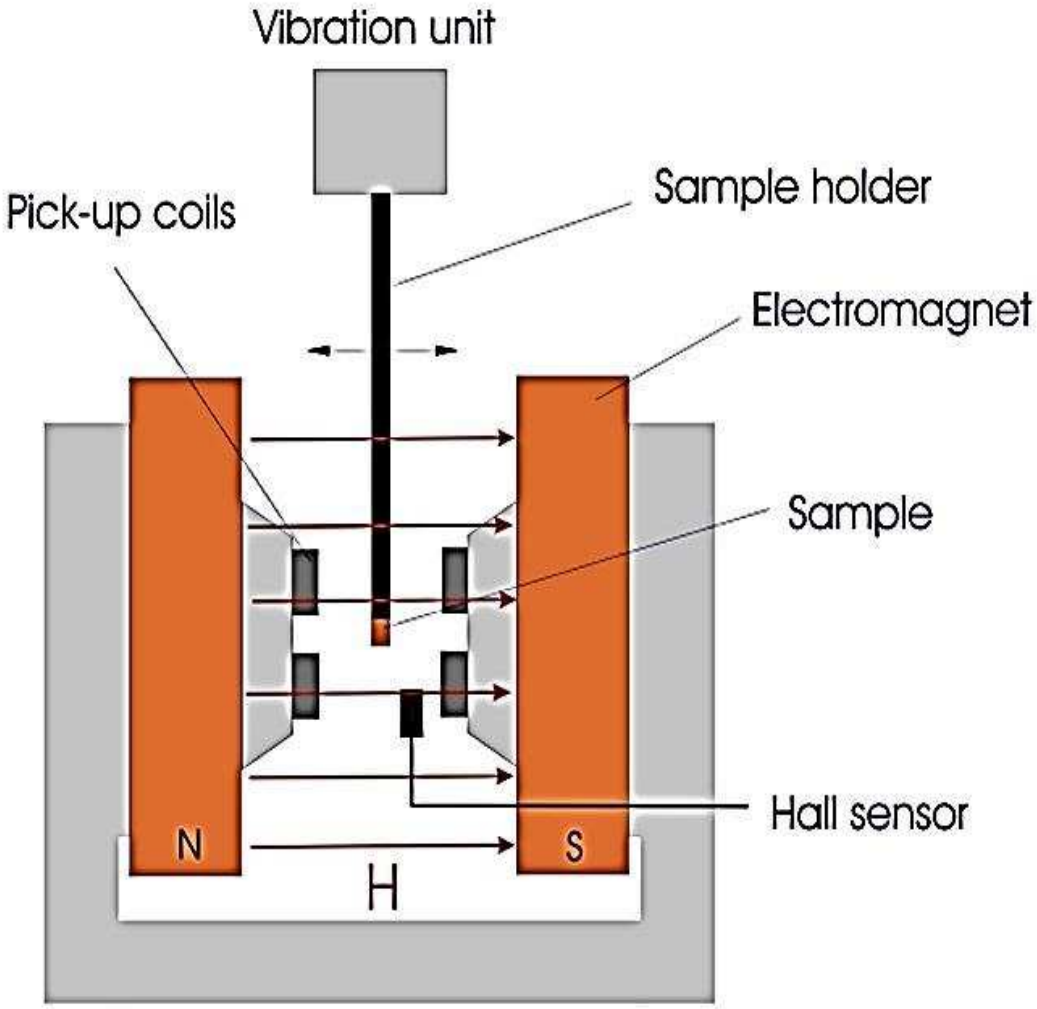

Figure 3.8: Schematic diagram of vibrating sample.

CHAPTER IV

STRUCTURAL, OPTICAL AND MAGNETIC STUDIES ON Ce DOPED ZnO NANOPARTICLES

4.1 INTRODUCTION

During the last few decades, nanomaterials such as nanorods, nanowires and nanotubes have been the subject of extensive interest because of their potential use in a wide range of field-effect transistors [249], single-electron transistor [250], photodiodes [251, 252] and sensing application [253, 254]. The physical, chemical, magnetic, electronic and optical properties of nanomaterials can differ significantly because of large surface area to volume ratio than their bulk counterparts [255]. In addition, metal oxide nanomaterials have drawn a special attention because of inheriting the fascinating properties such as piezoelectricity, chemical sensing, photo-detection and also possess unique properties associated with their highly anisotropic geometry and size confinement [256].

Among various metal oxides, many researchers have shown much interest in ZnO and its fundamental research and practical studies because of its excellent optical, electrical, optoelectronic, gas-sensing, piezoelectric and photochemical properties [104, 257]. ZnO has a large direct band gap of ~ 3.37 eV and a high exciton binding energy of 60 meV that makes it attractive for its emission tendency in UV and full color lighting [32, 35]. Another attractive property of ZnO is photocatalysis. It is because of its non-hazardous nature and tremendous physical and chemical stability [39, 198, 258]. Its photocatalytic efficiency depends on the competition between electron- hole recombination process and surface chemical reaction. If recombination process of electron and hole occurs too fast, we find that the surface chemical reaction does not occur. Due to very fast recombination of photogenerated electron- hole pairs, the photocatalytic efficiency of ZnO remains low. Therefore, to improve the photocatalytic activity of ZnO, numerous modification techniques have been developed. In literature it has been cited that photocatalytic efficiency of semiconductor photocatalyst i.e. ZnO can be enhanced by doping certain cation which

can act as electron trapping agents to decrease electron- hole recombination rate [259].

Doping is considered an effective way to enhance the properties of ZnO for various applications. There are numerous reports on the utilization of several metals for doping such as Sb [260], Sn [261], In [262], Mn [263], Ga [264] and Ce [39, 198, 258, 265]. In this framework, the doping of RE ion in ZnO is of great importance due to signs of tunable luminescence and ferromagnetism at room temperature.

RE ions are extensively used as activators in different host materials due to their high fluorescence efficiencies and very narrow line fluorescence bands. The ferromagnetism property of RE doped ZnO nanostructures is another such property which has drawn great interest. These nanostructures find applications in magneto-optical device applications i.e. communications, storage, quantum computation etc. [25, 26]. Due to only few percent of doping of RE ions into non-magnetic semiconductor and to achieve ferromagnetism are known as DMS. Specifically, room temperature ferromagnetism of Ce doped ZnO nanostructures have not been reported extensively. RE doped ZnO nanomaterials i.e. nanophosphors and DMS are an attractive class of materials with ferromagnetism and optical emission from 4*f*–4*f* or 4*f*–5*d* transition of rare earth ions [192, 265]. Ce doped ZnO nanophosphors have been comprehensively studied because of the unusual interaction between the excited states and the host lattice.

CeO_2 has a band gap of 3.0 eV and possesses a unique optical characteristic for visible LED and high power laser that are similar to ZnO [258–266]. Thus, the Ce doped ZnO nanomaterials also exhibited versatile properties and have been explored to assess the photoluminescence and photoelectrochemical activity under visible light, gas-sensing properties and ferromagnetism [265, 267, 268]. So, the preparation and characterization of Ce doped ZnO nanostructures still need further research and investigation. To date, various synthesis techniques of RE doped ZnO nanostructures have been reported, including the hydrothermal method, magnetron sputter deposition, pulsed laser deposition, photolithography and wet chemical etching. In present investigation, an attempt has been made for synthesis of ZnO nanoparticles and Ce doped ZnO nanoparticles by chemical precipitation technique and studied for effect of Ce doping on properties of ZnO nanoparticles.

Though it's not an easy task to incorporate RE ions into the lattice of semiconductors that efficiently via chemical method as Ce ion has large radius and there is a noticeable difference between their charges and chemical properties but this process was undertaken in this study effectively. In the method of synthesis of ZnO nanoparticles and Ce doped ZnO nanoparticles, the addition of reactant solutions of zinc nitrate to sodium hydroxide and zinc nitrate and cerium nitrate to sodium hydroxide begin the process of precipitation. In this technique, composition of the solvent is modified in such a way that the ZnO nanoparticles is formed, which in itself requires deep understanding of the growth mechanism of nanoparticles as ZnO has a significantly lower solubility than the concentration in solution whereas the formation of Ce doped ZnO nanoparticles made it evident that RE ion can be introduced into the ZnO nanoparticles and shift of energy from host to RE ions can be accomplished if synthesis process is well designed and charge discrepancy is compensated as per the purpose. Chemical precipitation technique is easily reproducible and applicable to large scale industrial fabrication of products at low cost.

4.2 EXPERIMENTAL DETAILS

4.2.1 Synthesis Procedure

In this study, ZnO nanoparticles and Ce doped ZnO nanoparticles were synthesized using chemical precipitation method. All chemicals used here were of analytical grade and highly pure. In this procedure for ZnO nanoparticles, 0.5M zinc nitrate hexahydrate [$Zn(NO_3)_2.6H_2O$] and 0.5M sodium hydroxide [NaOH] (as precipitant agent) were dissolved in de-ionized (DI) water and slowly mixed into constantly magnetic stirred. For Ce doped ZnO nanoparticles, 0.5M zinc nitrate hexahydrate [$Zn(NO_3)_2.6H_2O$] and 0.5M cerium nitrate hexahydrate [$Ce(NO_3)_3.6H_2O$] were dissolved in DI water. These solutions were slowly mixed in a container to produce the precipitate of Ce doped ZnO nanoparticles. In addition 0.5M sodium hydroxide [NaOH] and methanol [CH_3OH] were also added in this solution. In both cases the precipitates were collected, washed with DI water for several times and then separated by centrifugal method. These clean precipitates were dried at 100°C into the electric oven for 10 hours. Finally, the dried gels were sintered at 600°C for 1 hour to get ZnO nanoparticles and Ce doped ZnO nanoparticles.

XRD (Philips X'pert Materials Research X-ray diffractometer), HRTEM (Philips CM-12), PL (Perkin-Elmer LS55 Fluorescence spectrometer), UV visible (Hitachi U-3400 UV-VIS spectrometer) and magnetization measurements from commercial quantum design Physical Properties Measurement System (PPMS) were used to illustrate the crystal structures, size, luminescence and magnetic properties of ZnO nanoparticles and Ce doped ZnO nanoparticles.

4.2.2 Mechanism of Synthesis

In this sub-section, we are giving the reaction process and mechanism accountable for the formation of ZnO and Ce doped ZnO nanoparticles.

For the formation of ZnO nanoparticles, first of all the aqueous solution of zinc nitrate is mixed with methanol to form zinc alkoxide.

I Step: $Zn(NO_3)_2 + 2CH_3OH \rightarrow Zn(OCH_3)_2 + 2HNO_3$

Further the slow mixing of aqueous solution of sodium hydroxide gives rise to the reduction of zinc alkoxide to give ZnO precipitate:

II Step: $Zn(OCH_3)_2 + 2\ HNO_3 + 2NaOH \rightarrow ZnO\ (ppt) + 2NaNO_3 + C_2H_5OH + 2H_2O$

The reduction of zinc alkoxide is pursued by the condensation process which causes the creation of ZnO precipitate. The rest of sodium nitrate and ethanol are disposed and ZnO precipitate is collected. Thus, the chemical reaction showing the synthesis of ZnO nanoparticles can be shown by the summation of I and II step.

$Zn(NO_3)_2 + 2CH_3OH + 2NaOH \rightarrow ZnO + 2NaNO_3 + C_2H_5OH + 2H_2O$

Similarly for the synthesis of Ce doped ZnO nanoparticles the basic chemical reaction can be expressed as follows:

$$(1-x)\times[Zn(NO_3)_2] + x\times[Ce(NO_3)_3] + (1-x)\times[NaOH] + (1-x)\times[CH_3OH] \rightarrow Zn_{1-x}Ce_xO + (1-x)\times[NaNO_3] + (1-x)\times C_2H_5OH + (1-x)\times[H_2O]$$

In this reaction 'x' is used for the Ce doping concentration. In our case x = 0.5M Ce doping. The chemically balanced reaction is as follows:

$$[Zn(NO_3)_2] + 2\ [Ce(NO_3)_3] + 8\ [NaOH] + 2\ [CH_3OH] \rightarrow ZnCe_2O_4 + 8\ [NaNO_3] + C_2H_5OH + 5\ [H_2O]$$

The Gibbs free energy for these reactions ($\Delta G_{reaction}$) can be calculated as:

$$\Delta G_{reaction} = \Delta G_{products} - \Delta G_{reactants}$$

The ZnO and Ce doped ZnO nanoparticles are synthesized at room temperature. The Gibbs free energy of reactions for the formation of ZnO and Ce doped ZnO is calculated using the process reported in literature [212], and the negative values of Gibbs free energy for the above reactions is interpreted that an exothermic reaction will be supported for the spontaneous creation of ZnO and Ce doped ZnO nanoparticles.

It is established that during chemical reactions, precipitation arises particularly if an insoluble substance is mixed into the solution and the density of this insoluble substance occurs to be larger than that of solution (or else the precipitate would float or form a suspension); whereas with soluble substances, precipitation is accelerated once the solution becomes supersaturated [269]. Moreover, in our case the above-mentioned reactions are performed with the organized slow uniform mixing of reactants so that the seed nucleation rate exceeds the growth rate and subsequently confined precipitation of ZnO and Ce doped ZnO nanoparticles happens [270]. So, it is concluded that chemical precipitation method, adopted in this study, actually leads to the growth of solid nanoparticles of ZnO and Ce doped ZnO in the solution. The further details of discussion related to the growth mechanism and the role of various reaction parameters (e.g. pH, mixing rate, drying treatment) of ZnO nanoparticles using chemical precipitation method can be referred elsewhere [212, 269–272]. The flow charts for synthesis of ZnO and Ce doped ZnO nanoparticles are shown through the Fig. 4.1 and 4.2.

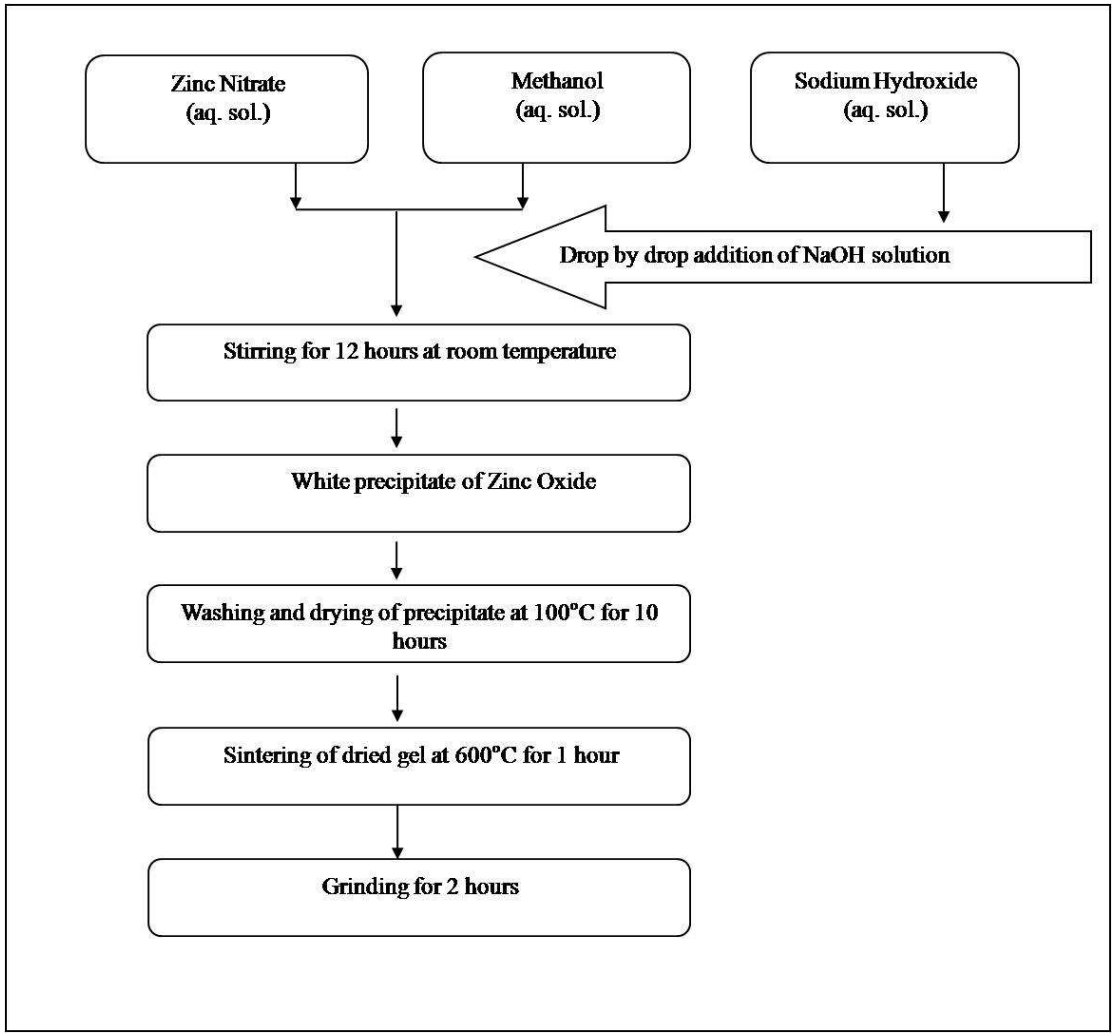

Figure 4.1: Flow chart for the synthesis of ZnO nanoparticles.

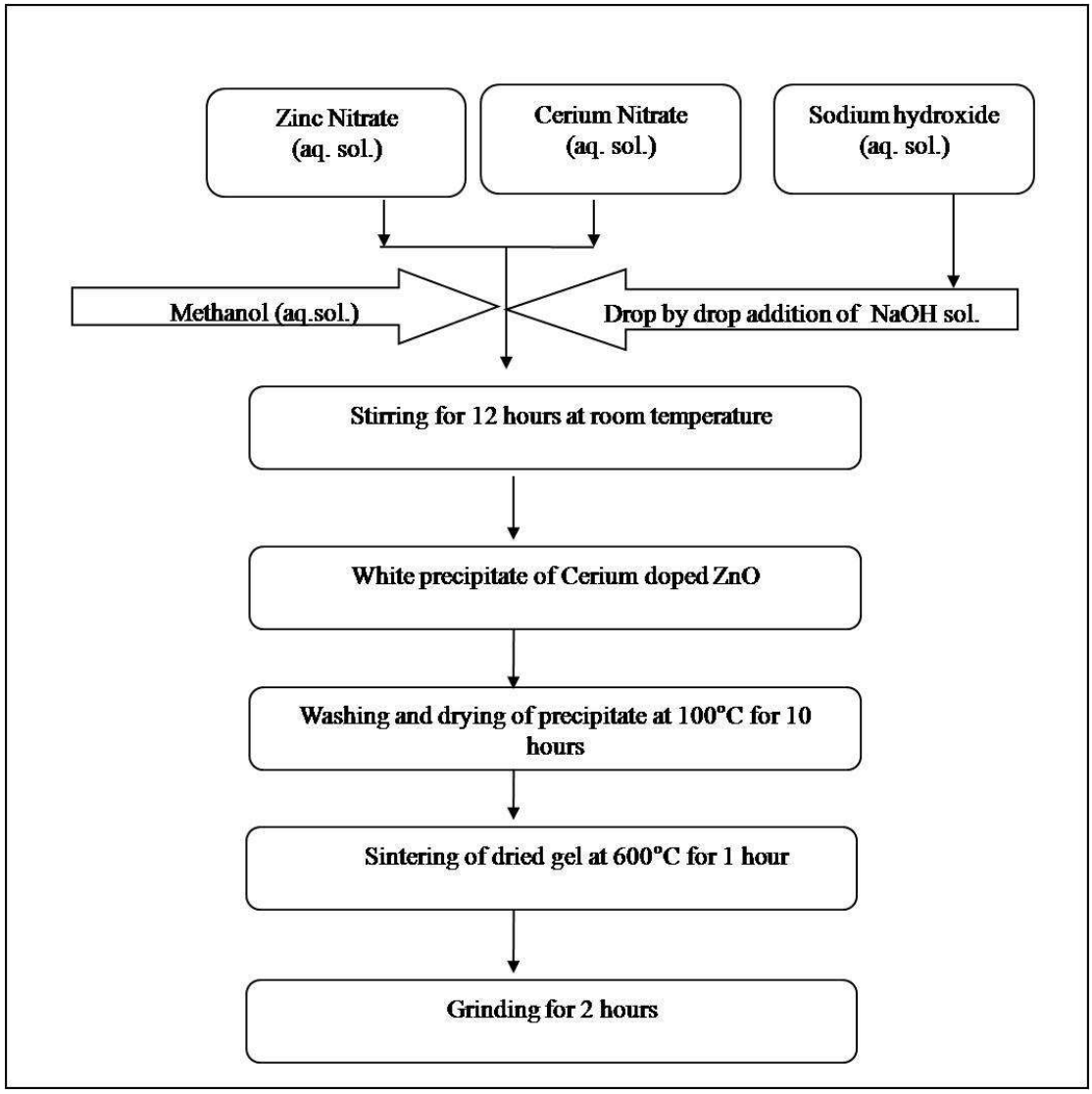

Figure 4.2: Flow chart for the synthesis of Ce doped ZnO nanoparticles.

4.3 RESULTS AND DISCUSSION

4.3.1 Structural Studies

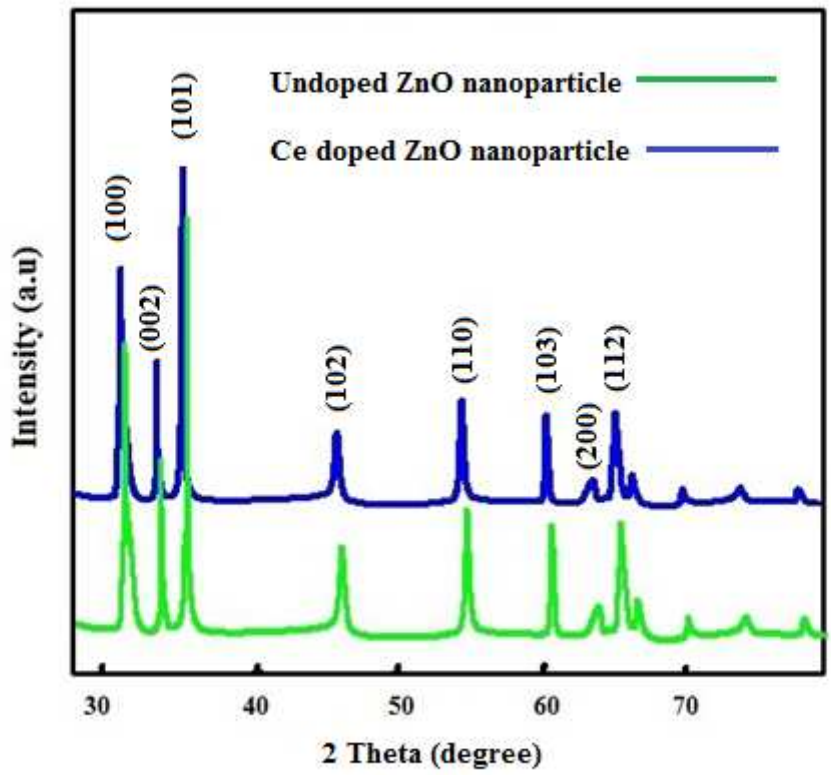

Figure 4.3: X-ray diffraction pattern of ZnO nanoparticles and Ce doped ZnO nanoparticles.

To examine the formation of crystal structure and crystal phase, the synthesized ZnO and Ce doped ZnO samples were examined by XRD. Fig. 4.3 shows the XRD pattern of ZnO nanoparticles and Ce doped ZnO nanoparticles. According to the XRD result of ZnO, it can be concluded that the prominent peaks labeled at 31.74°, 34.14°, 36.25°, 47.12°, 56.12°, 62.50°, 66.24° and 67.5° correspond to the (100), (002), (101), (102), (110), (103), (200) and (112) planes respectively, confirming the formation of hexagonal zinc oxide phase. No considerable difference could be observed between the XRD patterns of ZnO and Ce doped ZnO i.e. both these XRD patterns are analogous. Hence it was analyzed that ZnO nanoparticles and Ce doped ZnO nanoparticles have hexagonal wurtzite structure and diffraction data in Fig. 4.3 are in

agreement with the JCPDS card for ZnO (JCPDS 36-1451). Impurity peaks such as CeO_2 and CeO_3 are not observed in the XRD pattern of Ce doped ZnO nanoparticles. Due to the absence of any impurity peaks, it was clear that Ce^{3+} ions were uniformly substituted into the Zn^{2+} ions and the integration of Ce ion in the ZnO matrix has no effect in the complete crystal structure. George et al. [37] expected that the substitutional doping to change the bond distances reflected through the change in unit cell lattice parameters and the peak intensities can be affected by the change in electron density due to substitution of atoms. In addition they suggested that the increase in lattice parameters can be due to interstitial incorporation of Ce ions in ZnO matrix while decrease in lattice parameters can be due to replacement of Zn ions with Ce ions. In the XRD pattern (Fig. 4.3) of Ce doped ZnO nanoparticles prominent diffraction peaks were shift slightly towards smaller diffraction angle as compared to XRD pattern of ZnO nanoparticles. According to the reported literature this shift in the peak positions of Ce doped ZnO nanoparticles indicate in the change of lattice parameters values than ZnO nanoparticles. The lattice parameters were also calculated from these XRD patterns. The lattice parameters of Ce doped ZnO nanoparticles are a = 3.2457, c = 5.2019 and ZnO nanoparticles are a = 3.2435, c = 5.1984. The shift in the peak position of XRD data and increase in the lattice parameters reveals that Ce^{3+} ions (1.01Å) with bigger ionic radius have been successfully integrated into the Zn^{2+} ions (0.74Å) sites [32]. The formation of nanocrystalline ZnO and Ce doped ZnO were reflected through the broadening of the XRD characteristic lines for ZnO and Ce doped ZnO. So the average size of nanoparticles were calculated by using Debye-Scherrer's equation ($D = k\lambda/\beta \cos\theta$, k=0.99 for spherical particles). In this equation D is the average crystallite size, λ is the X-ray wavelength, θ is the Bragg's angle and β is the FWHM of the peak. The average size of ZnO nanoparticles and Ce doped ZnO nanoparticles was 22 nm.

4.3.2 Morphological Studies

The contents and compositions of the Ce doped sample were studied by EDX spectra equipped in HRTEM. Fig. 4.4 shows EDX spectra of the Ce doped ZnO nanoparticles. EDX analysis confirmed the presence of Zn, Ce and O element in the sample. The peaks of C and Cu may be due to Cu grid. The atomic percentage of Ce in the sample was estimated as ~ 2.0% which clearly confirmed that the Ce dopant was successfully incorporated into the ZnO nanoparticles.

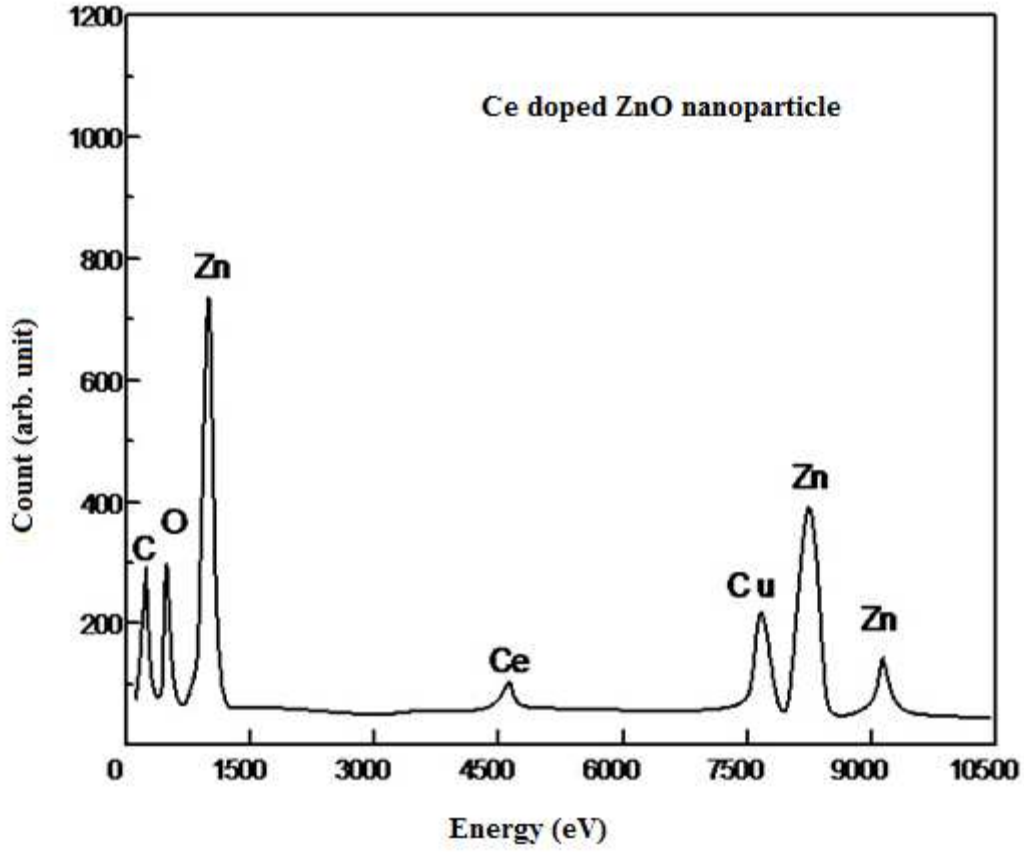

Figure 4.4: EDX image of Ce doped ZnO nanoparticles.

Fig. 4.5 (a) and (b) shows the TEM images of the ZnO nanoparticles and Ce doped ZnO nanoparticles. In both the images, no considerable difference was observed. In both characterizations, almost spherical nanoparticles were observed. The average size of nanoparticles was around 20 nm. In both cases the ZnO nanoparticles and Ce doped ZnO nanoparticles were observed in the size range of 20–60 nm.

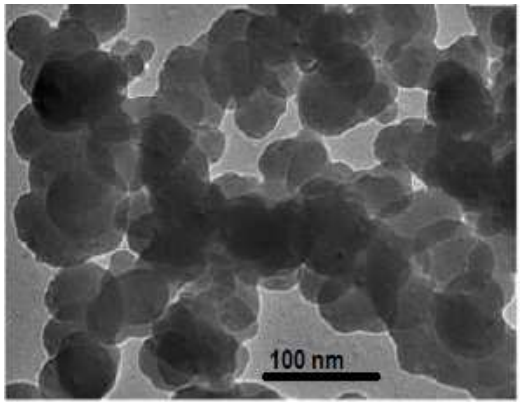

Figure 4.5 (a): TEM image of ZnO nanoparticles.

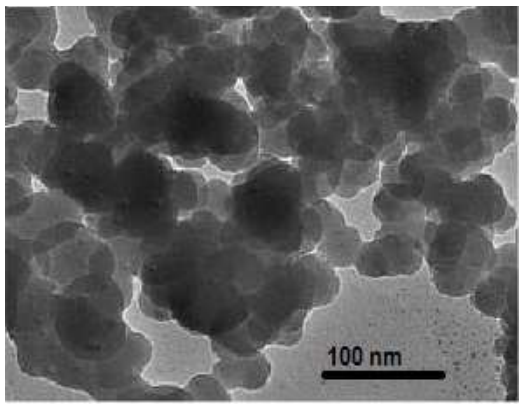

Figure 4.5 (b): TEM image of Ce doped ZnO nanoparticles.

4.3.3 Optical Studies

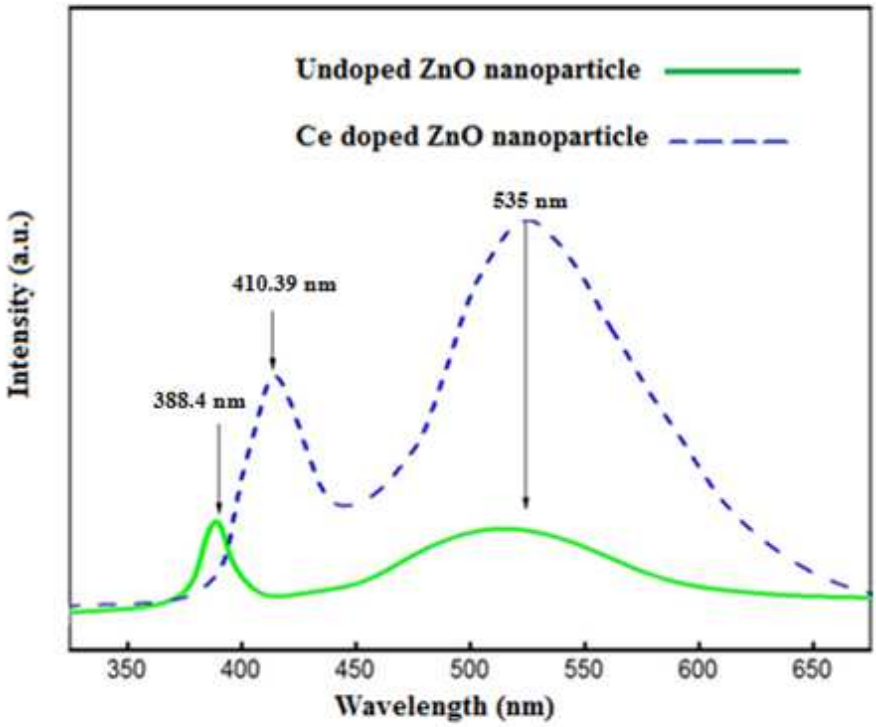

Figure 4.6: PL spectra of ZnO nanoparticles and Ce doped ZnO nanoparticles.

Fig. 4.6 shows the PL spectra of ZnO nanoparticles and Ce doped ZnO nanoparticles. The PL spectra of ZnO nanoparticles contain two strong emission peaks at UV (388.4 nm) and visible range (535 nm). The UV emission is due to the NBE emission of ZnO, which generates from the recombination of exciton- exciton through collision process [273]. The emission in the visible range is referred to as a green emission, which is the emission outcome from the radiative recombination of a photogenerated hole with an electron occupying the oxygen vacancy. This green emission is due to the defects i.e. oxygen vacancy, zinc vacancy, oxygen interstitial, zinc interstitial. Oxygen vacancies arise in three diverse charge states: a neutral oxygen vacancy (V_O), a singly ionized oxygen vacancy (V_O*) and a doubly ionized oxygen vacancy (V_O**) [274]. Vanheusden et al. [275] found that singly ionized oxygen vacancies are responsible for the green luminescence in the ZnO. On comparing the PL spectrum of Ce doped ZnO nanoparticles with the peak for ZnO nanoparticles, the peak position of

the UV emission shifts to a higher wavelength region (from 388.4 nm to 410.39 nm). The change in the peak position of UV emission is recognized to an increase in the concentration of Ce ion in ZnO nanoparticles [276]. In the PL spectra of Ce doped ZnO nanoparticles new emission spectra are developed which leads to the red shift in the UV emission [277, 278]. In addition the broad green emission also exists in the spectra which originate by Ce ion introduced into the ZnO nanoparticles i.e. electron energy transition from 5*d* to 4*f* orbital's in the Ce^{3+} ions. From this analysis Fig. 4.6 suggest that after doping of Ce ion in ZnO nanoparticles, the band gap of ZnO nanostructure can be tailored significantly.

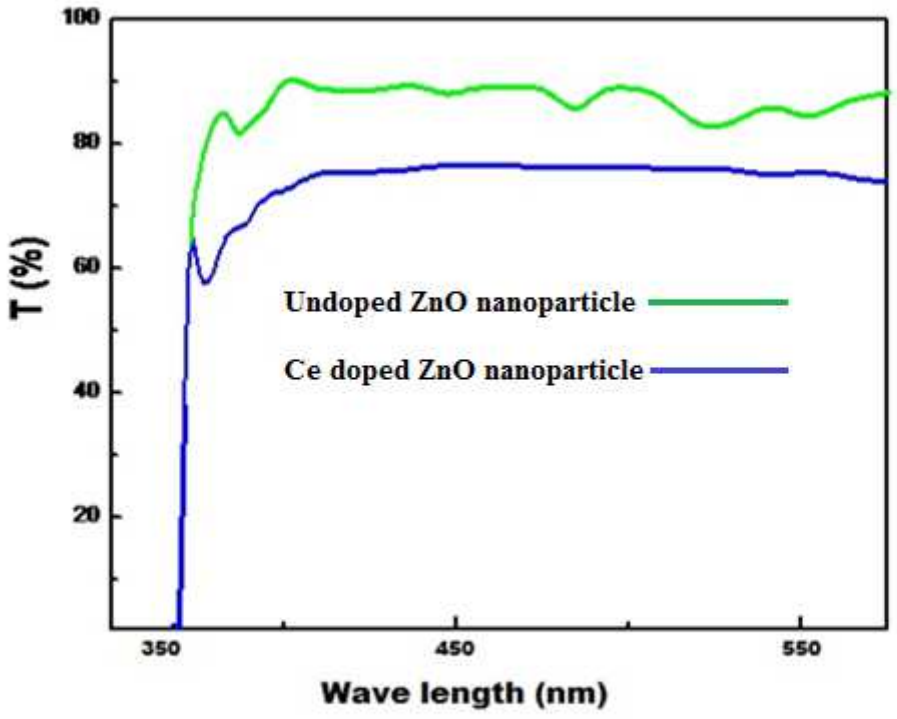

Figure 4.7(a): Transmission spectra of ZnO nanoparticles and Ce doped ZnO nanoparticles.

Fig. 4.7(a) shows the optical transmittance spectra of the ZnO nanoparticles and Ce

doped ZnO nanoparticles, which were measured at room temperature in 300-800 nm wavelength range using a UV/VIS spectrophotometer. The energy band gap of the ZnO nanoparticles and Ce doped ZnO nanoparticles were calculated from the transmittance spectra using Tauc relation. For determination of band gap we have plotted a graph between $(\alpha h\nu)^2$ vs $h\nu$ as shown in Fig. 4.7(b). The extrapolation of straight line on the energy ($h\nu$) axis gives a band gap for ZnO nanoparticles and Ce doped ZnO nanoparticles respectively at 3.35 eV and 3.2 eV. This clearly indicates a significant reduction in band gap after doping of Ce ion in ZnO. The net reduction in the band gap energy, upon Ce insertion, could be due to the formation of Ce related, localized, density of states closer to the conduction band minima of ZnO. Such localized electronic states have also been reported to form the new unoccupied molecular orbitals and facilitate band gap reduction of host compound [279].

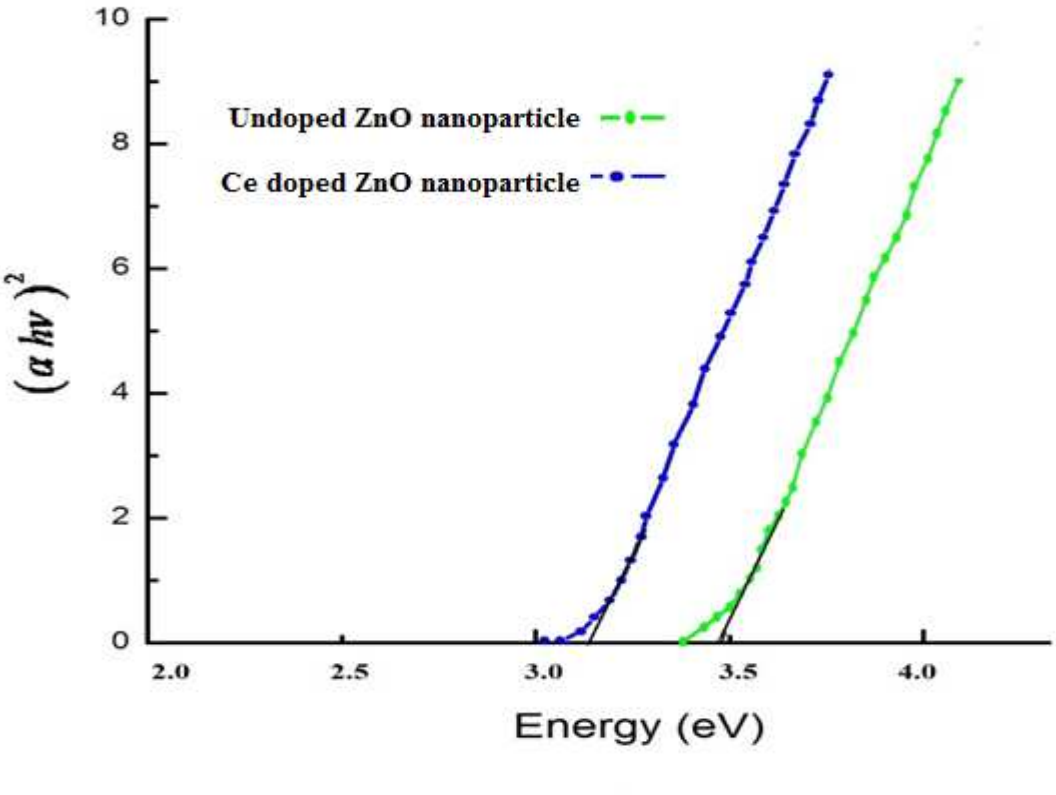

Figure 4.7(b): Determination of band gap of ZnO nanoparticles and Ce doped ZnO nanoparticles.

4.3.4 Magnetic Studies

Fig. 4.8 shows the magnetization curves of ZnO nanoparticles and Ce doped ZnO nanoparticles at room temperature. The ZnO nanoparticles demonstrate a diamagnetic behavior at room temperature, as indicated by magnetization curve shown in Fig. 4.8. It was observed that the Ce doped ZnO nanoparticles exhibit noticeable ferromagnetism at room temperature with Ms=0.023 μB/Ce and Hc=155 Oe, as shown in Fig. 4.8. The ferromagnetism at room temperature was rarely reported in the RE ions doped ZnO nanostructures [265]. To the best of our knowledge, this study is one of the preliminary description about ferromagnetism at room temperature of Ce doped ZnO nanoparticles. The faithful cause of this ferromagnetism is not clear until now due to be short of theoretical work.

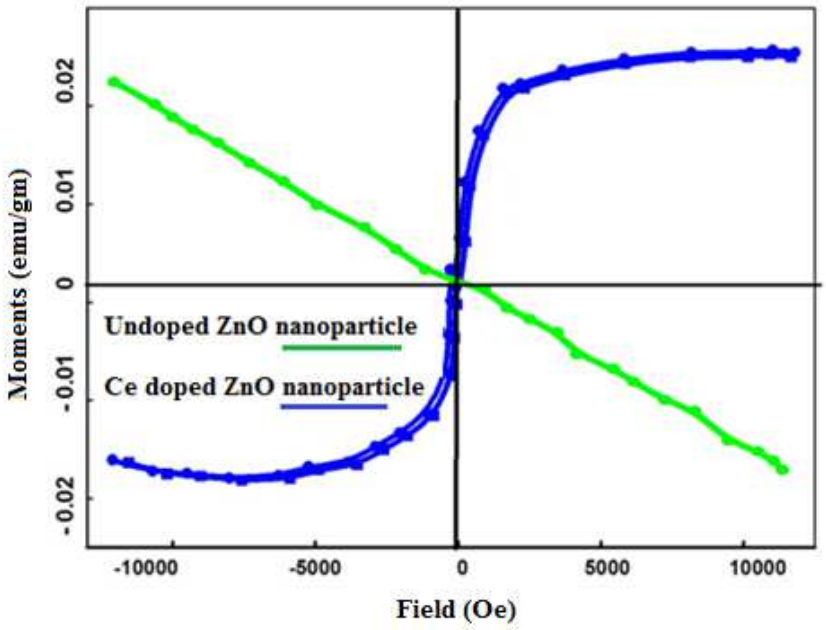

Figure 4.8: Ferromagnetism curve of ZnO nanoparticles and Ce doped ZnO nanoparticles.

RE atoms have incompletely filled 4*f* orbitals that bring magnetic moments and may get part in magnetic coupling as in the case of transitions metals with incompletely filled 3*d* orbitals which are delocalized, robustly direct exchange interactions and have high Curie temperature, but regularly the orbital momentum is zero, leading to small total magnetic moment per atom [280, 281]. The 4*f* electrons are localized,

exchange interactions are not direct via 5*d* or 6*s* conduction electrons, and the high orbital momentum leads to high total magnetic moments per atom. It is likely that the magnetic coupling strength of the *f* orbitals is much weaker than that of the *d* orbitals due to the stronger localization of the *f* electrons. Ce atom that has atomic configuration $1s^2 2s^2 2p^6 3s^2 3p^6 3d^{10} 4s^2 4p^6 4d^{10} 5s^2 5p^6 4f^1 5d^1 6s^2$ is a fascinating RE element that has equally incompletely filled 4*f* and 5*d* orbitals, which can take part in a new coupling mechanism happening via intra-ion 4*f*-5*d* swap over interaction, followed by inter-ion 5*d*-5*d* coupling mediated through charge carriers to show the observed ferromagnetism [265].

4.4 CONCULISON

To summarize, ZnO nanoparticles and Ce doped ZnO nanoparticles were synthesized by the chemical precipitation method. The XRD results exhibit that the ZnO nanoparticles and Ce doped ZnO nanoparticles were in hexagonal wurtzite phase and unnecessary Ce related compounds were not formed during the growth of Ce doped ZnO nanoparticles. EDX analysis showed the presence of the Ce ion into the ZnO lattice sites. The particle sizes estimated by TEM were in range of 20-60 nm. PL measurement of Ce doped ZnO nanoparticles revealed the red shift in the UV emission and green emission band for visible emission. UV-visible spectroscopy exhibited a considerable drop in the band gap after doping of Ce ions in ZnO nanoparticles. When observed keenly, it was found that the characteristic of ferromagnetism was prominent in Ce doped ZnO nanoparticles which was not at all visible in ZnO nanoparticles. It is projected that synthesized Ce doped ZnO nanoparticles could present a new potential application in the field of optical materials and spintronics in the future.

CHAPTER V

STRUCTURAL, OPTICAL AND MAGNETIC STUDIES ON Er DOPED ZnO NANOPARTICLES

5.1 INTRODUCTION

In recent years, great deals of research efforts have been done on developing uniquely versatile metal oxide nanomaterials with superior properties which are not observed in conventional materials in technological applications. ZnO is one of the most comprehensively studied materials in this category of II-VI semiconductors due to its high direct band gap ~3.4 eV, large exciton binding energy (60 meV) and a large conducting range from 10^{4}-10^{-12} ohm cm. In optoelectronic devices, ultraviolet lasers, gas sensors, solar cell, photo catalyst and light emitting diodes; ZnO is the most widely used due to its direct wide band gap energy, high electron mobility and luminescence etc. [282–286]. This oxide is economical, environment friendly having high sensibility, low cost and revealing a high thermal and chemical stability, which makes it even more usable and acceptable [287, 288]. In the present times, the greatest concern of researchers is to remove hazardous pollutants from air and water and ZnO has reflected better photocatalytic efficiencies in comparison to TiO_2, which can remove organic compounds in water matrices based on its larger initial activity rates and its efficient absorption of solar radiation [289, 290].

The crystal structure, morphology, size and surface defects are the important characteristics on which the properties of ZnO nanostructures depend. It's been proved that alteration of ZnO nanostructures could enrich their properties through doping of transition metals or RE elements [95, 291–294]. If RE elements are integrated into suitable matrices; which is an emerging topic of eminence for their partially filled 4*f* shells surrounded by completely filled 5*s* and 5*p* shells, their intra 4*f*–4*f* optical transitions become possible [295]. The modification with the incorporation of dopant ions significantly enhanced the photocatalytic and sensing performance of ZnO [296, 297]. Undoped ZnO exhibits the diamagnetic behaviour whereas the transition or RE element doped ZnO has been detected to exhibit ferromagnetic characteristic at room temperature [298–302]. The extensive studies

about RE elements doped ZnO is conducted for industrial application in the field of spintronic, photoluminescence, laser, fibre amplifier and so on [303–307]. Er, out of the various RE elements, is an important focus of attention because of its enormous potential in various applications. Although ZnO is a good matrix material to host the Er ions as it is not only responsible for the allowance of 4*f* transition, prohibited in isolated atom but also for the reason that it enhances the emission yield for the transition [308, 309].

Considering the above as base, this work explores the fact that using a simple chemical precipitation technique, undoped ZnO and a series of Er doped ZnO samples were prepared. Until now, RE doped ZnO nanostructures have been synthesized by different methods such as pulsed laser deposition, magnetron synthesis, chemical vapour deposition, spray pyrolysis, solution combustion and vapour transport route [310–313]. An important role is played by the synthesis method in enhancing the properties of materials. The production of huge amounts of high uncontaminated samples at low cost is facilitated by the conventional chemical precipitation method. Present work exposes and diminishes the controversies that still exist regarding whether RE elements could be incorporated into the semiconductor nanocrystals or not, and if; whether efficient energy transfer from the ZnO host to RE element could occur or not. This work exhibits that doping of Er ion can be effectively done in ZnO nanostructures with some parameters of chemical precipitation method such as solution properties, mixing rate, pH value and drying treatment. The prepared samples were characterized by XRD, HRSEM, EDX, UV/vis spectroscopy, PL and VSM. The improved structural transformation, luminescence, ferromagnetism characteristics and a decrease in band gap energy has been reported in this study. Its low cost, high yield and ability to attain high purity in fabrication of undoped ZnO and Er doped ZnO nanostructures proved that chemical precipitation is a highly advantageous method.

5.2 EXPERIMENTAL DETAILS

5.2.1 Synthesis Procedure

In the present investigation, Er doped ZnO and the undoped ZnO powders were prepared via the chemical precipitation route. All the reagents used were of analytical grade (Sigma-Aldrich) without further purification. Er doped ZnO powders were prepared by zinc acetate [$Zn(CH_3COO)_2.2H_2O$; 99.5% purity], erbium(III) oxide

[Er_2O_3; 99.9% purity], sodium hydroxide [NaOH; 98% purity] and ammonium hydroxide [NH_4OH; 99.99% purity]. Four batches of samples were prepared by varying the different molar concentration of doping erbium oxide in zinc acetate as 1, 3, 5 and 7 at.%. As per described Er doping concentration, the calculated amount of erbium oxide solution was added to zinc acetate solution. In this foundation solution, 1 M solution of ammonium hydroxide and sodium hydroxide was added drop-wise. The ammonium hydroxide and sodium hydroxide were used as OH^- source for forming the complexes and to control the pH value of solution respectively. During the entire process, magnetic stirring was carried out to achieve the precipitate of Er doped ZnO samples. Undoped ZnO powder was formed by zinc acetate, sodium hydroxide and ammonium hydroxide. Zinc acetate and ammonium hydroxide were dissolved into DI water with magnetic stirring until they form clear solutions. Sodium hydroxide (1M) solution was added drop-wise into the prepared clear solution of zinc acetate and ammonium hydroxide with constant magnetic stirring. In both cases, these precipitates were thoroughly washed several times with DI water to remove the unwanted ions. These washed precipitates were dried at 60°C for 2 hours. These dried precipitates were grinded and added 100 ml DI water and again dried at 60°C for 40 hours followed by normal cooling up to the room temperature; then final powder products were collected carefully. As per the established literature on chemical precipitation technique, the formation and controlling of undoped and Er doped ZnO nanostructures is critical. Due to this reason, the slow mixing of reactants and the pH value (~ 12) of all samples were kept constant during synthesis process. As illustrated by the flow chart, the synthesis procedure for the undoped ZnO and Er doped nanostructures via chemical precipitation method are shown in Fig. 5.1 and 5.2.

The crystalline phase and structural information of prepared samples were studied by using a Bruker D8 Advance X-ray diffractometer with CuKα radiation of wavelength λ=0.15405 nm. All XRD measurements were performed in the range of 2θ =20-90° at a scan speed of 3°/min at room temperature. Surface morphology and chemical composition of samples were investigated by using a JEOL JEM-2100F HRSEM equipped with EDAX equipment. The nanostructures were also analyzed by dissolving Er doped ZnO nanostructures in DI water followed by ultrabath sonication for 20 minutes. The samples were subjected to optical characterizations. The UV-visible spectra of prepared samples were carried out by using JASCO UV-Vis

spectrometers (Model-Lambda). PL measurements of prepared samples were made by employing Lab RAM UV-Vis-NIR spectrometer Horiba Yvon having The-Cd 325 nm. Magnetic properties of the synthesized samples were obtained from VSM at room temperature.

5.2.2 Mechanism of Synthesis

In continuation with the previous subsection 4.2.2, here we present the reaction process and mechanism applicable for the formation of undoped ZnO and Er doped ZnO nanostructures.

First of all, for the synthesis of ZnO nanostructures, the basic chemical reaction given as:

I step: $Zn(CH_3COO)_2 + NH_4OH \rightarrow Zn(OH)_2 + NH_4(CH_3COO)_2$

Additional slow mixing of aqueous solution of sodium hydroxide to the products of I step reaction gives rise to zinc hydroxide to give ZnO precipitate:

II Step: $Zn(OH)_2 + NH_4(CH_3COO)_2 + 2NaOH \rightarrow ZnO\ (ppt) + 2(CH_3COO)Na + NH_3 + H_2O$

The reduction of zinc hydroxide is preceded by the condensation process which causes the creation of ZnO precipitate. The rest of sodium acetate and ammonia are disposed off and precipitate of ZnO nanostructures is collected. Therefore the final chemical reaction showing the synthesis of ZnO nanostructures is shown by the summation of above mentioned steps.

$Zn(CH_3COO)_2 + 2NaOH + NH_4OH \rightarrow ZnO\ (ppt) + 2(CH_3COO)Na + NH_3 + 2H_2O$

Similarly the basic chemical reaction governing the formation of Er doped ZnO is as follows:

$(1- x)\times[Zn(CH_3COO)_2] + x\times[Er_2O_3] + 2(1-x)\times[NaOH] + 2(1-x)\times[NH_4OH] \rightarrow Zn_{1-x}Er_xO + 2(1-x)\times[CH_3COONa] + 2(1-x)\times[NH_3] + (1-x)\times[H_2O]$

'x' represents the Er doping concentration in the reaction.

In our study x = 0.01-0.07 for 1-7% Er doping. The balanced chemical reaction is as follows:

$[Zn(CH_3COO)_2] + [Er_2O_3] + 2\ [NaOH] + 2\ [NH_4OH] \rightarrow ZnEr_2O_4 + 2\ [CH_3COONa] + 2\ NH_3 + 3\ [H_2O]$

The Gibbs free energy for above reactions ($\Delta G_{reaction}$) can be evaluated as:

$$\Delta G_{reaction} = \Delta G_{products} - \Delta G_{reactants}$$

As the synthesis of undoped ZnO and Er doped ZnO nanostructures is made at room temperature, the values of Gibbs free energy of formation ($\Delta_f G$) of various ingredients is at standard conditions, The Gibbs free energy of reactions for the formation of undoped ZnO and Er doped ZnO is estimated by using the method suggested in literature [212], and found to be negative in magnitude, which is interpreted that such reactions will be favoured and will release energy during the spontaneous formation of undoped ZnO and ZnO:Er nanostructures. The flow charts for the synthesis of undoped ZnO and Er doped ZnO nanostructures are presented through the Fig. 5.1 and 5.2.

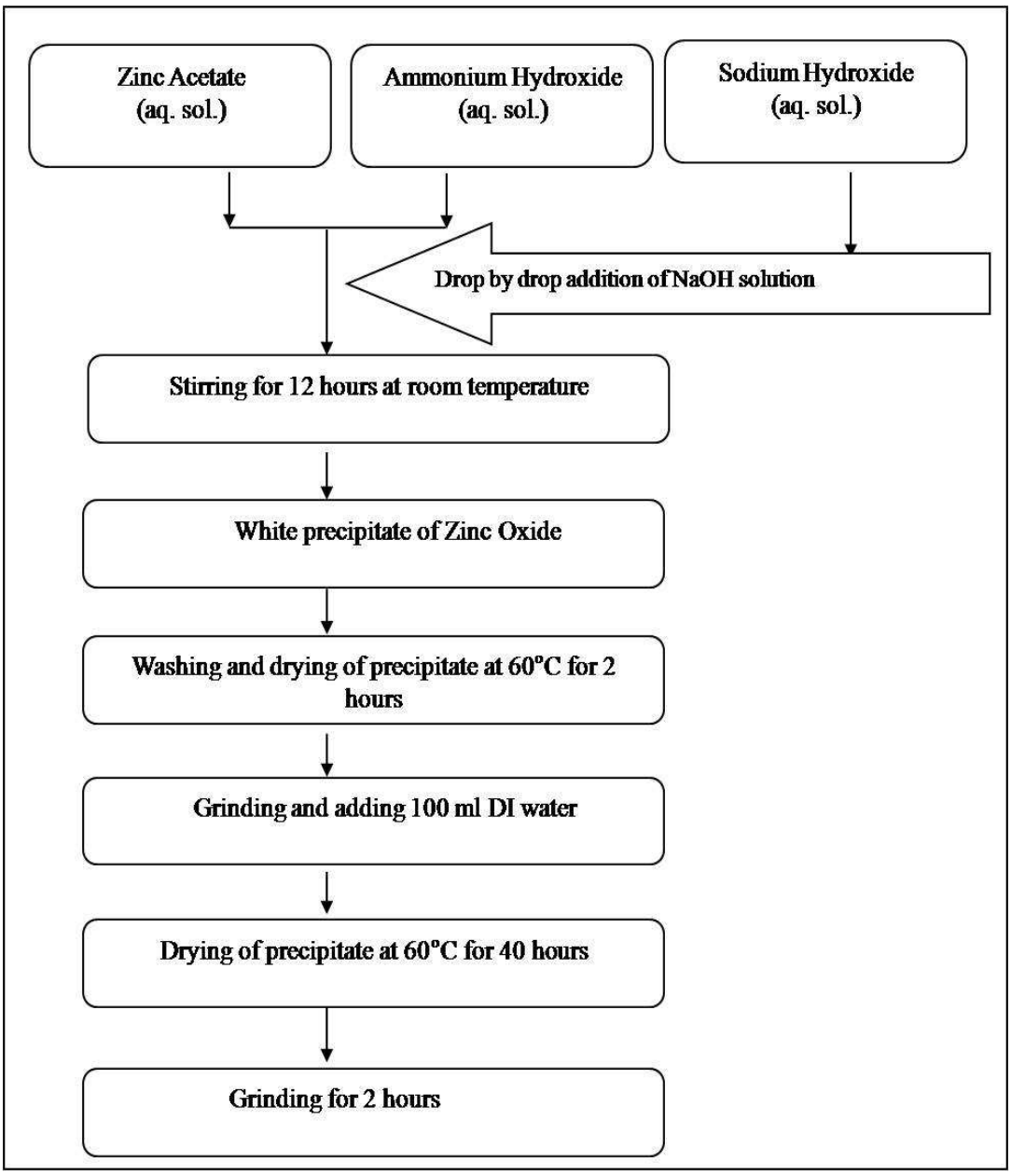

Figure 5.1: Flow chart for the synthesis of ZnO nanostructures.

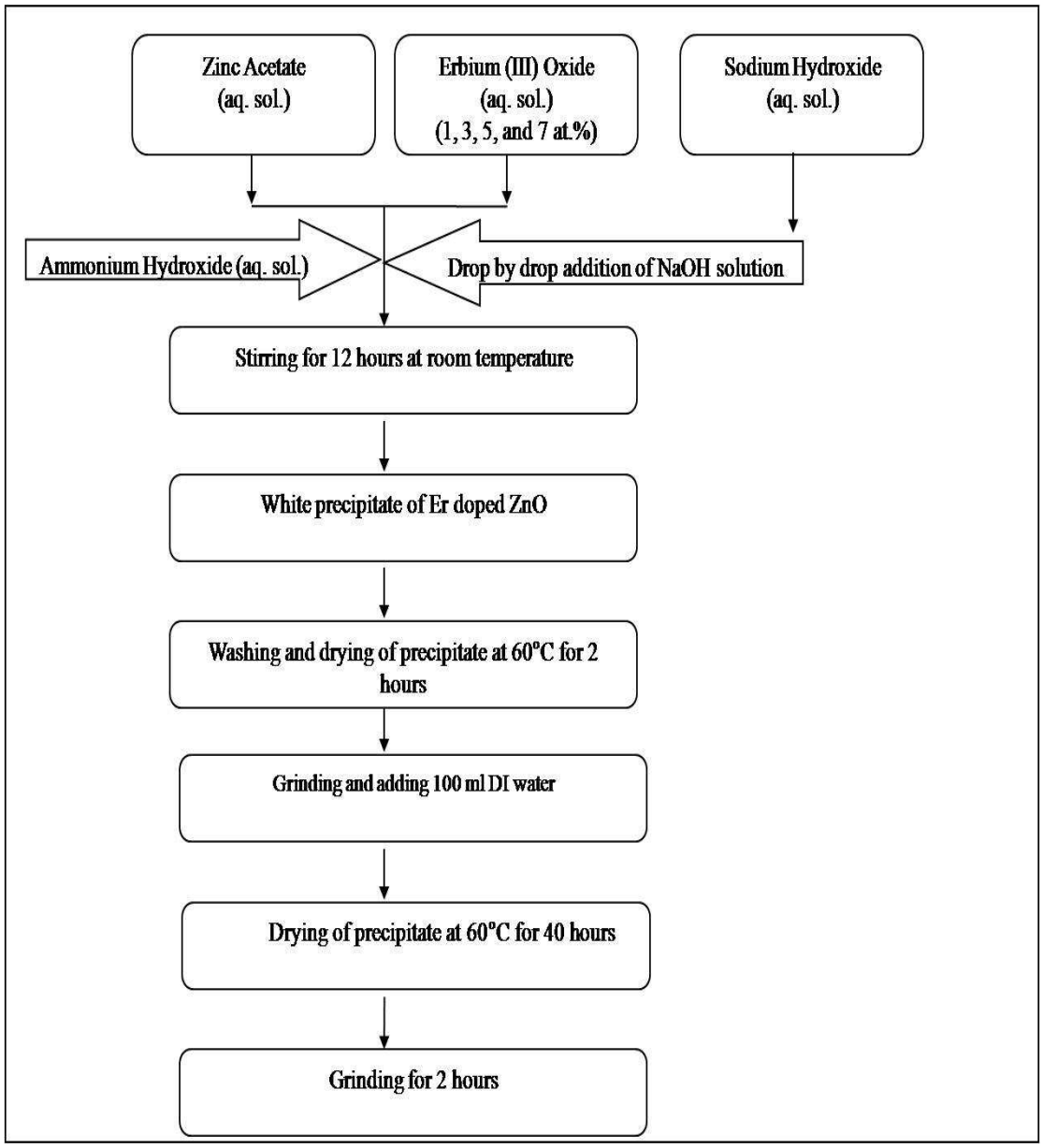

Figure 5.2: Flow chart for the synthesis of Er doped ZnO nanostructures.

5.3 RESULTS AND DISCUSSION

5.3.1 Structural Studies

The XRD patterns of undoped ZnO and Er doped nanostructures [$Zn_{1-x}Er_xO$, where x =1, 3, 5 and 7 at.%.] have been analysed for crystallographic and structural information. Powder XRD patterns of undoped ZnO and Er doped ZnO samples are plotted against intensity versus 2θ in range of 30-75° in the Fig. 5.3 (i). All the patterns are in close agreement with the standard XRD data (JCPDS file no. 36-1451) indicating the hexagonal wurtzite structure. The prominent diffraction peaks observed at 31.79°, 34.52°, 36.24°, 47.60°, 56.58°, 62.95°, 68.04°, and 69.12° respond from lattice planes (100), (002), (101), (102), (110), (103), (112) and (201) respectively. The graph shows that Er^{3+} ions sit at the host Zn^{2+} sites without disturbing the wurtzite structure because no extra peaks are obtained from Er related second phase than those of ZnO such as Er_2O_3. The peaks in the diffraction pattern of Er doped samples show slightly shifting towards lower angles as compared to undoped ZnO. The trend of (101) peak shifting with different Er doping as shown in Fig. 5.3 (ii), is of particular interest here. This shifting indicates that the lattice parameter increases with the Er doping which is an expected result because the ionic radius of Er^{3+} (0.88Å) is greater than the ionic radius of Zn^{2+} (0.74Å). The average crystallite size of samples has been calculated, using the Debye Scherrer's formula: $D = \frac{0.9\lambda}{\beta \cos\theta}$

where λ is wavelength of the CuKα radiation (0.15405 nm), β and θ are the FWHM and the diffraction angle of the observed peaks using the diffraction intensity of (101) lattice plane. In order to examine the doping effect of Er concentration on the crystal parameters of prepared nanostructures, the lattice parameters, bond length and volume of unit cell for hexagonal system have been calculated using lattice geometry equation.

$$\frac{1}{d^2} = \frac{4}{3}\left(\frac{h^2 + hk + k^2}{a^2}\right) + \frac{l^2}{c^2}$$

where d is the inter-planer spacing between the planes and h, k and l are miller indices. The bond length (Zn–O) can be calculated using this formula,

$$l = \sqrt{\frac{a^2}{3} + (0.5 - u^2)c^2}$$

where a and c are lattice constants of ZnO and u is the wurtzite structure parameter which can be calculated as,

$$u = \left(\frac{a^2}{3c^2}\right) + \frac{1}{4}$$

In addition, the volume of unit cell has been calculated using the formula,

$$V = 0.866a^2c$$

All these parameters of samples are summarized in Table 5.1. From the table 5.1, no fixed pattern of variation in the calculated crystal parameters could be observed for these nanostructures on comparing previously reported literature [42, 47, 48]. Only a fixed increasing pattern in D (crystallite size) is observed from 0 to 7 at.% Er doped ZnO. But as the doping concentration increases, the slight variation in lattice constants, bond length and volume of unit cell could be due to Zn and Er ionic size mismatch and the replacement of Zn^{2+} ions with the Er^{3+} ions in the crystal lattice.

Table 5.1: Average crystallite size, lattice constants, bond length and cell volume of undoped ZnO and Er doped ZnO samples

Concentration of Er (%)	Average crystallite size D (nm)	Lattice constant c (Å)	Lattice constants a=b (Å)	Bond length of anion-cation L (nm)	Cell volume V (Å^3)
0	15.99	5.2817	3.2344	1.9806	47.8846
1	17.03	5.2866	3.2374	1.9825	48.0196
3	17.57	5.2824	3.2348	1.9809	47.9022
5	21.10	5.2786	3.2324	1.9794	47.7959
7	27.84	5.2836	3.2355	1.9813	47.9357

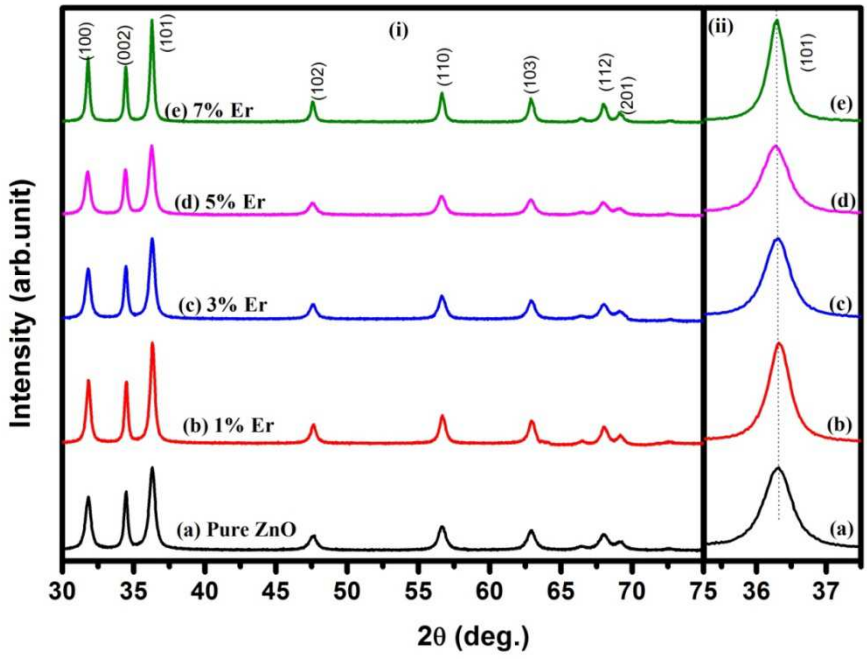

Figure 5.3: (i) XRD pattern of (a) undoped ZnO, (b) 1, (c) 3, (d) 5, and (e) 7 at.% Er doped ZnO nanostructures, (ii) Shifting of (101) peak for respective nanostructures.

5.3.2 Morphological Studies

In order to confirm the presence of Er^{3+} ion and determine its chemical composition, EDX analysis of Er doped samples was carried out. The EDX of 1 and 5 at.% Er doped samples is shown in Fig. 5.4 (a) and (b). For accuracy, EDX measurement was carried out at a number of locations all over the sample. From EDX analysis the presence of Zn, Er and O elements were confirmed in the sample. According to the EDX analysis Zn and Er contents in the composition of 1 and 5 at.% Er doped samples are close to the proposed doping concentration. All the above results of XRD and EDX indicate that the Er^{3+} ions are effectively doped into the crystal lattice of ZnO matrix without forming erbium oxides or any other impurities at the surface of ZnO.

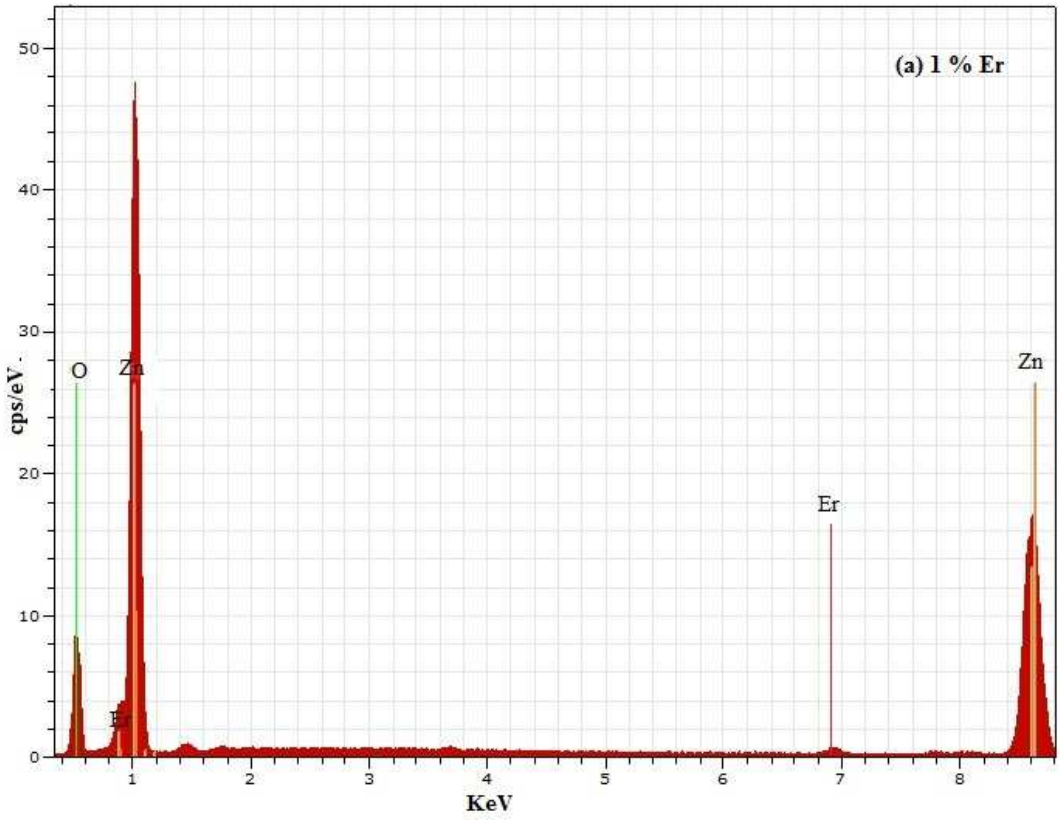

Figure 5.4 (a): EDX spectrum of 1 at.% Er doped ZnO nanostructures.

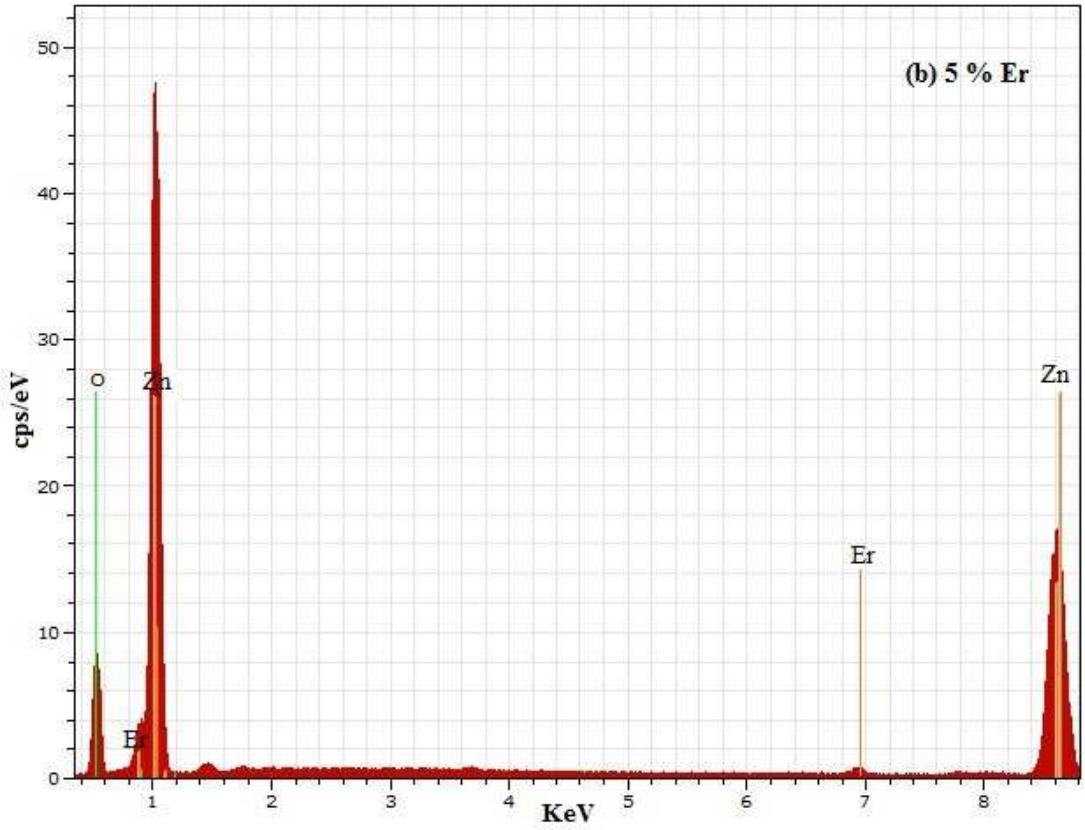

Figure 5.4 (b): EDX spectrum of 5 at.% Er doped ZnO nanostructures.

The morphological features of prepared samples were carried out by using HRSEM images. The incorporation of Er ion in Zn lattice sites makes the changes in the morphology of crystallites. Fig. 5.5 (a-e) shows HRSEM images of undoped ZnO and Er doped ZnO samples, where structures are in the nm range. The distribution of sizes as well as shape is irregular and this may be due to the damages occurred in the re-crystallisation or coalescence of nanostructures in formation of larger agglomeration of ZnO lattice during the heating process. As shown in Fig. 5.5 (a), the surface texture of undoped ZnO is irregular in shape and is found to be in 50 nm range.

It is observed that the doping of Er with ZnO remarkably changed the morphology of the nanostructures from nanorods-like to nanocones-like, as shown in Fig. 5.5 (b-e). For 1 at.% Er doped ZnO nanorods of approximately 100 nm long and 25 nm thick are observed in Fig. 5.5 (b), which is similar to undoped ZnO nanostructures, influence of Er doping on size or shape is not observed at this stage. For 3 at.% Er doped ZnO nanorods of approximately 200 nm long and 50 nm thick are seen in Fig. 5.5 (c). Infact onset of structural transformation is evident for 3 at.%

Er. At this stage, enhanced Er doping induced anisotropic growth not only causes the formation of nanorods but here onwards, the evolution of nanocones initiates as marked through the dashed lines in Fig. 5.5(c). The systematic transformation continues with further Er doping and is vividly evident for 5 and 7 at.% Er doped nanostructures, as shown respectively through Fig. 5.5(d-e). The dominant growth of structure for 7 at.% Er doping is demonstrated clearly through the formation of approximately 400 nm long and 70 nm thick structure of nanocones-like as exhibited in Fig. 5.5(e).

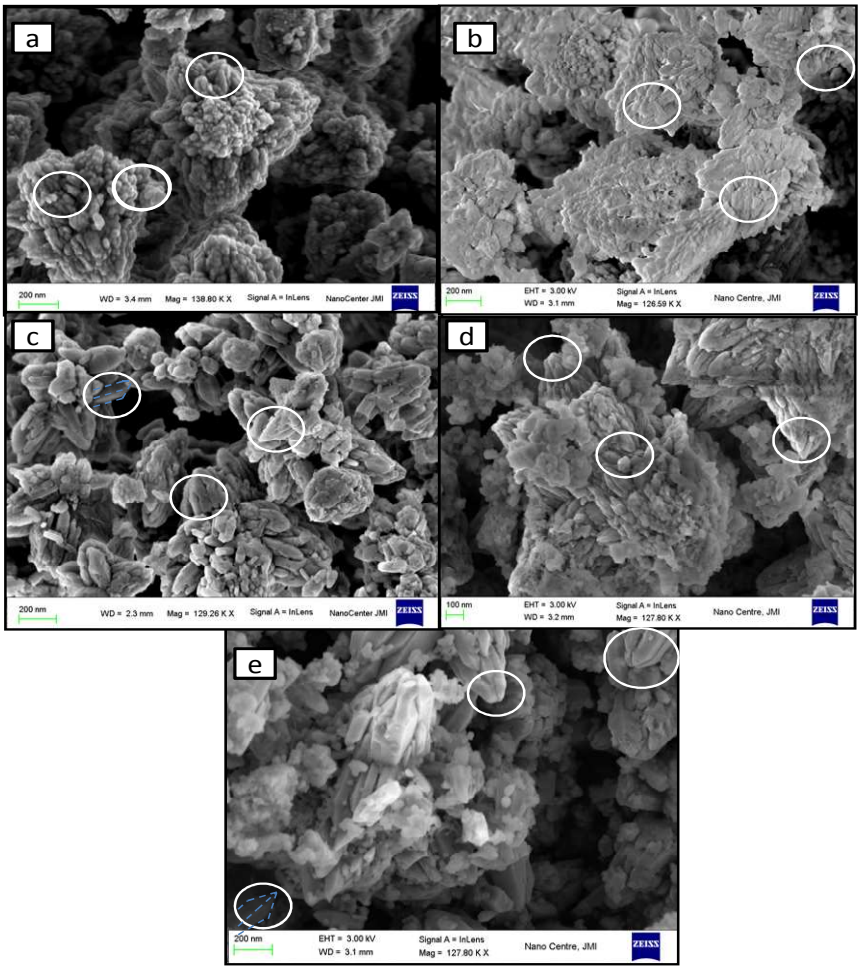

Figure 5.5: HRSEM images of (a) undoped ZnO, (b) 1, (c) 3, (d) 5, and (e) 7 at.% Er doped ZnO nanostructures.

Therefore the observed changes in structure can only be attributed to the effect of dopant, which might act as structure driving agents through selectively adsorbing

onto ZnO crystalline planes. Structurally ZnO has three types of crystalline planes - two non-polar $(2\bar{1}\bar{1}0)$ and $(01\bar{1}0)$ planes and a polar (0001) basal plane. The polar basal plane has high surface energy as compared to non-polar planes [314]. Furthermore, under thermodynamic equilibrium condition, the facets with higher surface energy are usually smaller in surface area whereas the lower energy facets are larger [315]. Therefore the growth of crystals in c axis direction is faster which leads to the formation of nanorod to nanocone shape crystal as it is indicated in Fig. 5.5(b-e).

5.3.3 Optical Studies

As doping is an effective way to alter the optical and electrical properties of semiconductor materials and to further improve the performance of their optoelectronic devices, RE elements have always attracted a large group of researchers [316-326]. RE elements such as Eu, Tb, Yb, and Nd are the famous visible luminescence centers once they are incorporated into the host matrix [316-318]. Therefore, it is widely expected that doping of RE element into the ZnO lattices would open channels for efficient visible light emissions [316]. Recently, Eu^{3+} ion as one of the most famous red emitting activators has been successfully incorporated into the ZnO nanoparticles, nanorods arrays, and nanospheres and most of them provide the red emission at 615 nm due to the intra 4*f* shell $5D_0 \rightarrow 7F_2$ transitions, which makes Eu doped ZnO a promising candidate for the white light-emitting diode and planar display due to their multi-colour emissions [316]. However, there are few reports for Er^{3+} ion doped ZnO nanoparticles [310, 319]. The interest of Er doping originates from the motivation to doping the dissimilar element (here in our case Er) in ZnO lattice due to the huge differences in their ionic radii (Er^{3+} = 0.88Å) and charges between Zn^{2+} and Er^{3+} ions [316]. Thus, based on previous data, it is crucial to detect the changes observed due to Er doping in electronic levels by recording the absorption spectra of UV-visible spectroscopy of the prepared nanostructures (as shown in Fig. 5.6).

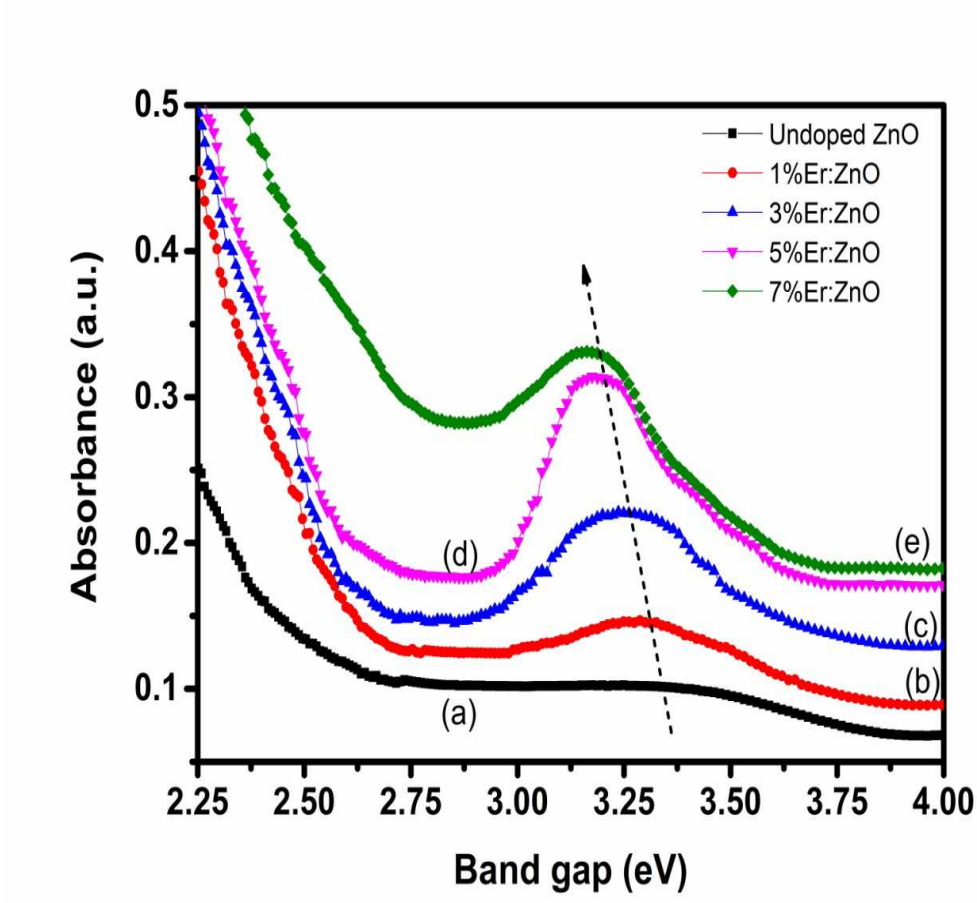

Figure 5.6: Room temperature UV-visible spectra of (a) undoped ZnO, (b) 1, (c) 3, (d) 5, and (e) 7 at.% Er doped ZnO nanostructures. The red shift in band gap is depicted by the line with dotted arrow with increasing Er doping.

As shown in Fig. 5.6 (a), one can observe a small hump at 3.34 eV (371 nm) for undoped ZnO nanostructures. This shows that the prepared nanostructures are depicting a slight blue shift as compared to bulk ZnO materials ($Bulk_{ZnO}$ = 3.2 eV) [95]. On doping the 1 at.% Er in ZnO (Fig. 5.6 (b)), the band gap shows a slight red shift from 3.34 eV to 3.3 eV (375 nm). This trend of red shift in band gap continues observed at 3.26 eV (380 nm), 3.20 eV (387.5 nm), and 3.19 eV (388.7 nm) for 3, 5 and 7 at.% doping concentration of Er^{3+} ion in ZnO nanostructures (Fig. 5.6 (b-e)) respectively. Our results are in good agreement with the previously published report [310]. Another observation which can be derived from Fig. 5.6 is the corresponding area and peak intensity increase with increasing doping concentration from 1-7 at.% Er in ZnO host lattice. This peak broadening and red shift in band gap signifies the incorporation of Er in ZnO nanostructures [310]. This red shift in band gap prompted us to further perform the luminescence study as is discussed ahead.

Optical properties of ZnO nanostructures become increasingly important as the size of structures is reduced to nanoscale [320]. The parameter related to surface and size confinement effects of nanomaterials not only vary the band gap but also influence their optical transitions, such as luminescence [95]. Generally, ZnO exhibits a visible deep level emission with a peak in the range from 450 to 730 nm [321]. Among the various luminescence properties of ZnO nanoparticles, the green emission around 521 nm is usually reported [320]. Another way to alter the luminescence centres in ZnO is to dope it with either transition elements or with RE elements like Eu, Er [316]. Previously, Eu doping in ZnO lattice pointed out that the host lattice transfer the energy resonantly to Eu^{3+} ion by trapping as oxygen vacancy and energy storage centers [316]. Furthermore, doping of RE elements helps in revealing the fundamental phenomenon of nano-order surface effects by utilizing the PL technique, since it is an effective method to gain a good understanding and systematically investigate the luminescence mechanism and the excitation pathways of the RE^{3+} ions in semiconductor hosts [316]. Therefore, we present the photoluminescence emission spectra of Er doped ZnO nanostructures as shown in Fig. 5.7. In Fig. 5.7, we have labelled the four peaks based on their intensities from peak 1-4 and elaborate their discussions in the order of decreasing intensities.

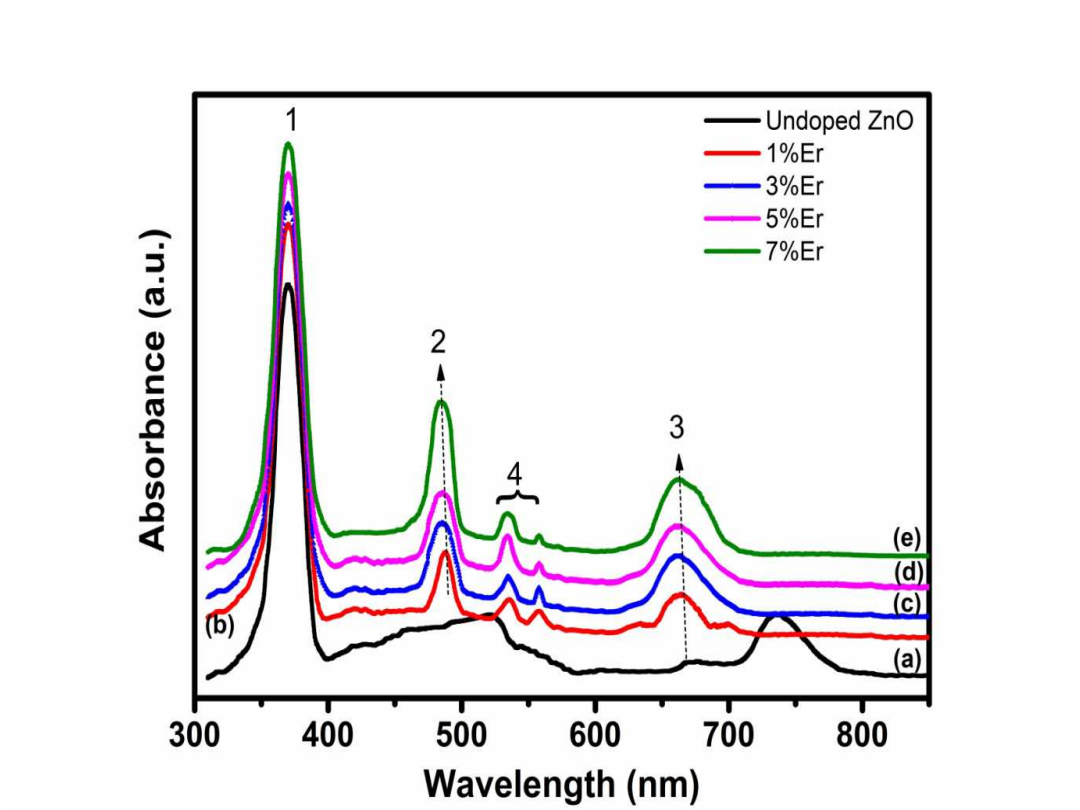

Figure 5.7: Room temperature Photoluminescence emission spectra of (a) undoped ZnO, (b) 1, (c) 3, (d) 5, and (e) 7 at.% Er doped ZnO nanostructures.

First, are defined the transitions occurring in undoped ZnO nanostructures shown by Fig. 5.7 (a). Peak '1' corresponds to the band energy transitions occurring at 371 nm thus depicting the quantum confinement effect of nanosize occurring therein [95]. A huge hump ranging from 400– 600 nm centred at 521 nm is widely reported for green emission. Although a variety of literature is reported for this emission but this peak in undoped ZnO nanostructures is corresponding to the radiative recombination of the photo-generated hole with an electron occupying the oxygen vacancy [320, 322]. As previously reported, for wurtzite structure of ZnO, valence band (VB) lies in O-2p state while Zn have a 4s-O 2p σ* interaction which is mainly responsible for two lowest conduction band (CB), covers a bandwidth of -10 eV. There is dispersion in the VB due to different factors out of which one major reason is overlapping of filled Zn 3d and O 2p orbitals [323]. Since ZnO is an *n*-type semiconductor, most defects are Zn interstitials and oxygen vacancies [95]. It is well known that visible luminescence is mainly due to defects that are related to deep level emissions such as zinc interstitials (I_{Zn}) and oxygen vacancies (V_O) [319]. Visible

luminescence in ZnO is primarily caused by the transition from deep donor level to VB due to oxygen vacancies and by the transition from CB to deep acceptor level due to impurities and defect states [320]. The structure of nanosize ZnO contains large voids, which can easily contain interstitial atoms and thus the appearance of blue emission in prepared ZnO nanostructures appear as a huge hump originating from 400-600 nm depicting the formation of interstitial defects of Zn [324]. ZnO has tightly bound 2p electrons of oxygen and 3d electrons of Zn, which have some attraction affinity [320]. Also, previous first principal calculations concluded that the Zn 3d electrons interact strongly with the 2p electron of O in ZnO structure [325]. As the centre energy of the green peak is different from the band gap energy of bulk ZnO (3.2 eV), this emission cannot be a result of direct recombination of a conduction electron in the Zn 3d band and a hole in the O 2p VB. Therefore, green emission must be related to the local level in band gap [320]. In fact the green emission results from the radiative recombination of photo generated hole with an electron occupying the oxygen vacancy [322]. We now explain the peak observed for orange-red emission around 736 nm corresponds to defects such as V_O [326].

Having explained the origin of green and orange-red emissions in undoped ZnO nanostructures, the changes observed in luminescence properties with Er doping in ZnO lattice is now explain. It has been previously reported that among the different RE ions, Er occupies a relevant position because of its crucial functioning in the upconversion phenomena and the intense 0.8 eV intra-ionic emission usually referred to as the 1.54 μm has a very special importance for the optical communications [310]. On the other hand, ZnO is a good matrix material to host the Er ions since not only is it responsible for 4*f* transitions, which were prohibited in isolated atoms, but also because it improves considerably the emission yield for these transitions [310]. It has been reported that lower dopant concentration leads to a noticeable quantity of nanostructures but also resulted in poor luminescent properties while higher Er concentrations give rise to very irregular and disordered structures [310]. The reason behind this was the probable stresses induced by the large Er ions in the ZnO structure [310]. Also, low doping concentration less than 3 at.% detection limit of XRD is difficult to be examined, as in our case no extra impurity or precursor phase was observed in XRD. But the luminescence characterizations bring out the probable transitions occurring therein. The results are discussed ahead.

As seen in Fig. 5.7 (a-e), the most prominent peaks are labelled as peak '1'. These peaks are observed at 371, 375, 380, 387, and 388 nm for undoped ZnO, 1, 3, 5 and 7 at.% Er doped ZnO nanostructures respectively. These most intense transitions observed in prepared nanostructures correspond to inter band transitions from VB to CB [310]. However, one can notice a slight red shift in the wavelength depicting the similar behaviour observed through UV-visible spectroscopy. Therefore, these peaks are in excellent agreement with UV-visible analysis thus endorsing our results. One can observe the second and third intense peaks, labelled as '2' and '3', respectively in Fig. 5.7 (a-e). These peaks represent the blue and yellowish-red band transitions occurring due to Er doping in ZnO lattice. The intensity of the emission of peak '2' at 488 nm (2.54 eV) increases with increase in Er doping in ZnO nanostructures. This blue emission at 488 nm has been reported for the transfer of energy between Er^{3+} excited ions present in the system and corresponds to $^4F_{7/2} \rightarrow {}^4I_{15/2}$ Er transitions [310]. On the other hand, the peak '3' at 652 nm (1.90 eV) emission is the third intense peak. This band is usually attributed to the oxygen excess taking into account the usage of doping with erbium oxide, is consistent with a major incorporation of oxygen present in dopant ZnO nanostructures [310]. This is also in good agreement with the absence of red band at 736 nm peaks, earlier present in Fig. 5.7 (a) for undoped ZnO nanostructures, for oxygen vacancy in ZnO nanostructures. Lastly, peaks at 558.6 nm (2.22 eV) and 536.8 nm (2.31 eV), corresponding to $^4S_{3/2} \rightarrow {}^4I_{15/2}$ and $^2H_{11/2} \rightarrow {}^4I_{15/2}$ transitions, respectively have much lower intensity as compared to other marked peaks. The relative intensities of these emissions are also a probe of the defect structure and quality of the nanostructures, since it is earlier reported that the transitions and their intensities are sensitive to local configuration of the particular ion involved in the transition and as a result their intensities diminish [310].

5.3.4 Magnetic Studies

To further understand the alternation in magnetic properties of undoped ZnO and Er doped ZnO nanostructures [$Zn_{1-x}Er_xO$, where x =1, 3, 5 and 7 at.%.] systematic room temperature hysteresis loops were recorded and presented in the Fig. 5.8. In the present case, undoped ZnO nanostructures show the diamagnetic behaviour and Er doped ZnO nanostructures expose the ferromagnetic hysteresis loop at room temperature. Since, there is no reason to attribute the introduction of ferromagnetism

to any dopant and moreover in this ZnO case, there is no 3*d* electron involved, one cannot think of any interaction that may originate from that and hence, the undoped ZnO bulk is expected to diamagnetic in nature [327, 328]. Multiple nanostructures of either inorganic or organic systems have been reported to show magnetic properties in the absence of magnetic elements [329-333] and even the suggestion of magnetism as a universal feature at the nanoscale has been proposed [334].

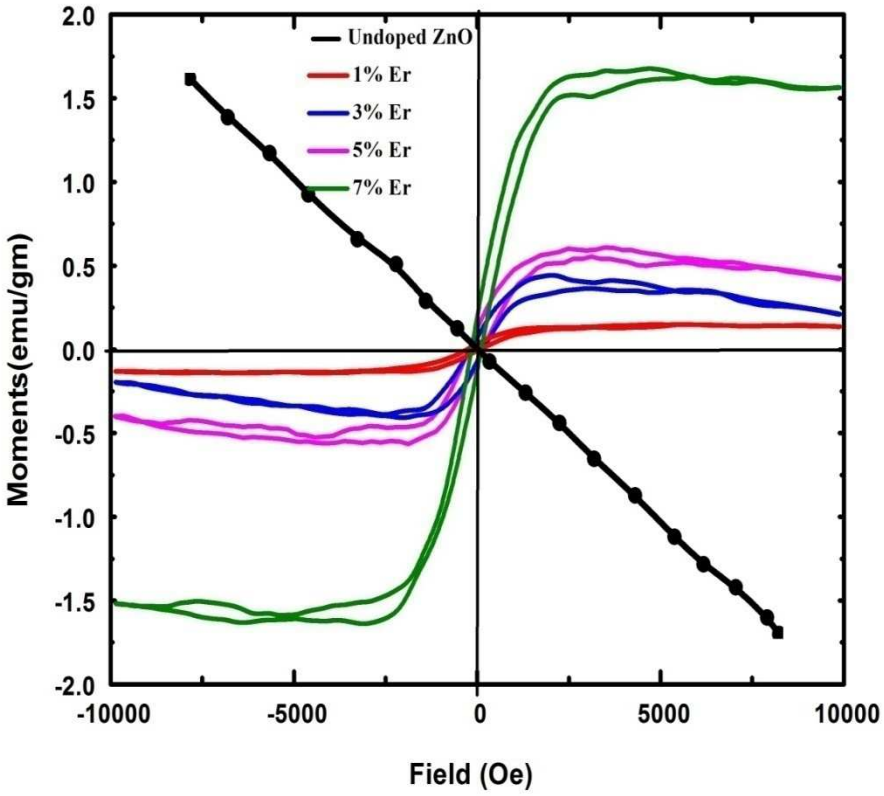

Figure 5.8: M-H curve for (a) undoped ZnO, (b) 1, (c) 3, (d) 5, and (e) 7 at.% Er doped ZnO nanostructures.

This study focuses on the outcome of Er^{3+} ions on the magnetic behaviour of ZnO nanostructures at room temperature. Er is one of the RE elements, which has more than a half filled 4*f* electron shells ($4f^{11}6s^{0}$). We observe that, the saturation magnetization (M_S), remanent magnetization (M_R) and the coercivity (H_C) value increases from x =1 at.% Er to x =7 at.% Er doped ZnO nanostructures, and are listed in Table 5.2.

Table 5.2: Values of saturation magnetization, remanent magnetization and coercivity of Er doped ZnO samples

Concentration of Er (%)	**Saturation magnetization M_S (emu/g)**	**Remanent magnetization M_R (emu/g)**	**Coercivity H_C (Oe)**
1%	0.1439	0.0554	0.002
3%	0.3691	0.1543	0.006
5%	0.5548	0.1926	0.017
7%	1.6297	0.3691	0.022

As the Er concentration increases, these all parameters are in appropriate increasing order. The magnetic moment per Er ion, which was obtained from the Ms/ total number of Er, decreased from 0.1439/ Er (x =1) to 0.5548/Er (x =5). The origin of ferromagnetism in Er doped ZnO nanostructures might be caused by the exchange interactions between unpaired electrons spins arising from oxygen vacancies and/or defects and confinement effects at the surface of nanostructures [334]. Furthermore RE ions introduce spin polarized localized states in the band gap. The impurity states are determined by the interaction between dopant atomic states and the host lattice. The interaction of the atomic states with the VB or CB would form bonding and anti-bonding states. After bonding, every RE atom loses three electrons and becomes RE^{3+} i.e. Er^{3+} ion. On the other hand, the magnetic ion is characterized by localized 3*d* or 4*f* shells. The magnetic properties are decided by the localized magnetic moments associated with the magnetic ions and their interaction with the host semiconductor. The desired magnetic behaviour in the case of RE ions is *s, p-f* atoms. As we know, 4*f* RE atoms have larger magnetic moments compared to those of the 3*d* transitions metal atoms [335, 336]. From this, it is clear that the magnetic moment was mainly contributed by the RE 4*f* orbital. Thus, Er doped ZnO nanostructures are observed to show dilute magnetic semiconducting behaviour.

5.4 CONCLUSION

In summary, undoped ZnO and a series of Er doped ZnO nanostructures samples were prepared by a chemical precipitation method and their structural, optical and magnetic properties as a function of doping concentration was undertaken. The foremost results from these studies are following: The XRD results showed that the undoped ZnO and Er doped ZnO nanostructures are single phase hexagonal ZnO and unwanted Er related compounds would not have formed during the growth of Er doped ZnO nanostructures. EDX studies also showed that the Er ions were successfully integrated into the ZnO lattice sites. HRSEM images illustrated that the inclusion of Er ions in crystal structure of ZnO could significantly the morphological evolution of ZnO nanoparticles from nanorods-like to nanocones-like. These morphological changes could be explained by an increase of ZnO crystal growth rate along vertical direction due to doping of Er^{3+} ions in its crystal structure. Er dopant has a strong consequence on structural and optical properties, which could be shown in a considerable red shift in the band gap, the formation of new states due to doping level and the presence of an oxygen vacancy. Values of optical band gap decrease from 3.34 eV to 3.19 eV for undoped ZnO nanostructures and 1–7 at.% Er doped ZnO nanostructures respectively. PL analysis revealed that the Er^{3+} ions doped ZnO has a high optical property and kind of fascinating PL material that shows multiemission peaks at the blue to yellowish-red region, which was attributed to the enhanced defects or oxygen vacancies in excess caused by erbium oxide dopant. At room temperature the hysteresis was observed in the M–H curves shows the presence of ferromagnetism in all Er doped ZnO samples, and it is found that the coercivity, remanent magnetization and the saturation magnetization values of these samples increases as the doping concentration is gradually increased from 1–7 at.% Er. The results suggest the possibility that the introduction of Er into ZnO material prepared by chemical precipitation method have the potential to be used in photonic and spintronic device applications.

CHAPTER VI

CONCLUSION AND FUTURE WORK

6.1 CONCLUSION

The main objective of present investigation was synthesis of undoped and rare earth element (Ce and Er) doped ZnO nanostructures using chemical precipitation method. The prepared nanostructures were dried and annealed at different temperatures whose details are mentioned in chapter 4 and 5. Further, to characterize these nanostructures for their structural, compositional, morphological, optical, magnetic properties different characterization techniques were used.

The effect of optimum doping concentration on the structural, compositional, morphological, optical and magnetic properties was analyzed. The structural, compositional and morphological analysis were carried out using XRD, EDX, TEM and HRSEM, while optical properties were analyzed via UV-Visible and PL spectroscopy. The magnetic properties were studied through VSM. Based on the observation of the analysis during the course of this study, two major steps were explored which depict the following key conclusions as summarized.

The first step was to study the structural, optical, photoluminescence and magnetic properties of Ce-doped ZnO nanoparticles prepared by chemical precipitation method at room temperature. On the basis of this study, it was concluded that:

- Pure ZnO and Ce doped ZnO nanostructures were found to have a hexagonal crystal structure with the diffraction peaks coming from (100), (002), (101), (102), (110), (103), (200) and (112) planes. Impurity peaks such as CeO_2 and CeO_3 were not observed in the XRD pattern of Ce doped ZnO nanoparticles. The lattice parameters were slightly changed due to doping of Ce^{3+} ions into the Zn^{2+} ions. The estimated grain size of the ZnO and Ce doped ZnO nanoparticles was 22 nm.

- EDX analysis showed all expected elements. It was observed that the Ce dopant was successfully incorporated into the ZnO nanoparticles.
- TEM micrographs indicated that the addition of Ce^{3+} does not influence the morphology of the samples. The spherical nanoparticles like structures were obtained for the undoped and Ce doped ZnO samples in the size range of 20-60 nm.
- PL showed that the pure and Ce doped ZnO nanoparticles exhibited a green emission, peaking at about 535 nm. On comparing the PL spectrum of Ce doped ZnO nanoparticles with the peak for ZnO nanoparticles, the peak position of the UV emission shifts to a higher wavelength region (from 388.4 to 410.39 nm) i.e. in the PL spectra of Ce doped ZnO nanoparticles new emission spectra were developed which leads to the red shift in the UV emission. In addition, the broad green emission also exists in the spectra which originate by Ce ion introduced into the ZnO nanoparticles i.e. electron energy transition from 5*d* to 4*f* orbital's in the Ce^{3+} ions.
- UV-vis spectroscopy showed the band gap for ZnO nanoparticles and Ce doped ZnO nanoparticles respectively at 3.35 eV and 3.2 eV. This clearly indicates a significant reduction in band gap after doping of Ce ion in ZnO. The net reduction in the band gap energy, upon Ce insertion, could be due to the formation of Ce related localized, density of states closer to the conduction band minima of ZnO.
- VSM characterization showed the magnetization curves of ZnO nanoparticles and Ce doped ZnO nanoparticles at room temperature. The ZnO nanoparticles demonstrate a diamagnetic behaviour at room temperature while Ce doped ZnO nanoparticles revealed ferromagnetism behaviour at room temperature.

In the second step, a similar kind of investigation was done for a series of samples of Er doped ZnO (0-7 at.%) cone-like nanostructures by chemical precipitation method. The effect of Er doping on the structural, compositional, morphological, optical and magnetic properties were analyzed, which are summarized as:

- XRD pattern of undoped ZnO and Er doped ZnO samples were in close agreement with the standard X-ray diffraction data of ZnO (JCPDS file no. 36-1451). No extra peaks were obtained from ZnO and Er related compound such

as Er_2O_3. Lattice parameters, bond length and volume of unit cell have been calculated for all samples to examine the doping effect of Er on ZnO. In the calculated parameters, no fixed pattern of variation could be observed for these samples. But we found that crystallite size (D) increased in a proper manner from 0-7 at.% Er doped ZnO samples.

- EDX analysis confirmed the presence of Zn, Er and O elements in the samples. XRD and EDX indicate that doping of Er^{3+} is effectively done without forming any impurities.
- HRSEM micrographs indicate that the doping amount of Er influence the morphology of the samples. The irregular structures obtained for the undoped ZnO in 50 nm range and low concentration of Er doped ZnO changed into a nanorods structure of ~100 nm long. When the Er concentration was increased to 3-7 at.%, the morphology of the Er doped ZnO has changed from nanorod to nanocone-like nanostructures.
- UV-vis study showed that Er doped ZnO nanostructure has a trend of slight red shift as compared to undoped ZnO nanostructures.
- The PL spectrum revealed that undoped ZnO and Er doped ZnO nanostructures had an UV emission and a defect emission and the Er ions doping induced a red shift in the UV emission and a small enhancement in the defect emission.
- Magnetic study revealed that the undoped ZnO nanostructures shows diamagnetic behaviour and Er doped ZnO nanostructures shows ferromagnetic behaviour. We also found that parameters of ferromagnetism such as M_S, M_R and H_C increases as doping content increased.

6.2 FUTURE WORK

The ZnO is a very prominent material for a number of applications like sensing, photovoltaic, antibacterial and biomedical, gas sensing, optoelectronic device and dilute magnetic semiconductors when doped with RE elements. In this study, ZnO was doped with Ce and Er. In the future work, it will be based on the optical, structural and elemental investigation of other lanthanides such as Lanthanum (La), Europium (Eu), Holmium (Ho), Ytterbium (Yb), etc. Also their lifetime and quantum efficiency can be studied. We need to analyse the influence of the annealing temperature on the properties of the prepared phosphors. Today's research world

indicates that the current research interest on luminescent materials is moving to solar cells and biological imaging. Also the prepared phosphors are effective materials for photovoltaic applications in order to improve the efficiency of device. The analysis of the work suggests that the structural, elemental, morphological and optical properties on the annealed samples is a promising research project that still needs to be undertaken. Considering its future significance, this work can be extended in the following different ways as given below:

1. Research could be done by comparative study of similar materials where synthesized methods could vary.
2. In this work the samples were annealed at ambient conditions only. Though in future, work could be done by annealing samples at higher temperatures and in different environment (e.g. Nitrogen, oxygen and hydrogen).
3. While in this work, absorption and photoluminescence were only measured for powder samples. But in further studies, it can be done on samples that are still in solution before and after washing of the impurities to examine if washing and drying of the samples will affect the structure, morphology, optical and luminescence properties.
4. In present research work, it is observed that the band gap of materials will increase with decrease in particle size. This blue shift in the band gap is due to quantum confinement effects. So further in depth study can be conducted to see what impact of various morphologies can have on quantum confinement or band gap increase.
5. ZnO nanostructures showed ferromagnetic behaviour after doping against both Ce and Er. In future research work, one could observe their behaviour for spintronic applications.
6. In the present investigations, doped ZnO nanostructures showed good luminescence properties. In further research we can work to understand the transport property and non-linear optical (NLO) property for optoelectronics applications.
7. The future study can be done by synthesizing and studying the properties of thin films for biomedical and photocatalytic applications.

REFERENCES

[1] A.L. Basham, "The practice of medicine in ancient and medieval India", in "Asian medical systems: a comparative study", C.M. Leslie, 1st ed., University of California Press, Berkeley, 1976, pp. 18–43.

[2] Nanotechnology Timeline, (2016, October 10). National Nanotechnology Initiative [Online] Available: http://www.nano.gov/nanotech-101/.

[3] U. Leonhardt, "Invisibility cup", Nature Photonics, Vol. 1, 2007, pp. 207–208.

[4] M.F.Ashby, P.J.Ferreira, and D.L.Schodek, "Nanomaterials, nanotechnologies and design: an introduction for engineers and architects", Butterworth-Heinemann, 2009.

[5] M. Reibold, P. Paufler, A.A. Levin, W. Kochmann, N. Pätzke, and D.C. Meyer, "Materials: carbon nanotubes in an ancient damascus sabre", Nature, Vol. 444, 2006, pp. 286.

[6] M. Faraday, "The bakerian lecture: experimental relations of gold (and other metals) to light", Philosophical Transactions of the Royal Society A, Vol. 147, 1857, pp. 145–181.

[7] V.I. Klimov, "Semiconductor and metal nanocrystals: synthesis and electronic and optical properties", CRC Press, USA, 2003.

[8] R.P. Feynman, "There's plenty of room at the bottom (data storage)", Journal of Microelectromechanical Systems, Vol. 1, 1992, pp.60–66.

[9] R. Feynman, "There is plenty of room at the bottom", Caltech Engineering and Science,Vol.23,1960,pp22–36, [Online] Available: www.zyvex.com/nanotech/feynman.html.

[10] N. Taniguchi, "On the basic concept of 'nano-technology", Proceedings of the Internationals Conference on Production Engineering, Tokyo, Part II, Japan Society of Precision Engineering, 1974.

[11] M.C. Roco, C.A. Mirkin, and M.C. Hersam, "Nanotechnology research directions for societal needs in 2020: summary of international study", Journal of Nanoparticle Research, Vol. 13, 2011, pp. 897– 919.

[12] C.N.R. Rao, A. Muller, and A.K. Cheetham, "The chemistry of nanomaterials: synthesis, properties and applications", WILEY VCH Verlag GmbH & Co. KGaA, Weinheim, 2004.

[13] J. Ramsden, “Essentials of nanotechnology”, Jeremy Ramsden & Ventus Publishing, 2009, pp. 1.

[14] What is nanotechnology? http://mrsec.wisc.edu/Edetc/nanotech/index.html

[15] P. Boisseau, and B. Loubaton, “Nanoscience and nanotechnologies: hopes and concerns nano-medicine, nanotechnology in medicine”, Comptes Rendus Physique, Vol. 12, 2011, pp. 620–636.

[16] L.A. DeLouise, “Applications of nanotechnology in dermatology”, Journal of Investigative Dermatology, Vol. 132, 2012, pp. 964–975.

[17] S.K. Arora, R.W. Foley, J. Youtie, P. Shapira, and A. Wiek, “Drivers of technology adoption- the case of nanomaterials in building construction”, Technological Forecasting and Social Change, Vol. 87, 2014, pp. 232–244.

[18] S. Chattopadhyay, L.-C. Chen, and K.-H. Chen, “Energy production and conversion applications of one-dimensional semiconductor nanostructures”, NPG Asia Materials, Vol. 3, 2011, pp. 74–81.

[19] B. Valeur, and M.N.B.-Santos, “A brief history of fluorescence and phosphorescence before the emergence of quantum theory”, Journal of Chemical Education, Vol. 88, 2011, pp. 731–738.

[20] N.Y.-Gross, “Colloidal semiconductor nanocrystals based solar cells”, [PhD Thesis], 2012.

[21] H.N. Bose, “Luminescence and allied phenomena”, Indian Journal of History of Science, Vol. 27, 1992, pp. 409–419.

[22] L. Ozawa, “Cathodoluminescence and photoluminescence: theories and practical applications”, CRC Press, Boca Raton, FL, 2007.

[23] G. Blasse, “New luminescent materials”, Chemistry of Materials, Vol. 1, 1989, pp. 294–301.

[24] T. Trupke, M.A. Green, and P. Wurfel, “Improving solar cell efficiencies by down conversion of high-energy photons”, Journal of Applied Physics, Vol. 92, 2002, pp. 4117.

[25] S.J. Pearton, C.R. Abernathy, M.E. Overberg, G.T. Thaler, D.P. Norton, N. Theodoropoulou, A.F. Hebard, Y.D. Park, F. Ren, J. Kim, and L.A. Boatner, “Wide band gap ferromagnetic semiconductors and oxides”, Journal of Applied Physics, Vol. 93, 2003, pp. 1–13.

[26] K. Ando, “Magneto-optics of diluted magnetic semiconductors: new materials and applications”, Magneto-Optics, Springer Series in Solid-State Science, Vol. 128, 2000, pp. 211–244.

[27] J. Xu, “Luminescence in ZnO”, [MSc Thesis], 2004.

[28] G. Galli, “Solid-state physics: doping the undopable”, Nature, Vol. 436, 2005, pp. 32–33.

[29] S.C. Erwin, L. Zu, M.I. Haftel, A.L. Efros, T.A. Kennedy, and D.J. Norris, “Doping semiconductor nanocrystals”, Nature, Vol. 436, 2005, pp. 91–94.

[30] J.-C.G. Bunzli, and S.V. Eliseeva, “Basics of lanthanide photophysics”, Lanthanide Luminescence: Photophysical, Analytical and Biological Aspects”, Vol. 7, 2010, pp. 1–45.

[31] M.A. Lim, S.I. Seok, and S.I. Hong, “Near infrared luminescence of Er ions in sol-gel ZnO/ zirconium-oxo-alkylsiloxane nanocomposite films”, Thin Solid Films, Vol. 515, 2006, pp. 2423–2427.

[32] G.-R. Li, X.-H. Lu, W.-X. Zhao, C.-Y. Su, and Y.-X. Tong, “Controllable electrochemical synthesis of Ce^{4+}-doped ZnO nanostructures from nanotubes to nanorods and nanocages”, Crystal Growth and Design, Vol. 8, 2008, pp. 1276–1281.

[33] J. Yang, M. Gao, L. Yang, Y. Zhang, J. Lang, D. Wang, Y. Wang, H. Liu, and H. Fan, “Low-temperature growth and optical properties of Ce-doped ZnO nanorods”, Applied Surface Science, Vol. 255, 2008, pp. 2646–2650.

[34] N.F. Djaja, and R. Saleh, “Characteristics and photocatalytics activities of Ce-doped ZnO nanoparticles”, Materials Sciences and Applications, Vol. 4, 2013, pp. 145–152.

[35] J. Lang, Q. Han, J. Yang, C. Li, X. Li, L. Yang, Y. Zhang, M. Gao, D. Wang, and J. Cao, “Fabrication and optical properties of Ce-doped ZnO nanorods”, Journal of Applied Physics, Vol. 107, 2010, pp. 074302.

[36] Y.-Il Jung, B.-Y. Noh, Y.-S. Lee, S.-Ho Baek, J.H. Kim, and Il-K. Park, “Visible emission from Ce-doped ZnO nanorods grown by hydrothermal method without a post thermal annealing process”, Nanoscale Research Letters, Vol. 7, 2012, pp. 43.

[37] A. George, S.K. Sharma, S. Chawla, M.M. Malik, and M.S. Qureshi, “Detailed of X-ray diffraction and photoluminescence studies of Ce doped

ZnO nanocrystals", Journal of Alloys and Compounds, Vol. 509, 2011, pp. 5942–5946.

[38] K. Singh, A.A. Ibrahim, A. Umar, A. Kumar, G.R. Chaudhary, S. Singh, and S.K. Mehta, "Synthesis of CeO_2–ZnO nanoellipsoids as potential scaffold for the efficient detection of 4-nitrophenol", Sensors and Actuators B: Chemical, Vol. 202, 2014, pp. 1044–1050.

[39] M. Faisal, A.A. Ismail, A.A. Ibrahim, H. Bouzid, and S.A. Al-Sayari, "Highly efficient photocatalyst based on Ce doped ZnO nanorods: controllable synthesis and enhanced photocatalytic activity", Chemical Engineering Journal, Vol. 229, 2013, pp. 225–233.

[40] J.-C. Sin, S.-M. Lam, K.-T. Lee, and A.R. Mohamed, "Fabrication of erbium-doped spherical-like ZnO hierarchical nanostructures with enhanced visible light-driven photocatalytic activity", Materials Letters, Vol. 91, 2013, pp. 1–4.

[41] A. Khataee, S. Saadi, M. Safarpour, and S.W. Joo, "Sonocatalytic performance of Er-doped ZnO for degradation of a textile dye", Ultrasonic Sonochemistry, Vol. 27, 2015, pp. 379–388.

[42] E. Asikuzun, O. Ozturk, L. Arda, A.T. Tasci, F. Kartal, and C. Terzioglu, "High-quality c-axis oriented non-vacuum Er doped ZnO thin films", Ceramics International, Vol. 42, 2016, pp. 8085–8091.

[43] J. Lang, J. Wang, Q. Zhang, S. Xu, D. Han, J. Yang, Q. Han, L. Yang, Y. Sui, X. Li, and X. Liu, "Synthesis and photoluminescence characterizations of the Er^{3+}-doped ZnO nanosheets with irregular porous microstructure", Materials Science in Semiconductor Processing, Vol. 41, 2016, pp. 32–37.

[44] R. Vettumperumal, S. Kalyanaraman, and R. Thangavel, "Optical constants and near infrared emission of Er doped ZnO sol–gel thin films", Journal of Luminescence, Vol.158, 2015, pp. 493–500.

[45] Y. Chen, and X.L. Xu, "Effect of oxygen deficiency on optical band gap shift in Er-doped ZnO thin films", Physica B, Vol. 406, 2011, pp. 3121–3124.

[46] L. Miao, S. Tanemura, L. Zhao, X. Xiao, and X.T. Zhang, "Ellipsometric studies of optical properties of Er-doped ZnO thin films synthesized by sol–gel method", Thin Solid Films, Vol. 543, 2013, pp. 125–129.

[47] N.K. Divya, and P.P. Pradyumnan, "Solid state synthesis of erbium doped ZnO with excellent photocatalytic activity and enhanced visible light

emission", Materials Science in Semiconductor Processing, Vol. 41, 2016, pp. 428–435.

[48] R. John, and R. Rajakumari, "Synthesis and characterization of rare earth ion doped nano ZnO", Nano-Micro Letters, Vol. 4, 2012, pp. 65–72.

[49] H. Yang, and P.H. Holloway, "Water-soluble silica-over coated CdS:Mn/ZnS semiconductor quantum dots", Journal of Chemical Physics, Vol. 121, 2004, pp. 7421.

[50] P. Yang, C.F. Song, M.K. Lu, X. Yin, G.J. Zhou, D. Xu, and D.R. Yuan, "The luminescence of PbS nanoparticles embedded in sol–gel silica glass", Chemical Physics Letters, Vol. 345, 2001, pp. 429–434.

[51] M.-H. Lee, S.-G. Oh, and S.-C. Yi, "Preparation of Eu-doped Y_2O_3 luminescent nanoparticles in nonionic reverse microemulsions", Journal of Colloid and Interface Science, Vol. 226, 2000, pp. 65–70.

[52] R.N. Bhargava, "Doped nanocrystalline materials - physics and applications", Journal of Lumiescence, Vol. 70, 1996, pp. 85–94.

[53] M.S. Dhlamini, "Luminescent properties of synthesized PbS nanoparticles phosphors", [PhD Thesis], 2008.

[54] J.-C.G. Bünzli, and S.V. Eliseeva, "Lanthanide NIR luminescence for telecommunications, bioanalyses and solar energy conversion", Journal of Rare Earths, Vol. 28, 2010, pp. 824–842.

[55] J.-C.G. Bünzli, S. Comby, A.S. Chauvin, and C.D.B. Vandevyver, "New opportunities for lanthanide luminescence", Journal of Rare Earths, Vol. 25, 2007, pp. 257–274.

[56] H. Suzuki, "Organic light-emitting materials and devices for optical communication technology", Journal of Photochemistry and Photobiology A: Chemistry, Vol. 166, 2004, pp. 155–161.

[57] Z.-Q. Chen, Z.-Q. Bian, and C.-H. Huang, "Functional Ir^{III} complexes and their applications", Advanced Materials, Vol. 22, 2010, pp. 1534–1539.

[58] S.V. Eliseeva, and J.-C.G. Bünzli, "Lanthanide luminescence for functional materials and bio-sciences", Chemical Society Reviews, Vol. 39, 2010, pp. 189–227.

[59] J.-C.G. Bünzli, "Lanthanide luminescence for biomedical analyses and imaging", Chemical Reviews, Vol. 110, 2010, pp. 2729–2755.

[60] F. Wang, D. Banerjee, Y. Liu, X. Chen, and X. Liu, “Upconversion nanoparticles in biological labeling, imaging, and therapy”, Analyst, Vol. 135, 2010, pp. 1839–1854.

[61] H. Uh, and S. Petoud, “Novel antennae for the sensitization of near infrared luminescent lanthanide cations”, Comptes Rendus Chimie, Vol. 13, 2010, pp. 668–680.

[62] J.-C.G. Bünzli, A.-S. Chauvin, C.D.B. Vandevyver, S. Bo, and S. Comby, “Lanthanide bimetallic helicates for in vitro imaging and sensing”, Annals of the New York Academy of Sciences, Vol. 1130, 2008, pp. 97–105.

[63] C.L. Amiot, S.P. Xu, S. Liang, L.Y. Pan, and J.X.J. Zhao, “Near-infrared fluorescent materials for sensing of biological targets, Sensors, Vol. 8, 2008, pp. 3082–3105.

[64] D.E. Cooper, A. D'Andrea, G.W. Faris, B. MacQueen, and W.H. Wright, “Up-converting phosphors for detection and identification using antibodies”, J.M. Van Emon, Ed. Immunoassay and Other Bioanalytical Techniques, Boca Raton: CRC Press, Taylor and Francis group, 2007, Ch. 9, pp. 217–247.

[65] S. Comby, and J.-C.G. Bünzli, “Lanthanide near-infrared luminescence in molecular probes and devices, K.A. Gschneidner Jr., J.-C.G. Bünzli, V.K. Pecharsky, Eds. “Hand book on the physics and chemistry of rare earths”, Amsterdam: Elsevier Science B.V., Vol. 37, 2007, Ch. 235, pp. 217–470.

[66] Q.Y. Zhang, and X.Y. Huang, “Recent progress in quantum cutting phosphors”, Progress in Material Science, Vol. 55, 2010, pp. 353–427.

[67] B.M. Van der Ende, L. Aarts, and A. Meijerink, “Lanthanide ions as spectral converters for solar cells”, Physical Chemistry Chemical Physics, Vol. 11, 2009, pp. 11081–11095.

[68] D.L. Andrews, “Energy harvesting: a review of the interplay between structure and mechanism”, Journal of Nanophotonics, Vol. 2, 2008, pp. 022502.

[69] C. Strümpel, M. McCann, G. Beaucarne, V. Arkhipov, A. Slaoui,V. Svrcek, C. del Canizo, and I. Tobias, “Modifying the solar spectrum to enhance silicon solar cell efficiency-an overview of available materials”, Solar Energy Materials and Solar Cells, Vol. 91, 2007, pp. 238–249.

[70] A. Shalav, B.S. Richards, and M.A. Green, “Luminescent layers for enhanced silicon solar cell performance: up-conversion”, Solar Energy Materials and Solar Cells, Vol. 91, 2007, pp. 829–842.

[71] A. Goetzberger, and W. Greube, “Solar energy conversion with fluorescent collectors”, Applied Physics A, Vol. 14, 1977, pp. 123–139.

[72] B.S. Richards, “Luminescent layers for enhanced silicon solar cell performance: down-conversion”, Solar Energy Materials and Solar Cells, Vol. 90, 2006, pp. 1189–1207.

[73] J. deWild, A. Meijerink, J.K. Rath, W.G.J.H.M. van Sark, and R.E.I. Schropp, “Upconverter solar cells: materials and applications”, Energy and Environmental Science, Vol. 4, 2011, pp. 4835–4848.

[74] E. Klampaftis, D. Ross, K.R. McIntosh, and B.S. Richards, “Enhancing the performance of solar cells via luminescent down-shifting of the incident spectrum: a review”, Solar Energy Materials and Solar Cells, Vol. 93, 2009, pp. 1182–1194.

[75] B.S. Richards, “Enhancing the performance of silicon solar cells via the application of passive luminescence conversion layers”, Solar Energy Materials and Solar Cells, Vol. 90, 2006, pp. 2329–2337.

[76] C.P. Thomas, A.B. Wedding, and S.O. Martin, “Theoretical enhancement of solar cell efficiency by the application of an ideal ‘down-shifting’ thin film”, Solar Energy Materials and Solar Cells, Vol. 98, 2012, pp. 455–464.

[77] V. Svrcek, A. Slaoui, and J.C. Muller, “Silicon nanocrystals as light converter for solar cells”, Thin Solid Films, Vol. 451, 2004, pp. 384–388.

[78] Y. Wang, D.-J. Wu, Y.-T. Yang, and X.-J. Liu, “Nd-doping induced lattice distortion in TiO_2 nanoparticles”, Chinese Physics Letters, Vol. 28, 2011, pp. 027804.

[79] W. Luo, R. Li, and X. Chen, “Host-sensitized luminescence of Nd^{3+} and Sm^{3+} ions incorporated in anatase titania nanocrystals”, Journal of Physical Chemistry C, Vol. 113, 2009, pp. 8772–8777.

[80] C.M. Leroy, T. Cardinal, V. Jubera, M.T.- Delapierre, J. Majimel, J.P. Manaud, R. Backov, C. Boissière, D. Grosso, C. Sanchez, B. Viana, and F. Pellé, “Europium-doped mesoporous titania thin films: rare-earth locations and emission fluctuations under illumination”, Chem Phys Chem, Vol. 9, 2008, pp. 2077–2084.

[81] P. Ghigna, A. Speghini, and M. Bettinelli, “Unusual Ln^{3+} substitutional defects: the local chemical environment of Pr^{3+} and Nd^{3+} in nanocrystalline

TiO_2 by Ln–K edge EXAFS", Journal of Solid State Chemistry, Vol. 180, 2007, pp. 3296–3301.

[82] W. Li, A.I. Frenkel, J.C. Woicik, C. Ni, and S.I. Shah, "Dopant location identification in Nd^{3+}-doped TiO_2 nanoparticles", Physical Review B, Vol. 72, 2005, pp. 155315.

[83] K.L. Frindell, M.H. Bartl, M.R. Robinson, G.C. Bazan, A.Popitsch, and G.D. Stucky, "Visible and near-IR luminescence via energy transfer in rare earth doped mesoporous titania thin films with nanocrystalline walls", Journal of Solid State Chemistry, Vol. 172, 2003, pp. 81–88.

[84] A. Burns, G. Hayes, W. Li, J. Hirvonen, J.D. Demaree, and S.I. Shah, "Neodymium ion dopant effects on the phase transformation in sol–gel derived titania nanostructures", Material Science and Engineering: B, Vol. 111, 2004, pp. 150–155.

[85] M.-H. Park, J.-H. Li, A. Kumar, G. Li, and Y. Yang, "Doping of the metal oxide nanostructure and its influence in organic electronics", Advanced Functional Materials, Vol. 19, 2009, pp. 1241–1246.

[86] J.C. Yu, J. Yu, W. Ho, Z. Jiang, and L. Zhang, "Effects of F- doping on the photocatalytic activity and microstructures of nanocrystalline TiO_2 powders", Chemistry of Materials, Vol. 14, 2002, pp. 3808–3816.

[87] C. Burda, Y. Lou, X. Chen, A.C.S. Samia, J. Stout, and J.L. Gole, "Enhanced nitrogen doping in TiO_2 nanoparticles", Nano Letters, Vol. 3, 2003, pp. 1049–1051.

[88] J. Kossanyi, D. Kouyate, J. Pouliquen, J.C.R. -Haret, P. Valat, D. Oelkrug, U. Mammel, G.P. Kelly, and F. Wilkinson, "Photoluminescence of semiconducting zinc oxide containing rare earth ions as impurities", Journal of Luminescence, Vol. 46, 1990, pp. 17–24.

[89] M. Leskela, "Rare earths in electroluminescent and field emission display phosphors", Journal of Alloys and Compounds, Vol. 275, 1998, pp. 702–708.

[90] B. Jacquier, E. Lebrasseur, S. Guy, A. Belarouci, and F. Menchini, "Rare earth-doped confined structures for amplifiers and lasers", Journal of Alloys and Compounds, Vol. 303, 2000, pp. 207–213.

[91] G. Blasse, and B.C. Grabmaier, "Luminescent Materials", Springer: New York, 1994.

[92] M. Gratzel, “Photoelectrochemical cells”, Nature, Vol. 414, 2001, pp. 338–344.

[93] R. Janisch, P. Gopal, and N.A. Spaldin, “Transition metal-doped TiO_2 and ZnO-present status of the field”, Journal of Physics: Condensed Matter, Vol. 17, 2005, pp. R657–R689.

[94] K. Nomura, H. Ohta, K. Ueda, T. Kamiya, M. Hirano, and H. Hosono, “Thin-film transistor fabricated in single-crystalline transparent oxide semiconductor”, Science, Vol. 300, 2003, pp. 1269–1272.

[95] Ü. Özgür, Ya.I. Alivov, C. Liu, A. Teke, M.A. Reshchikov, S. Doğan, V. Avrutin, S.-J. Cho, and H. Morkoç, “A comprehensive review of ZnO materials and devices”, Journal of Applied Physics, Vol. 98, 2005, pp. 041301.

[96] C. Klingshirn, “ZnO: material, physics and applications”, Chem Phys Chem, Vol. 8, 2007, pp. 782–803.

[97] C. Klingshirn, R. Hauschild, H. Priller, M. Decker, J. Zeller, and H. Kalt, “ZnO rediscovered — once again!?”, Superlattices and Microstructures, Vol. 38, 2005, pp. 209–222.

[98] R. Thangavel, R.S. Moirangthem, W.-Shan Lee, Y.-C. Chang, P.-K. Wei, and J. Kumar, “Cesium doped and undoped ZnO nanocrystalline thin films: a comparative study of structural and micro-Raman investigation of optical phonons”, Journal of Raman Spectroscopy, Vol. 41, 2010, pp. 1594–1600.

[99] E.K. Ellmer, A. Klein, and B. Rech, “Transparent conductive zinc oxide”, Springer, Berlin, 2008.

[100] L. Zhang, Y. Jiang, Y. Ding, M. Povey, and D. York, “Investigation into the antibacterial behaviour of suspensions of ZnO nanoparticles (ZnO nanofluids)”, Journal of Nanoparticle Research, Vol. 9, 2007, pp. 479–489.

[101] J. Strunk, K. Kähler, X. Xia, and M. Muhler, “The surface chemistry of ZnO nanoparticles applied as heterogeneous catalysts in methanol synthesis”, Surface Science, Vol. 603, 2009, pp. 1776–1783.

[102] B. Shahmoradi, I.A. Ibrahim, N. Sakamoto, S. Ananda, T.N. Row, K. Soga, K. Byrappa, S. Parsons, and Y. Shimizu, “In situ surface modification of molybdenum-doped organic–inorganic hybrid TiO_2 nanoparticles under hydrothermal conditions and treatment of pharmaceutical effluent”, Environmental Technology, Vol. 31, 2010, pp. 1213–1220.

[103] A. Nuruddin, and J.R. Abelson, “Improved transparent conductive oxide/p^+/i junction in amorphous silicon solar cells by tailored hydrogen flux during growth”, Thin Solid Films, Vol. 394, 2001, pp. 48–62.

[104] Z.L. Wang, and J.H. Song, “Piezoelectric nanogenerators based on zinc oxide nanowire arrays”, Science, Vol. 14, 2006, pp. 242–246.

[105] P.X. Gao, J.H. Song, J. Liu, and Z.L. Wang, “Nanowire piezoelectric nanogenerators on plastic substrates as flexible power sources for nanodevices”, Advanced Materials, Vol. 19, 2007, pp. 67–72.

[106] Z.L. Wang, “Nanopiezotronics”, Advanced Materials, Vol. 19, 2007, pp. 889–892.

[107] J.H. Song, X.D. Wang, J. Liu, H.B. Liu, Y.L. Li, and Z.L. Wang, “Piezoelectric potential output from ZnO nanowire functionalized with p-type oligomer”, Nano Letters, Vol. 8, 2008, pp. 203–207.

[108] M.P. Lu, J.H. Song, M.Y. Lu, M.T. Chen, Y.F. Gao, L.J. Chen, and Z.L. Wang, “Piezoelectric nanogenerator using p-type ZnO nanowire arrays”, Vol. 9, 2009, pp. 1223–1227.

[109] H. Morko, and U. Özgür, “Zinc Oxide: fundamentals, materials and device technology”, Wiley-VCH, 2009.

[110] A. Janotti, and C.G. Van de Walle, “Fundamentals of zinc oxide as a semiconductor”, Reports on Progress in Physics, Vol. 72, 2009, pp. 126501–29.

[111] A.B. Djurisic, and Y.H. Leung, “Optical properties of ZnO nanostructures", Small, Vol. 2, 2006, pp. 944–961.

[112] Z.L. Wang, “Zinc oxide nanostructures: growth, properties and applications”, Journal of Physics: Condensed Matter, Vol. 16, 2004, pp. R829–R858.

[113] J. Cui, “Zinc oxide nanowires”, Materials Characterization, Vol. 64, 2012, pp. 43–52.

[114] M. Willander, O. Nur, Q.X. Zhao, L.L. Yang, M. Lorenz, B.Q. Cao, J.Z. Pérez, C.Czekalla, G.Zimmermann, M.Grundmann, A.Bakin, A. Behrends, M. Al-Suleiman, A. El-Shaer, A.C. Mofor, B. Postels, A. Waag, N. Boukos, A. Travlos, H.S. Kwack, J. Guinard, and D.L. Si Dang, “Zinc oxide nanorod based photonic devices: recent progress in growth, light emitting diodes and lasers”, Nanotechnology, Vol. 20, 2009, pp. 332001.

[115] H. Ohno, “Making nonmagnetic semiconductors ferromagnetic”, Science, Vol. 28l, 1998, pp. 951.

[116] S.J. Han, T.H. Jang, Y.B. Kim, B.G. Park, J.H. Park, and Y.H. Jeong, “Magnetism in Mn-doped ZnO bulk samples prepared by solid state reaction” Applied Physics Letters, Vol. 83, 2003, pp. 920.

[117] H.J. Schulz, and M. Thiede, “Optical spectroscopy of $3d^7$ and $3d^8$ impurity configuration in a wide-gap semiconductor (ZnO:Co, Ni, Cu)”, Physical Review B, Vol. 35, 1987, pp. 8.

[118] T. Yasahira, K. Uchida, Y.H. Matsuda, N. Miura, and A. Twardowski, “Magnetic and non-magnetic Faraday rotation in ZnMnSe in high magnetic fields”, Semiconductor Science and Technology, Vol. 14, 1999, pp. 1161.

[119] K. Ando, A.K. Bhattacharjee, H. Tanoue, T. Takamasu, Y. Imanaka, G. Kido, T. Yasuhira Y.H. Matsuda, and N. Miura, “Nickel-based diluted magnetic semiconductor (Zn, Ni)Te”, Physica Status Solidi (b), Vol. 229, 2002, pp.733–736.

[120] S.W. Yoon, S.B. Cho, S.C. We, S. Yoon, and Y.J. Shin, “Magnetic properties of ZnO-based diluted magnetic semiconductors”, Journal of Applied Physics, Vol. 93, 2003, pp. 7879.

[121] J. Dreyhsig, and B.L. Zenburger, “Nature of optical transitions in the charge-transfer region of ZnS:Co and ZnSe:Co”, Physical Review B, Vol. 54, 1996, pp. 10516.

[122] J.L. Costa -Kramer, F. Briones, J.F. Fernandez, A.C. Caballero, M. Villegas, M. Diaz, and M.A. Garcia, “Nanostructure and magnetic properties of the MnZnO system, a room temperature magnetic semiconductor”, Nanotechnology, Vol. 16, 2005, pp. 214.

[123] J. Chen, M.H. Yu, W.L. Zhou, K. Sun, and L. Mwang, “Room-temperature ferromagnetic Co-doped ZnO nanoneedle array prepared by pulsed laser deposition”, Applied Physics Letters, Vol. 87, 2005, pp. 173119.

[124] D.A. Schwartz, N.S. Norberg, Q.P. Ngayen, J.M. Parker, and D.R. Gamelin, “Magnetic quantum dots: synthesis, spectroscopy, and magnetism of Co^{2+}- and Ni^{2+}-doped ZnO nanocrystals”, Journal of American Chemical Society, Vol. 125, 2003, pp. 13205–13218.

[125] R. Viswanatha, S. Sapra, S.S. Gupta, B. Satpati, P.V. Satyam, B.N. Dev, and D.D. Sarma, "Synthesis and characterization of Mn-doped ZnO nanocrystals", Journal of Physical Chemistry B, Vol. 108, 2004, pp. 6303–6310.

[126] T. Dietl, H. Ohno, F. Matsukura, J. Cibert, and D. Ferrand, "Zener model description of ferromagnetism in zinc-blende magnetic semiconductors", Science, Vol. 287, 2000, pp. 1019–1022.

[127] J.M.D. Coey, M. Venkatesan, and C.B. Fitzgerald, "Donor impurity band exchange in dilute ferromagnetic oxides", Nature Materials, Vol. 4, 2005, pp. 173–179.

[128] R.N. Bhargava, D. Gallagher, X. Hong, and Nurmikko, "Optical properties of manganese-doped nanocrystals of ZnS", Physical Review Letters, Vol. 72, 1994, pp. 416.

[129] F.V. Mikulec, M. Kuno, M. Bennati, D.A. Hall, R.G. Griffin, and M.G. Bawendi, "Organometallic synthesis and spectroscopic characterization of manganese-doped CdSe nanocrystals", Journal of American Chemical Society, Vol. 122, 2000, pp. 2532–2540.

[130] D.J. Norris, N. Yao, F.T. Charnock, and T.A. Kennedy, "High-quality manganese-doped ZnSe nanocrystals", Nano Letters, Vol. 1, 2001, pp. 3–7.

[131] G.M. Dalpian, and J.R. Chelikowsky, "Self-purification in semiconductor nanocrystals", Physical Review Letters, Vol. 96, 2006, pp. 226802.

[132] Q. Xu, H. Schmidt, S. Zhou, K. Potzger, M. Helm, H. Hochmuth, M. Lorenz, A. Setzer, P. Esquinazi, C. Meinecke, and M. Grudmann, "Room temperature ferromagnetism in ZnO films due to defects", Applied Physics Letters, Vol. 92, 2008, pp. 082508.

[133] M.A. Garcia, M.L. Ruiz-Gonzalez, A. Quesada, J.L. Costa-Kramer, J.F. Fernandez, S.J. Khatib, A. Wennberg, A.C. Caballero, M.S. Martin-Gonzalez, M. Villegas, F. Briones, J.M. Gonzalez-Calbet, and A. Hernando, "Interface double-exchange ferromagnetism in the Mn-Zn-O system: new class of biphase magnetism", Physical Review Letters, Vol. 94, 2005, pp. 217206.

[134] A. Sundaresan, R. Bhargavi, N. Rangarajan, U. Siddesh, and C.N.R. Rao, "Ferromagnetism as a universal feature of nanoparticles of the otherwise nonmagnetic oxides", Physical Review B, Vol. 74, 2006, pp. 161306(R).

[135] M.A. Garcia, J.M. Merino, P.E. Fernandez, A. Quesada, J.de la Venta, M.L. Ruiz Gonzalez, G.R. Castro, P. Crespo, J. Llopis, J.M.G. Calbet, A. Hernando,

"Magnetic Properties of ZnO Nanoparticles", Nano Letters, Vol. 7, 2007, pp. 1489–1494.

[136] Q. Wang, Q. Sun, and P. Jena, "Ligand induced ferromagnetism in ZnO nanostructures", Journal of Chemical Physics, Vol. 129, 2008, pp. 164714.

[137] K. Potzger, S. Zhou, J. Grenzer, M. Helm, and J. Fassbender, "An easy mechanical way to create ferromagnetic defective ZnO", Applied Physics Letters, Vol. 92, 2008, pp. 182504.

[138] M.S. Arnold, P. Avouris, Z.W. Pan, and Z.L. Wang, "Field-effect transistors based on single semiconducting oxide nanobelts", Journal of Physical Chemical B, Vol. 107, 2003, pp. 659–663.

[139] J. Xu, Y. Chen, Y. Li, and J. Shen, "Gas sensing properties of ZnO nanorods prepared by hydrothermal method", Journal of Materials Science, Vol. 40, 2005, pp. 2919–2921.

[140] H.T. Wang, B.S. Kang, F. Ren, L.C. Tien, P.W. Sadik, D.P. Norton, S.J. Pearton, and J. Lin, "Hydrogen-selective sensing at room temperature with ZnO nanorods", Applied Physics Letters, Vol. 86, 2005, pp. 24.

[141] Q.H. Li, Y.X. Liang, Q. Wan, and T.H. Wang, "Oxygen sensing characteristics of individual ZnO nanowire transistors", Applied Physics Letters, Vol. 85, 2004, pp. 6389–6391.

[142] Z. Fan, D. Wang, P.C. Chang, W.Y. Tseng, and J.G. Lu, "ZnO nanowire field-effect transistor and oxygen sensing property", Applied Physics Letters, Vol. 85, 2004, pp. 5923–5925.

[143] J. Xu, N. Wu, C. Jiang, M. Zhao, M.J. Li, Y. Wei, and S.X. Mao, "Impedance characterization of ZnO nanobelt/Pd Schottky contacts in ammonia", Small, Vol. 2, 2006, pp. 1458–1461.

[144] N. Zhang, K. Yu, L. Li, and Z. Zhu, "Investigation of electrical and ammonia sensing characteristics of Schottky barrier diode based on a single ultra-long ZnO nanorod", Applied Surface Science, Vol. 254, 2008, pp. 5736–5740.

[145] J. Yu, M. Shafiei, M. Breedon, K. Kalantar-zadeh, and W. Wlodarski, "A comparison of forward and reverse bias operation in a Pt/nanostructured ZnO Schottky diode based hydrogen sensor", Procedia Chemistry, Vol. 1, 2009, pp. 979–982.

[146] S.N. Das, J.P. Kar, J.H. Choi, T. Lee, K.J. Moon, and J.M. Myoung, "Fabrication and characterization of ZnO single nanowire-based hydrogen sensor", Journal of Physical Chemistry C, Vol. 114, 2010, pp. 1689–1693.

[147] M. Gratzel, "Dye-sensitized solar cell", Journal of Photochemistry and Photobiology C, Vol. 4, 2003, pp. 145–153.

[148] Z.Z. Yang, T. Xu, Y.S. Ito, U. Welp, and W.K. Kwoko, "Enhanced electron transport in dye-sensitized solar cells using short ZnO nanotips on a rough metal anode", Journal of Physical Chemistry C, Vol. 113, 2009, pp. 20521–20526.

[149] F. Xu, M. Dai, Y. Lu, and L. Sun, "Hierarchical ZnO nanowire-nanosheet architectures for high power conversion efficiency in dye-sensitized solar cells", Journal of Physical Chemistry C, Vol. 114, 2010, pp. 2776–2782.

[150] M. Law, L.E. Greene, J.C. Johnson, R. Saykally, and P. Yang, "Nanowire dye-sensitized solar cells", Nature Materials, Vol. 4, 2005, pp. 455–459.

[151] A.B.F Martinson, J.W. Elam, J.T. Hupp, and M.J. Pellin, "ZnO nanotube based dye-sensitized solar cells", Nano Letters, Vol. 7, 2007, pp. 2183–2187.

[152] C.T. Wu, W.P. Liao, and J.J. Wu, "Three-dimensional ZnO nanodendrite/nanoparticle composite solar cells", Journal of Materials Chemistry, Vol. 21, 2011, pp. 2871–2876.

[153] G.V. Irene, and L.C. Monica, "Vertically-aligned nanostructures of ZnO for excitonic solar cells: a review", Energy & Environmental Science, Vol. 2, 2009, pp. 19–34.

[154] D. Costenaro, F. Carniato, G. Gatti, L. Marchese , and C. Bisio, "Preparation of luminescent ZnO nanoparticles modified with aminopropyltriethoxy silane for optoelectronic applications", New Journal of Chemistry, Vol. 37, 2013, pp. 2103–2109.

[155] B. Liu, Z. Wang, Y. Dong, Y. Zhu, Y. Gong, S. Ran, Z. Liu, J. Xu, Z. Xie, D. Chen, and G. Shen, "ZnO-nanoparticle-assembled cloth for flexible photodetectors and recyclable photocatalysts", Journal of Materials Chemistry, Vol. 22, 2012, pp. 9379–9384.

[156] A. Bagabas, A. Alshammari, M. FA. Aboud, and H. Kosslick, "Room-temperature synthesis of zinc oxide nanoparticles in different media and their application in cyanide photodegradation", Nanoscale Research Letters, Vol. 8, 2013, pp. 516.

[157] R.Y. Hong, J.H. Li, L.L. Chen, D.Q. Liu, H.Z. Li, Y. Zheng, and J.Ding, "Synthesis, surface modification and photocatalytic property of ZnO nanoparticles", Powder Technology, Vol. 189, 2009, pp. 426–432.

[158] Y. Zhang, T.R. Nayak, H. Hong, and W. Cai1, "Biomedical applications of zinc oxide nanomaterials", Current Molecular Medicine, Vol. 13, 2013, pp. 1633–1645.

[159] H.-M. Xiong, "ZnO nanoparticles applied to bioimaging and drug delivery", Advance Materials, Vol. 25, 2013, pp. 5329–5335.

[160] K. Matsuyama, N. Ihsan, K. Irie, K. Mishima, T. Okuyama, and H. Mutod, "Bioimaging application of highly luminescent silica-coated ZnO-nanoparticle quantum dots with biotin", Journal of Colloid and Interface Science, Vol. 399, 2013, pp. 19–25.

[161] J.W. Rasmussen, E. Martinez, P. Louka, and D.G. Wingett, "Zinc oxide nanoparticles for selective destruction of tumor cells and potential for drug delivery applications", Expert Opinion on Drug Delivery, Vol. 7, 2010, pp. 1063–1077.

[162] A. Al-Kahlout, "ZnO nanoparticles and porous coatings for dye-sensitized solar cell application: photoelectrochemical characterization" Thin Solid Films, Vol. 520, 2012, pp. 1814–1820.

[163] T.G Smijs, and S. Pavel, "Titanium dioxide and zinc oxide nanoparticles in sunscreens: focus on their safety and effectiveness", Nanotechnology Science and Applications, Vol. 4, 2011, pp. 95–112.

[164] H. Sun, H. Tian, Y. Yang, D. Xie, Y.-C. Zhang, X. Liu, S. Ma, H.-M. Zhao, and T-L. Ren, "A novel flexible nanogenerator made of ZnO nanoparticles and multiwall carbon nanotube", Nanoscale, Vol. 5, 2013, pp. 6117–6123.

[165] S.-M. Chang, and W.-S. Liu, "Surface doping is more beneficial than bulk doping to the photocatalytic activity of vanadium-doped TiO_2", Applied Catalysis B: Environmental, Vol. 101, 2011, pp. 333–342.

[166] http://en.academic.ru/pictures/enwiki/68/Defecttypes.png

[167] I. Luciu, "RF plasma synthesis and characterization of thin films for transparent conductors", [PhD Thesis], 2012.

[168] J. Geng, G.-H. Song, and J.-J. Zhu, "Sonochemical synthesis of Er^{3+}-doped ZnO nanospheres with enhanced upconversion photoluminescence", Journal of Nanomaterails, Vol. 2012, 2012, pp. 1–5.

[169] R. Zamiria, A.F. Lemos, A. Reblo, H.A. Ahangar, and J.M.F. Ferreira, “Effects of rare-earth (Er, La and Yb) doping on morphology and structure properties of ZnO nanostructures prepared by wet chemical method”, Ceramics International, Vol. 40, 2014, pp. 523–529.

[170] J. Slunecko, and M. Kosec, “Morphology and crystallization behaviour of sol–gel-derived titania”, Journal of the American Ceramic Society, Vol. 81, 1998, pp. 1121–1133.

[171] P.K. Dutta, and P.K. Gallagher, “Raman spectroscopic and thermoanalytical studies of the reaction of barium hydroxide with anatase and titanium oxide gels”, Journal of Materials Chemistry, Vol. 4, 1992, pp. 847–851.

[172] S. Gao, H. Zhang, R. Deng, X. Wang, D. Sun, and G. Zheng, “Engineering white light-emitting Eu-doped ZnO urchins by biopolymer-assisted hydrothermal method”, Applied Physics Letters, Vol. 89, 2006, pp. 123125.

[173] X.M. Teng, H.T. Fan, S.S. Pan, C. Ye, and G.H. Li, “Influence of annealing on the structural and optical properties of ZnO:Tb thin films”, Journal of Applied Physics, Vol. 100, 2006, pp. 053507.

[174] R.P.- Casero, A.G.- Llorente, O.P.Y. Moll, W. Seiler, R.M. Defourneau, D. Defourneau, E. Millon, J. Perrie`re, P. Goldner, and B. Viana, “Er-doped ZnO thin films grown by pulsed-laser deposition”, Journal of Applied Physics, Vol. 97, 2005, pp. 054905.

[175] E. Rita, E. Alves, U. Wahl, J.G. Correia, A.J. Neves, M.J. Soares, and T. Monteiro, “Optical doping of ZnO with Tm by ion implantation”, Physica B: Condensed Matter, Vol. 340, 2003, pp. 235–239.

[176] IUPAC: http://www.chem.qmul.ac.uk/iupac/.

[177] Cotton, and A. Simon, “Lanthanides and actinides”, Oxford University Press, New York, 1991.

[178] N. Sabbatini, M. Guardigli, and I. Manet, “Handbook on the physics and chemistry of rare earths: including actinides”, Elsevier, Amsterdam, 1996.

[179] A. Dossing, “Luminescence from lanthanide (3+) ions in solution”, European Journal of Inorganic Chemistry, Vol. 8, 2005, pp. 1413–1434.

[180] T. Christie, B. Brathwhite, and A. Tullach, “Mineral commodity report 17: rare earths and related elements”, New Zealand Mining, Vol. 24, 1998, pp. 1–13.

[181] S.V. Eliseeva, and J.-C.G. Bunzli, “Rare earths: jewels for functional materials of the future”, New Journal of Chemistry, Vol. 35, 2011, pp. 1165–1176.

[182] G.H. Dieke, “Spectra and energy levels of rare earth ions in crystals”, Interscience Publishers, New York, 1968.

[183] T. Justel, H. Nikol, and C. Ronda, “New developments in the field of luminescent materials for lighting and displays”, Angewandte Chemie International Edition, Vol. 37, 1998, pp. 3084–3103.

[184] K.W. Krämer, P. Dorenbos, H.U. Güdel, and C.W.E. van Eijk, “Development and characterization of highly efficient new cerium doped rare earth halide scintillator materials”, Journal of Materials Chemistry, Vol. 16, 2006, pp. 2773–2780.

[185] N. Sabbatini, M. Guardigli, and J.-M. Lehn, “Luminescent lanthanide complexes as photochemical supramolecular devices”, Coordination Chemistry Review, Vol. 123, 1993, pp. 201–228.

[186] A. Meijerink, R. Wegh, P. Vergeer, and T. Vlugt, “Photon management with lanthanides”, Optical Materials, Vol. 28, 2006, pp. 575–581.

[187] K.S. Pitzer, “Relativistic effects on chemical properties”, Accounts of Chemical Research, Vol. 12, 1974, pp. 271–276.

[188] G. Accorsi, “Trivalent lanthanide ions: luminescence and applications”, [PhD Thesis], 2007.

[189] D. Chen, Y. Wang, and M. Hong, “Lanthanide nanomaterials with photon management characteristics for photovoltaic application”, Nano Energy, Vol. 1, 2012, pp. 73–90.

[190] J.S. John, and J.L. Coffer, “Size control of erbium-doped silicon nanocrystals”, Applied Physics Letters, Vol. 77, 2000, pp. 1635–1637.

[191] J.-R. Duclère, B. Doggett, M.O. Henry, E. McGlynn, R.T.R. Kumar, and J.-P. Mosnier, “(20–23) ZnO thin films grown by pulsed laser deposition on CeO_2-buffered r-sapphire substrate”, Journal of Applied Physics, Vol. 101, 2007, pp. 013509.

[192] S.K. Shukla, E.S. Agorku, H. Mittal, and A.K. Mishra, “Synthesis, characterization and photoluminescence properties of Ce^{3+}-doped ZnO-nanophosphors”, Chemical Papers, Vol. 68, 2014, pp. 217–222.

[193] C. Chariditis, P. Patsalas, and S. Logothetidis, “Optical and mechanical performance of nanostructured cerium oxides for applications in optical devices”, Journal of Physics: Conference Series, Vol. 10, 2005, pp. 226–229.

[194] B.G. Mishra, and G.R. Rao, “Promoting effect of CeO_2 on cyclohexanol conversion over CeO_2-ZnO mixed oxide materials prepared by amorphous citrate process”, Bulletin of Material Science, Vol. 25, 2002, pp. 155–162.

[195] Y. He, B. Yang, and G. Cheng, “On the oxidative coupling of methane with carbon dioxide over CeO_2/ZnO nanocatalysts”, Catalysis Today, Vol. 98, 2004, pp. 595–600.

[196] L. Mo, X. Zheng, and C.-T. Yeh, “A novel CeO_2/ZnO catalyst for hydrogen production from the partial oxidation of methanol”, Chem Phys Chem, Vol. 6, 2005, pp. 1470–1472.

[197] T.-Y. Ma, Z.-Y. Yuan, and J.-L. Cao, “Hydrangea-like meso-/macroporous ZnO–CeO_2 binary oxide materials: synthesis, photocatalysis and CO oxidation”, European Journal of Inorganic Chemistry, Vol. 2010, 2010, pp. 716–724.

[198] C. Karunakaran, P. Gomathisankar, and G. Manikandan, “Preparation and characterization of antimicrobial Ce-doped ZnO nanoparticles for photocatalytic detoxification of cyanide”, Materials Chemistry and Physics, Vol. 123, 2010, pp. 585–594.

[199] D. Fangli, W. Ning, Z. Dongmei, and S. Yingzhong, “Preparation, characterization and infrared emissivity study of Ce-doped ZnO films”, Journal of Rare Earths, Vol. 28, 2010, pp. 391–395.

[200] L. Yan, L. Xiulin, and L. Jiangang, “Preparation and characterization of CeO_2 doped ZnO nanotubes fluorescent composite”, Journal of Rare Earths, Vol. 28, 2010, pp. 571–575.

[201] L.-A. Ying, J. Liu, L. Mo, H. Lou, and X. Zheng, “Hydrogen production by oxidative steam reforming of methanol over Ce_{1-x} Zn_xO_y catalysts prepared by combustion method”, International Journal of Hydrogen Energy, Vol. 37, 2012, pp. 1002–1006.

[202] J. Flor, S.A. Marques de Lima, and M.R. Davolos, “Effect of reaction time on the particle size of ZnO and ZnO:Ce obtained by a sol–gel method”, Progress in Colloid and Polymer Science, Vol. 128, 2004, pp. 239–243.

[203] J.X. Meng, K.W. Cheah, Z.P. Shi, and J.Q. Li, "Intense 1540 nm emission from Er doped Ce:YAG phosphor", Applied Physics Letters, Vol. 91, 2007, pp. 151107.

[204] G. Lakshminarayana, R.V. Sagar, and S. Buddhudu, "NIR luminescence from Er^{3+}/Yb^{3+}, Tm^{3+}/Yb^{3+}, Er^{3+}/Tm^{3+} and Nd^{3+} ions-doped zincborotellurite glasses for optical amplification", Journal of Luminescence, Vol. 128, 2008, pp. 690–695.

[205] R.G. Wilson, R.N. Schwartz, C.R. Abernathly, S.J. Pearton, N. Newman, M. Rubin, T. Fu, and J.M. Zavada, "1.54- μm photoluminescence from Er-implanted GaN and AlN", Applied Physics Letters, Vol. 65, 1994, pp. 992.

[206] K. Takahei, and K. Taguchi, "Selective formation of an efficient Er–O luminescencecenter in GaAs by metalorganic chemical vapor deposition under an atmosphere containing oxygen", Journal of Applied Physics, Vol. 74, 1993, pp. 1979.

[207] A. Polman, "Erbium implanted thin film photonic materials", Journal of Applied Physics, Vol. 82, 1997, pp. 1.

[208] S. Komuro, T. Katsumata, T. Morikawa, Y. Zhao, H. Isshiki, and Y. Aoyagi, "1.54 μm emission dynamics of erbium-doped zinc-oxide thin films", Applied Physics Letters, Vol. 76, 2000, pp. 3935.

[209] T. Williams, D. Hunter, A. Pradhan, and I. Kityk, "Photoinduced piezo-optical effect in Er doped ZnO films", Applied Physics Letters, Vol. 89, 2006, pp. 043116.

[210] A.J. Steckl, J.H. Park, and J.M. Zavada, "Prospects for rare earth doped GaN lasers on Si", Materials Today, Vol. 10, 2007, pp. 20–27.

[211] H. Hahn, "Gas phase synthesis of nanocrystalline materials", Nanostructured Materials, Vol. 9, 1997, pp. 3–12.

[212] N. Goswami, and D.K. Sharma, "Structural and optical properties of unannealed and annealed ZnO nanoparticles prepared by a chemical precipitation technique", Physica E, Vol. 42, 2010, pp. 1675–1682.

[213] C.J. Brinker, and G. W. Scherer, "Sol -gel science: the physics and the chemistry of sol gel processing", Academic Press, London, 1990.

[214] L.L. Hench, and J.K. West, "The sol-gel process", Chemical Reviews, Vol. 90, 1990, pp. 33–72.

[215] L.J. Fu, H. Liu, C. Li, Y.P. Wu, E. Rahm, R. Holze, and H.Q. Wu, "Electrode materials for lithium secondary batteries prepared by sol–gel methods", Progress in Materials Science", Vol. 50, 2005, pp. 881–928.

[216] H. Liu, Y.P. Wu, E. Rahm, R. Holze, and H.Q. Wu, "Cathode materials for lithium ion batteries prepared by sol-gel methods", Journal of Solid State Elelrochemistry, Vol. 8, 2004, pp. 450466.

[217] D.H. Chen, and X.R. He, "Synthesis of nickel ferrite nanoparticles by sol-gel method", Materials Research Bulletin, Vol. 36, 2001, pp. 1369–1377.

[218] B.J. Hwang, R. Santhanam, and D.G. Liu, "Characterization of nanoparticles of $LiMn_2O_4$ synthesized by citric acid sol–gel method", Journal of Power Sources, Vol. 97-98, 2001, pp. 443–446.

[219] Y.D. Zhong, X.B. Zhao, G.S. Cao, J.P. Tu, and T.J. Zhu, "Characterization of particulate sol–gel synthesis of $LiNi_{0.8}Co_{0.2}O_2$ via maleic acid assistance with different solvents", Journal of Alloys and Compounds, Vol. 420, 2006, pp. 298–305.

[220] J.T. Son, and H.G. Kim, "New investigation of fluorine-substituted spinel $LiMn_2O_{4-x}F_x$ by using sol–gel process", Journal of Power Sources, Vol. 147, 2005, pp. 220–226.

[221] T. Adschiri, Y. Hakuta, K. Sue, and K. Arai, "Hydrothermal synthesis of metal oxide nanoparticles at supercritical conditions", Journal of Nanoparticle Reserach, Vol. 3, 2001, pp. 227–235.

[222] M.S. Whittingham, J.D. Guo, R. Chen, T. Chirayl, G. Janauer, and P. Zavalij, "The hydrothermal synthesis of new oxide materials", Solid State Ionics, Vol. 75, 1995, pp. 257–268.

[223] A. Burubin, O. Brylev, P. Hany, and B.R. Churagulov, "Hydrothermal synthesis of $LiCoO_2$ for lithium rechargeable batteries", Solid State Ionics, Vol. 151, 2002, pp. 259–263.

[224] T. Kanasaku, K. Amezawa, and N. Yamamoto, "Hydrothermal synthesis and electrochemical properties of Li–Mn-spinel", Solid State Ionics, Vol. 133, 2000, pp. 51–56.

[225] Y.Y. Lianga, S.J. Baoa, and H.L. Li, "A series of spinel phase cathode materials prepared by a simple hydrothermal process for rechargeable lithium batteries", Journal of Solid State Chemistry, Vol. 179, 2006, pp. 2133–2140.

[226] H.M. Wu, J.P. Tu, Y.F. Yuan, X.T. Chen, J.Y. Xlang, X.B. Zhao, and G.S. Cao, "One-step synthesis $LiMn_2O_4$ cathode by a hydrothermal method", Journal of Power Sources, Vol. 161, 2006, pp. 1260–1263.

[227] S.T. Myung, S. Komaba, and N. Kumagai, "Hydrothermal synthesis and electrochemical behavior of orthorhombic $LiMnO_2$", Eiectrochimica Acta, Vol. 47, 2002, pp. 3287–3295.

[228] T. Zhang, C.G. Jin, T. Qian, X.L. Lu, J.M. Baia, and X.G. Li, "Hydrothermal synthesis of single-crystalline $La_{0.5}Ca_{0.5}MnO_3$ nanowires at low temperature", Journal of Materials Chemistry, Vol. 14, 2004, pp. 2787–2789.

[229] F. Chen, K. Zhu, G.J. Gan, S. Shen, and F. Kooli, "Hydrothermal processing of amorphous hydrous zirconia gels in the presence of 1,12-diaminododecane", Materials Research Bulletin, Vol. 42, 2007, pp. 1128–1136.

[230] P.Y. Silvert, and K.T. Elhsissen, "Synthesis of monodisperse submicronic gold particles by the polyol process", Solid State Ionics, Vol. 82, 1995, pp. 53–60.

[231] B. Wiley, Y. Sun, B. Mayers, and Y. Xia, "Shape-controlled synthesis of metal nanostructures: the case of silver", Chemistry a European Journal, Vol. 11, 2005, pp. 454–463.

[232] Y. Wang, X. Xuchuan, X. Jiang, and Y. Xia, "A solution-phase, precursor route to polycrystalline SnO_2 nanowires that can be used for gas sensing under ambient conditions", Journal of American Chemical Society, Vol. 125, 2003, pp. 16176–16177

[233] C. Feldmann, and H.O. Jungk, "Polyol-mediated preparation of nanoscale oxide Particles", Angewandte Chemie International Edition, Vol. 40, 2001, pp. 359.

[234] L. Poul, S. Arnmar, N. Jouini, and F. Fievet, "Synthesis of inorganic compounds (metal, oxide and hydroxide) in polyol medium: a versatile route related to the sol-gel process", Journal of Sol-gel Science and Technology, Vol. 26, 2003, pp. 261–265.

[235] C. Feldmann, "Preparation of nanoscale pigment particles", Advanced Materials, Vol. 13, 2001, pp. 1301–1303.

[236] S. Ammar, A. Helfen, N. Jouini, F. Fievet, L. Rosenman, F. Villain, P. Molinie, and M. Danot, "Magnetic properties of ultrafine cobalt ferrite

particles synthesized by hydrolysis in a polyol medium", Journal of Materials Chemistry, Vol. 11, 2001, pp. 186–192.

[237] B.H. Kim, J.H. Kim, I.H. Kwon, and M.Y. Song, "Electrochemical properties of $LiNiO_2$ cathode material synthesized by the emulsion method", Ceramics International, Vol. 33, 2007, pp. 837–841.

[238] V.G. Kumar, and K.B. Kim, "Organized and highly dispersed growth of MnO_2 nano-rods by sonochemical hydrolysis of Mn(3) acetate", Ultrasonics Sonochemistry, Vol. 13, 2006, pp. 549–556.

[239] Y.P. Fu, Y.H. Su, S.H. Wu, and C.H. Lin, "$LiMn_{2-y}M_yO_4$ (M = Cr, Co) cathode materials synthesized by the microwave-induced combustion for lithium ion batteries", Journal of Alloys and Compounds, Vol. 426, 2006, pp. 228–234.

[240] H.S. Kang, Y.C. Kang, H.Y. Koo, S.H. Ju, D.Y. Kim, S.K. Hong, J.R. Sohn, K. Y. Jung, and S.B. Park, "Nano-sized ceria particles prepared by spray pyrolysis using polymeric precursor solution", Materials Science and Engineering : B, Vol. 127, 2006, pp. 99–104.

[241] A.I.Y. Tok, F.Y.C. Boey, and X. L. Zhao, "Novel synthesis of Al_2O_3 nano-particles by flame spray pyrolysis", Journal of Materials Processing Technology, Vol. 178, 2006, pp. 270–273.

[242] Y. Zhang, H. Cao, J. Zhang, and B. Xia, "Synthesis of $LiNi_{0.6}Co_{0.2}Mn_{0.2}O_2$ cathode material by a carbonate co-precipitation method and its electrochemical characterization", Solid State Ionics, Vol. 177, 2006, pp. 3303–3307.

[243] T.H. Cho, Y. Shiosaki, and H. Noguchi, "Preparation and characterization of layered $LiMn_{1/3}Ni_{1/3}Co_{1/3}O_2$ as a cathode material by an oxalate co-precipitation method", Journal of Power Sources, Vol. 159, 2006, pp. 1322–1327.

[244] M.J. Godinho, R.F. Goncalves, L.P.S. Santos, J.A. Varela, E. Longo, and E.R. Leite, "Room temperature co-precipitation of nanocrystalline CeO_2 and $Ce_{0.8}Gd_{0.2}O_{1.9-\delta}$ powder", Materials Letters, Vol. 61, 2007, pp. 1904–1907.

[245] A.R. West, "Solid state chemistry and its applications", John Wiely Sons, India, 2005.

[246] A.B. Gaikwad, S.C. Navale, V. Samuel, A.V. Murugan, and V. Ravi, "A co-precipitation technique to prepare $BiNbO_4$, $MgTiO_3$ and $Mg_4Ta_2O_9$ powders", Materials Research Bulletin, Vol. 41, 2006, pp. 347–353.

[247] G. Xu, X. Zhang, W. He, H. Liu, H. Li, and R.I. Boughton, "Preparation of highly dispersed YAG nano-sized powder by co-precipitation method", Materials Letters, Vol. 60, 2006, pp. 962–965.

[248] B.D. Cullity, "Elements of X-ray Diffraction", Addison-Wesley, Reading, 1978.

[249] S.W. Chung, J.Y. Yu, and J.R. Heath, "Silicon nanowire devices", Applied Physics Letters, Vol. 76, 2000, pp. 2068.

[250] A. Notargiacomo, L. Di Gaspare, G. Scappucci, G. Mariottini, E. Giovine, R. Leoni, and F. Evangelisti, "A single electron transistor based on Si/SiGe wires", Materials Science and Engineering: C, Vol. 23, 2003, pp. 671–673.

[251] O. Hayden, R. Agarwal, and C.M. Lieber, "Nanoscale avalanche photodiodes for highly sensitive and spatially resolved photon detection", Nature Materials, Vol. 5, 2006, pp. 352–356.

[252] P. Feng, J.Y. Zhang, Q.H. Li, and T.H. Wang, "Individual β-Ga_2O_3 nanowires as solar-blind photodetectors", Applied Physics Letters, Vol. 88, 2006, pp. 153107.

[253] C. Li, D. Zhang, X. Liu, S. Han, T. Tang, J. Han, and C. Zhou, "In_2O_3 nanowires as chemical sensors", Applied Physics Letters, Vol. 82, 2003, pp. 1613.

[254] A. Kolmakov, Y. Zhang, G. Cheng, and M. Moskovits, "Detection of CO and O_2 using tin oxide nanowire sensors", Advanced Materials, Vol. 15, 2003, pp. 997–1000.

[255] E. Elssfah, and C. Tang, "From $Al_4B_2O_9$ nanowires to $Al_{18}B_4O_{33}$: Eu nanowires", Journal of Physical Chemistry C, Vol. 111, 2007, pp. 8176–8179.

[256] J.G. Lu, P. Chang, and Z. Fan, "Quasi-one-dimensional metal oxide materials-synthesis, properties and applications", Materials Science and Engineering: R, Vol. 52, 2006, pp. 49–91.

[257] K.X. Yao, and H.C. Zeng, "Asymmetric ZnO nanostructures with an interior cavity", Journal of Physical Chemistry B, Vol. 110, 2006, pp. 14736–14743.

[258] A.A. Ismail, A.A. El-Midany, E.A. Abel-Aal, and H. El-Shall, "Application of statistical design to optimize the preparation of ZnO nanoparticles via hydrothermal technique", Materials Letters, Vol. 59, 2005, pp. 1924–1928.

[259] W. Zhang, Z.Y. Zhong, Y.S. Wang, and R. Xu, "Doped solid solution: $(Zn_{0.95}Cu_{0.05})_{1-x}Cd_xS$ nanocrystals with high activity for H_2 evolution from aqueous solutions under visible light", Journal of Physical Chemistry C, Vol. 112, 2008, pp. 17635–17642.

[260] G. Vijayaprasath, R. Murugan, S. Palanisamy, N.M. Prabhu, T. Mahalingam, Y. Hayakawa, and G. Ravi, "Structural, optical and antibacterial activity studies of neodymium doped ZnO nanoparticles", Journal of Materials Science: Materials in Electronics, Vol. 26, 2015, pp. 7564–7576.

[261] X. Jia, H. Fan, M. Afzaal, X. Wu, and P. O'brien, "Solid state synthesis of tin-doped ZnO at room temperature: characterization and its enhanced gas sensing and photocatalytic properties", Journal of Hazardous Materials, Vol. 193, 2011, pp. 194–199.

[262] S. Kumar, V. Singh, and A. Tanwar, "Structural, morphological, optical and photocatalytic properties of Ag-doped ZnO nanoparticles", Journal of Materials Science: Materials in Electronics, Vol. 27, 2016, pp. 2166–2173.

[263] C. Jing, Y. Jiang, W. Bai, J. Chu, and A. Liu, "Synthesis of Mn-doped ZnO diluted magnetic semiconductors in the presence of ethyl acetoacetate under solvothermal conditions", Journal of Magnetism and Magnetic Materials, Vol. 322, 2010, pp. 2395–2400.

[264] N. Wang, P. Li, J. Xu, C. Cui, H. Li, and P. Yao, "Simple low-temperature chemical bath route to synthesize novel Ga-doped ZnO nanostructures for high photoresponse", Journal of Materials Science: Materials in Electronics, Vol. 26, 2015, pp. 671–676.

[265] J. Iqbal, X. Liu, H. Zhu, C. Pan, Y. Zhang, D. Yu, and R. Yu, Trapping of Ce electrons in band gap and room temperature ferromagnetism of Ce^{4+}doped ZnO nanowires", Journal of Applied Physics, Vol. 106, 2009, pp. 083515.

[266] B.C. Cheng, Y.H. Xiao, G.S. Wu, and L.D. Zhang, "Controlled growth and properties of one-dimensional ZnO nanostructures with Ce as activator/dopant", Advanced Functional Materials, Vol. 14, 2004, pp. 913–919.

[267] M. El Jouad, M.A. Lamrani, Z. Sofiani, M. Addou, T. El Habbani, N. Fellahi, K. Bahedi, L. Dghoughi, A. Monteil, B. Sahraoui, S. Dabos, and N. Gaumer, "Roughness effect on photoluminescence of cerium doped zinc oxide thin films", Optical Materials, Vol. 31, 2009, pp. 1357–1361.

[268] M. Yousefi, M. Amiri, R. Azimirad, and A.Z. Moshfegh, “Enhanced photoelectrochemical activity of Ce doped ZnO nanocomposite thin films under visible light”, Journal of Electroanalytical Chemistry, Vol. 661, 2011, pp. 106–112.

[269] G. Oskam, “Metal oxide nanoparticles: synthesis, characterization and application”, Journal of Sol-Gel Science and Technology, Vol. 37, 2006, pp.161–164.

[270] S. Steinfel, A.V. Gleich, and U. Petschow, “Nanotechnologies hazards and resource efficiency”, Springer Verlag, London, 2007.

[271] E.M. Wong, J.E. Bonevich, and P.C. Searson, “Growth kinetics of nanocrystalline ZnO particles from colloidal suspensions”, Journal of Physical Chemistry B, Vol. 102, 1998, pp. 7770–7775.

[272] Y. Hu, and H.J. Chen, “Preparation and characterization of nanocrystalline ZnO particles from a hydrothermal process”, Journal of Nanoparticle Research, Vol. 10, 2008, pp. 401–407.

[273] Y.W. Chen, Y.C. Liu, S.X. Lu, C.S. Xu, C.L. Shao, C. Wang, J.Y. Zhang, Y.M. Lu, D.Z. Shen, and X.W. Fan, Optical properties of ZnO and ZnO:In nanorods assembled by sol-gel method”, Journal of Chemical Physics, Vol. 123, 2005, pp. 134701.

[274] W. Li, D. Mao, F. Zhang, X. Wang, X. Liu, S. Zou, Y. Zhu, Q. Li, and J. Xu, “Characteristics of ZnO:Zn phosphor thin films by post-deposition annealing”, Nuclear Instruments and Methods in Physics Research Section B: Beam Interactions with Materials and Atoms, Vol. 169, 2000, pp. 59–63.

[275] K. Vanheusden, W.L. Warren, C.H. Seager, D.R. Tallant, J.A. Voigt, and B.E. Gnade, “Mechanisms behind green photoluminescence in ZnO phosphor powders”, Journal of Applied Physics, Vol. 79, 1996, pp. 7983.

[276] Z. Sofiani, B. Derkowska, P. Dalasiński, M. Wojdyła, S.D. -Seignon, M.A. Lamrani, L. Dghoughi, W. Bała, M. Addou, and B. Sahraoui, “Optical properties of ZnO and ZnO:Ce layers grown by spray pyrolysis”, Optics Communications, Vol. 267, 2006, pp. 433–439.

[277] A. Majid, and A. Ali, “Red shift of near band edge emission in cerium implanted GaN”, Journal of Physics D: Applied Physics, Vol. 42, 2009, pp. 045412.

[278] W. Li, Y. Wang, H. Lin, S.I. Shah, C.P. Huang, D.J. Doren, S.A. Rykov, J.G. Chen, and M.A. Barteau, "Band gap tailoring of Nd^{3+}-doped TiO_2 nanoparticles", Applied Physics Letters, Vol. 83, 2003, pp. 4143.

[279] V. Kumar, K.K. Sharma, D.K. Sharma, and D. K. Dwivedi, "Growth and characterization of $Cd_{0.8}Zn_{0.2}S$ thin films by spray pyrolysis method", Optik, Vol. 126, 2015, pp. 3203–3205.

[280] H.S. Li, Y.P. Li, and J.M.D. Coey, "R-T and R-R exchange interactions in the rare-earth (R)- transition-metal (T) intermetallics: an evaluation from relativistic atomic calculations", Journal of Physics: Condensed Matter, Vol. 3, 1991, pp. 7277–7290.

[281] T. Story, M. Gorska, A. Lusakowski, M. Arciszewska, W. Dobrowolski, E. Grodzicka, Z. Golacki, and R.R. Galazka, New mechanism of f-f exchange interactions controlled by Fermi level position", Physical Review Letters, Vol. 77, 1996, pp. 3447–3450.

[282] M. Timpel, M.V. Nardi, S. Krause, G. Ligorio, C. Christodoulou, L. Pasquali, A. Giglia, J. Frisch, B. Wegner, P. Moras, and N. Koch, "Surface modification of ZnO (0001)–Zn with phosphonate-based self-assembled monolayers: binding modes, orientation and work function", Chemistry of Materials, Vol. 26, 2014, pp. 5042–5050.

[283] M.H. Huang, S. Mao, H. Feick, H. Yan, Y. Wu, H. Kind, E. Weber, R. Russo, and P. Yang, "Room-temperature ultraviolet nanowire nanolasers", Science, Vol. 292, 2001, pp. 897–1899.

[284] D. Kim, K.Y. Lee, M.K. Gupta, S. Majumder, and S.-W. Kim, "Self-compensated insulating ZnO-based piezoelectric nanogenerators", Advanced Functional Materials, Vol. 24, 2014, pp. 6949–6955.

[285] Y.-W. Wang, A. Cao, Y. Jiang, X. Zhang, J.-H. Liu, Y. Liu, and H. Wang, "Superior antibacterial activity of zinc oxide/graphene oxide composites originating from high zinc concentration localized around bacteria", ACS Applied Materials Interfaces, Vol. 6, 2014, pp. 2791–2798.

[286] Y. Sun, J. Yang, L. Yang, M. Gao, X. Shan, Z. Zhang, M. Wei, Y. Liu, L. Fei, and H. Song, "Less contribution of nonradiative recombination in ZnO nails compared with rods", Journal of Luminescence, Vol. 134, 2013, pp. 35–41.

[287] G. Zhu, Y. Zhou, S. Wang, R. Yang, Y. Ding, X. Wang, Y. Bando, and Z. Wang, "Synthesis of vertically aligned ultra-long ZnO nanowires on

heterogeneous substrates with catalyst at the root", Nanotechnology, Vol. 23, 2012, pp. 055604.

[288] F.D. Nayeri, and E.A. Soleimani, "Influence of seed layers on the vertical growth of ZnO nanowires by low-temperature wet chemical bath deposition on ITO-coated glass Substrate", Experimental Techniques, Vol. 38, 2014, pp. 13–20.

[289] S. Anandan, A. Vinu, K.L.P. Sheeja Lovely, N. Gokulakrishnan, P. Srinivasu, T. Mori, V. Murugesan, V. Sivamurugan, and K. Ariga, "Photocatalytic activity of La-doped ZnO for the degradation of monocrotophos in aqueous suspension", Journal of Molecular Catalysis A : Chemical, Vol. 226, 2007, pp. 149–157.

[290] P.V. Kamat, "Photochemistry on nonreactive and reactive (semiconductor) surfaces", Chemical Reviews, Vol. 93, 1993, pp. 267–300.

[291] N. Kilinc, S. Ozturk, L. Arda, A. Altindal, and Z.Z. Ozturk, "Structural, electrical transport and NO_2 sensing properties of Y-doped ZnO thin films", Journal of Alloys and Compounds, Vol. 536, 2012, pp. 138–144.

[292] Z.K. Heiba, L. Arda, and M.B. Mohamed, "Structural and magnetic properties of $Zn_{0.95}Cr_{0.05}O$ annealed at different temperatures", Journal of Magnetism and Magnetic Materials, Vol. 389, 2015, pp. 153–156.

[293] N. Kilinc, L. Arda, S. Ozturk, and Z.Z. Ozturk, "Structure and electrical properties of Mg-doped ZnO nanoparticles", Crystal Research and Technology, Vol. 45, 2010, pp. 529–538.

[294] Z.K. Heiba, and L. Arda, "Structural properties of $Zn_{1-x}Mg_xO$ nanomaterials prepared by sol-gel method", Crystal Research and Technology, Vol. 44, 2009, pp. 845–850.

[295] S. Gburt, D. Stichtenoth, S. Muller, W. Dewald, C. Ronning, J. Wang, Y. Jiao, Y.Y. Rao, S.K. Hark, and Q. Li, "Rare earth doped zinc oxide nanowires", Nanoscience and Nanotechnology, Vol. 8, 2008, pp. 244–251.

[296] Y.R. Jang, K.H. Yoo, J.S. Ahn, C. Kim, and S.M. Park, "1.54 μm emission mechanism of Er-doped zinc oxide thin films", Applied Surface Science, Vol. 257, 2011, pp. 2822–2824.

[297] R. Vettumpperumal, S. Kalyanaraman, and R. Thangavel, "Optical constants and near infrared emission of Er doped ZnO sol–gel thin films", Journal of Luminescence, Vol. 158, 2015, pp. 493–500.

[298] J.H. Shim, T. Hwang, S. Lee, J.H. Park, S.J. Han, and Y.H. Jeong, "Origin of ferromagnetism in Fe- and Cu-codoped ZnO", Applied Physics Letters, Vol. 86, 2005, pp. 082503.

[299] B. Khalil, S. Naji, H. Labrim, M. Bhihi, A.G. EL Hachimi, M. Lakhal, A. Belhaj, A. Benyoussef, and A. El Kenz, "Magnetic properties of SrO doped with 3d transition Metals", Journal of Superconductivity and Novel Magnetism, Vol. 27, 2014, pp. 203– 208.

[300] X. Ma, "The magnetic properties of Gd doped ZnO nanowires", Thin Solid Films, Vol. 520, 2012, pp. 5752–5755.

[301] Y. Tan, Z. Fang, W. Chen, and P. He, "Structural, optical and magnetic properties of Eu-doped ZnO films", Journal of Alloys and Compounds, Vol. 509, 2011, pp. 6321–6324.

[302] D.K. Sharma, K.K. Sharma, V. Kumar, and A. Sharma, "Effect of Ce doping on the structural, optical and magnetic properties of ZnO nanoparticles", Journal of Materials Science: Materials in Electronics, Vol. 27, 2016, pp. 10330–10335.

[303] T. Schmidit, G. Muller, L. Spanhel, K. Kerkel, and A. Forchel, "Activation of 1.54 μm Er^{3+} fluorescence in concentrated II–VI semiconductor cluster environments", Chemistry of Materials, Vol. 10, 1998, pp. 65–71.

[304] D. Rute, and W. Bauhofe, "Highly luminescent Eu^{3+} or Tb^{3+} doped and ZnO sensitized optical fibers drawn from silicon compatible sealing glasses", Applied Physics Letters, Vol. 69, 1996, pp. 892.

[305] B. Yan, X. Chen, and J. Wu, "Induced assembly and photoluminescence of lanthanum (Tb, Eu, Dy) complexes/ZnO/polyethylene glycol hybrid phosphors", Applied Surface Science, Vol. 253, 2007, pp. 8575–8580.

[306] R. Rolli, K. Gatterer, M. Wachtler, M. Beettinelli, A. Speghini, and D. Ajo, "Optical spectroscopy of lanthanide ions in ZnO–TeO_2 glasses", Spectrochimica Acta Part A, Vol. 57, 2001, pp. 2009–2017.

[307] M. Kohls, T. Schimidt, H. Katschorek, L. Spanhel, G. Muller, N. Mais, A. wolf, and A. Forchel, "A simple colloidal route to planar micropatterned Er@ZnO amplifiers", Advanced Materials, Vol. 11, 1999, pp. 288–292.

[308] H.L. Han, L.W. Yang, Y.X. Liu, Y.Y. Zhang, and Q.B. Yang, "Up-conversion Luminescence switching in Er^{3+}-containing ZnO nanoparticles through Li^{+} co-doping", Optical Materials, Vol. 31, 2008, pp. 338–341.

[309] Y. Sun, Y. Chen, L. Tian, Y. Yu, X. Kong, Q. Zeng, Y. Zhang, and H. Zhang, "Morphology-dependent upconversion luminescence of ZnO:Er^{3+} nanocrystals", Journal of Luminescence, Vol. 128, 2008, pp. 15–21.

[310] Y.K. Ryu, P. Fernández, and J. Piqueras, "Growth and characterization of Er-doped ZnO elongated nanostructures", Physica Status Solidi A, Vol. 208, 2011, pp. 868–873.

[311] Y.H. Yang, Y. Feng, H.G. Zhu, and G.W. Yang, "Growth, structure, and cathodeluminescence of Eu-doped ZnO nanowires prepared by high-temperature and high-pressure pulsed-laser deposition", Journal of Applied Physics, Vol. 107, 2010, pp. 053502.

[312] Y. Terai, K. Yoshida, M.H. Kamarudin, and Y. Fujiwara, "Photoluminescence properties of Eu^{3+} ions in Eu-doped ZnO grown by sput- tering-assisted metalorganic chemical vapour deposition", Physica Status Solidi C, Vol. 8, 2010, pp. 519–521.

[313] S.L. -Romero, M.J.Q. -Jiménez, M.H. García, and A.A. -Castillo, "Bright Red Luminescence and Structural Properties of Eu^{3+} Ion doped ZnO by solution combustion technique", World Journal of Condensed Matter Physics Vol. 4, 2014, pp. 227–234.

[314] R. Zamiri, A.F. Lemos, A. Reblo, H.A. Ahangar, and J.M.F. Ferreira, "Effects of rare-earth (Er, La and Yb) doping on morphology and structure properties of ZnO nanostructures prepared by wet chemical method", Ceramics International, Vol. 40 2014, pp. 523–529.

[315] X.Y. Kong, and Z.L. Wang, "Polar-surface dominated ZnO nanobelts and the electrostatic energy induced nanohelixes, nanosprings, and nanospirals", Applied Physics Letters, Vol. 84, 2004, pp. 975.

[316] L. Yang, Z. Wang, Z. Zhang, Y. Sun, M. Gao, J. Yang, and Y. Yan, "Surface effects on the optical and photocatalytic properties of graphene like ZnO:Eu^{3+} nanosheets", Journal of Applied Physics, Vol. 113, 2013, pp. 033514.

[317] F. Li, X.-C. Liu, R.-W. Zhou, H.-M. Chen, S.-Y. Zhuo, and E.-W. Shi, "Strong correlation between oxygen vacancy and ferromagnetism in Yb-doped ZnO thin films", Journal of Applied Physics, Vol. 116, 2014, pp. 243910.

[318] S. Chauhan, M. Kumar, S. Chhoker, S.C. Katyal, and V.P.S. Awana, "Structural, vibrational, optical and magnetic properties of sol–gel derived Nd

doped ZnO nanoparticles", Journal of Materials Science: Materials in Electronics, Vol. 24, 2013, pp. 5102–5110.

[319] M. Kachi, W. Sakamoto, M. Ichida, T. Wada, H. Ando, and T. Yogo, "Synthesis of Er-doped ZnO nanoparticle/organic hybrid from metal-organics", Journal of Materials Science, Vol. 47, 2012, pp. 5128–5133.

[320] L. Irimpan, V.P.N. Nampoori, P. Radhakrishnan, A. Deepthy, and B. Krishnan, "Size dependent fluorescence spectroscopy of nanocolloids of ZnO", Journal of Applied Physics, Vol. 102, 2007, pp. 063524.

[321] R.M. Nyffenegger, B. Craft, M. Shaaban, S. Gorer, G. Erley, and R.M. Penner, "A hybrid electrochemical/chemical synthesis of zinc oxide nanoparticles and optically intrinsic thin films", Chemistry of Materials, Vol. 10, 1998, pp. 1120–1129.

[322] A. Mohanta, and R.K. Thareja, "Photoluminescence study of ZnO nanowires grown by thermal evaporation on pulsed laser deposited ZnO buffer layer", Journal of Applied Physics, Vol. 104, 2008, pp. 044906.

[323] O. Madelung, "Semiconductors: Data Handbook", 3rd Edition, Springer, 2003.

[324] L.V. Azaroff, "Introduction to Solids", McGraw-Hill, New York, 1960, pp. 371–372.

[325] P. Schröer, P. Krüger, and J. Pollmann, "First-principles calculation of the electronic structure of the wurtzite semiconductors ZnO and ZnS", Physical Review B, Vol. 47 1993, pp. 6971.

[326] V. Kumar, H.C. Swart, O.M. Ntwaeaborwa, R.E. Kroon, J.J. Terblans, S.K.K. Shaat, A. Yousif, and M.M. Duvenhage, "Origin of the red emission in zinc oxide nanophosphors", Materials Letters, Vol. 101, 2013, pp. 57–60.

[327] S. Zhou, K. Potzger, H. Reuther, K. Kuepper, W. Skorupa, M. Helm, and J. Fassbender, "Absence of ferromagnetism in V-implanted ZnO single crystals", Journal of Applied Physics, Vol. 101, 2007, pp. 09H109.

[328] N.H. Hong, J. Sakai, and V. Brizé, "Observation of ferromagnetism at room temperature in ZnO thin films", Journal of Physics: Condensed Matter, Vol. 19, 2007, pp. 036219.

[329] R. Nascimento, A.J.A. de Oliveira, A.A. Correa, L.O. Bulhoes, E.C. Pereira, V.M. Souza, and L. Walmsley, "Magnetic behavior of poly(3-

methylthiophene): metamagnetism and room-temperature weak ferromagnetism", Physical Review B, Vol. 67, 2003, pp. 144422.

[330] F.R. de Paula, L. Walmsley, E.C. Pereira, and A.J.A. Oliveira, "Magnetic properties of poly(3-hexylthiophene)", Journal of Magnetism and Magnetic Materials, Vol. 320, 2008, pp. e193–e195.

[331] D. Gao, Z. Zhang, J. Fu, Y. Xu, J. Qi, and D. Xue, "Room temperature ferromagnetism of pure ZnO nanoparticles", Journal of Applied Physics, Vol. 105, 2009, pp. 113928.

[332] S. Deng, K.P. Loh, J.B. Yi, J. Ding, H.R. Tan, M. Lin, Y.L. Foo, M. Zheng, and C.H. Sow, "Room temperature ferromagnetism at self-assembled monolayer modified Ag nanocluster–ZnO nanowire interface", Applied Physics Letters, Vol. 93, 2009, pp. 193111.

[333] O.V. Yazyev, "Emergence of magnetism in graphene materials and nanostructures", Reports on Progress in Physics, Vol.73, 2010, pp. 056501.

[334] A. Sundaresan, and C.N. Rao, "Implications and consequences of ferromagnetism universally exhibited by inorganic nanoparticles", Solid State Communications, Vol. 149, 2009, 1197–1200.

[335] A.G. El Hachimi, H. Zaari, A. Benyoussef, M. El Yadari, and A. El Kenz, "First principles prediction of the magnetism of 4f rare-earth-metal-doped wurtzite zinc oxide", Journal of Rare Earths, Vol. 32, 2014, pp. 715–721.

[336] J. Xie, "First-principles study on the magnetism in ZnS-based diluted magnetic semiconductors", Journal of Magnetism and Magnetic Materials, Vol. 322, 2010, pp. L37–L41.